

Evolution and Speciation in North American Toads

by

Kerry Allen Cobb

A dissertation submitted to the Graduate Faculty of
Auburn University
in partial fulfillment of the
requirements for the Degree of
Doctor of Philosophy

Auburn, Alabama
December 9, 2023

Keywords: speciation, hybridization, hybrid zone, phylogenetics, introgression, admixture

Copyright 2023 by Kerry Allen Cobb

Approved by

Jamie R. Oaks, Chair, Associate Professor, Department of Biological Sciences
Rita M. Graze, Associate Professor, Department of Biological Sciences
Tonia S. Schwartz, Associate Professor, Department of Biological Sciences
Laurie S. Stevison, Associate Professor, Department of Biological Sciences

Abstract

Understanding speciation, the evolutionary process by which new species evolve, is a central goal of evolutionary biology. Yet many important questions regarding this process remain unanswered. In this dissertation, I investigate speciation within North American toads in the genus *Anaxyrus*, a group belonging to the family Bufonidae, which has been the focus of many studies on speciation. I integrate data from hybrid zones, range-wide sampling of species in the genus, and simulations to illuminate patterns of diversification. I provide the first genetic characterization of two putative hybrid zones and demonstrate that both ancient and ongoing introgression is substantial. I also show that previous inferences of the evolutionary relationships among species of *Anaxyrus* have been unable to accurately reconstruct the true history of this group. With a better representation of the evolutionary history of these species, I obtain estimates of the timing of events and discuss the consequences of these findings as they relate to diversification and hybridization in *Anaxyrus*. Finally, I show through simulations that commonly used methods in evolutionary biology suffer from violations of assumptions we make about the evolutionary process. This highlights the need for caution when interpreting results and continued evaluation of the performance of methods in real-world scenarios. This study significantly enhances our understanding of speciation in *Anaxyrus* as well as the promise of this group for furthering our understanding of this fundamental evolutionary process.

Acknowledgments

I would like to express my deep appreciation to the individuals who have played pivotal roles leading to the successful completion of my PhD dissertation. Their support, encouragement, and guidance have been instrumental in shaping my academic journey. First and foremost, I am grateful to my advisor Jamie Oaks for his generosity, kindness, and mentorship throughout my time at Auburn. You have been a wonderful teacher and a fantastic role model. I would also like to thank my committee member Laurie Stevison for your advice and words of encouragement. And thank you to my other committee members Tonia Schwartz and Rita Graze for your valuable input and expertise. To my dear friend and labmate, Randy Klabacka, I will always cherish the fond memories we created and the enlightening conversations that we've had during our time at Auburn. I would also like to acknowledge my other labmates, Matt Buehler, Saman Jahangiri, Tanner Meyers, Morgan Muell, Claire Tracy, J.R. Wood, for making my time at Auburn an enjoyable and enriching experience. The stimulating environment created by all of you along with your camaraderie, have made my time at Auburn an incredibly enriching and enjoyable experience. To my parents Mark and Jane and my sister Claire, I am immensely grateful for the love, support, and encouragement you have provided me throughout my life. I also thank you Mom and Dad for fostering my curiosity for the natural world from a young age, for being wonderful role models, and for making education a high priority in my upbringing. Lastly, I want to thank my wonderful wife, Aura Cobb, for her unwavering support, love, and patience and for the sacrifices you have made for me to accomplish this dream. I am profoundly grateful to have you in my life and to have had you by my side during this endeavor.

Table of Contents

Abstract	2
Acknowledgments	3
List of Tables	7
List of Figures	9
1 Introduction	10
References	14
2 Genomic Evidence for Hybridization and Introgression in a North American Toad (<i>Anaxyrus</i>) Hybrid Zone	18
2.1 Introduction	18
2.2 Methods	22
2.2.1 Sampling and DNA Isolation	22
2.2.2 RADseq Library Preparation	23
2.2.3 Data Processing	25
2.2.4 Genetic Clustering & Ancestry Proportions	25
2.2.5 Genomic Cline Analysis	26
2.2.6 Genetic differentiation and Introgression	27
2.3 Results	28
2.3.1 Sampling and Data Processing	28
2.3.2 Genetic Clustering & Ancestry Proportions	28
2.3.3 Patterns of Introgression	29
2.3.4 Genomic Differentiation	30
2.4 Discussion	30

2.4.1	Evidence for ongoing hybridization	30
2.4.2	Variability of introgression	32
2.4.3	Relationship between introgression and differentiation	34
2.4.4	Conclusion	35
References	35
2.5 Figures	42
2.6 Tables	48
3 Phylogenomic Insights Into the Evolutionary History of <i>Anaxyrus</i> Toads (Anura: Bufonidae)	56
3.1 Introduction	56
3.2 Methods	60
3.2.1 Sampling and DNA Isolation	60
3.2.2 RADseq Library Preparation	60
3.2.3 Phylogenetic Data Processing	62
3.2.4 Phylogenetic Inference	62
3.2.5 Introgression	64
3.2.6 Population Structure	64
3.3 Results	66
3.3.1 Assembly and alignment with <i>ipyrad</i>	66
3.3.2 Maximum Likelihood Phylogeny	66
3.3.3 Coalescent Phylogeny	67
3.3.4 Introgression	67
3.3.5 Population Structure	68
3.4 Discussion	70
3.4.1 Phylogenetic relationships	70
3.4.2 Divergence Time	71
3.4.3 Hybridization	73
3.4.4 Population Structure	76
3.4.5 Conclusion	78

References	79
3.5 Figures	85
3.6 Tables	108
4 Comparison of Linked versus Unlinked Character Models for Species	
Tree Inference	117
4.1 Introduction	117
4.2 Methods	120
4.2.1 Simulations of error-free data sets	120
4.2.2 Introducing Site-pattern Errors	121
4.2.3 Assessing Sensitivity to Errors	121
4.2.4 Project repository	122
4.3 Results	123
4.3.1 Behavior of linked (<i>StarBEAST2</i>) versus unlinked (<i>ecoevolity</i>) character models	123
4.3.2 Analyzing all sites versus SNPs with <i>ecoevolity</i>	124
4.3.3 Coverage of credible intervals	124
4.3.4 MCMC convergence and mixing	125
4.4 Discussion	125
4.4.1 Robustness to character-pattern errors	126
4.4.2 Relevance to empirical data sets	128
4.4.3 Recommendations for using unlinked-character models	129
4.4.4 Other complexities of empirical data in need of exploration	130
References	131
4.5 Figures	135

List of Tables

2.1	Samples collected for this study	48
2.2	Samples loaned from museums	55
3.1	Samples used in this study	109

List of Figures

2.1.	Evanno method for optimal value of K in <i>STRUCTURE</i>	42
2.2.	All independent <i>STRUCTURE</i> runs	43
2.3.	Summarized <i>STRUCTURE</i> results for each value of K.	44
2.4.	Genetic evidence of hybridization between <i>A. americanus</i> and <i>A. terrestoris</i>	45
2.5.	Shape of genomic clines	46
2.6.	Patterns of genomic divergence.	46
2.7.	Relationship between genetic divergence and introgression.	47
3.1.	Distribution map of <i>americanus</i> group samples	86
3.2.	Maximum likelihood tree part 1	87
3.3.	Maximum likelihood tree part 2	88
3.4.	Simplified maximum likelihood tree	89
3.5.	Multispecies coalescent phylogeny	90
3.6.	<i>f</i> -branch statistics	91
3.7.	<i>A. americanus</i> population structure, K=2	92
3.8.	<i>A. americanus</i> population structure, K=3	93
3.9.	<i>A. terrestoris</i> population structure	94
3.10.	<i>A. fowleri</i> population structure	95
3.11.	<i>A. woodhousii</i> population structure	96
3.12.	Estimate of admixture between <i>A. fowleri</i> and <i>A. woodhousii</i>	97
3.13.	ΔK for <i>A. americanus</i> <i>STRUCTURE</i> analysis	98
3.14.	ΔK for <i>A. fowleri</i> <i>STRUCTURE</i> analysis	99
3.15.	ΔK for <i>A. terrestoris</i> <i>STRUCTURE</i> analysis	100
3.16.	ΔK for <i>A. woodhousii</i> <i>STRUCTURE</i> analysis	101
3.17.	ΔK for combined <i>A. fowleri</i> and <i>A. woodhousii</i> <i>STRUCTURE</i> analysis	102

3.18. All <i>A. americanus</i> <i>STRUCTURE</i> runs	103
3.19. All <i>A. fowleri</i> <i>STRUCTURE</i> runs	104
3.20. All <i>A. terrestris</i> <i>STRUCTURE</i> runs	105
3.21. All <i>A. woodhousii</i> <i>STRUCTURE</i> runs	106
3.22. All combined <i>A. fowleri</i> and <i>A. woodhousii</i> <i>STRUCTURE</i> runs	107
 4.1. Simulation model	135
4.2. Accuracy and precision of divergence-time estimates (in units of expected substitutions per site) with 1000 base pair loci	136
4.3. Accuracy and precision of divergence-time estimates (in units of expected substitutions per site) with 500 base pair loci	137
4.4. Accuracy and precision of divergence-time estimates (in units of expected substitutions per site) with 250 base pair loci	138
4.5. Accuracy and precision of estimates of root effective population size scaled by the mutation rate ($N_e^R \mu$) with 1000 base pair loci	139
4.6. Accuracy and precision of estimates of root effective population size scaled by the mutation rate ($N_e^R \mu$) with 500 base pair loci	140
4.7. Accuracy and precision of estimates of root effective population size scaled by the mutation rate ($N_e^R \mu$) with 250 base pair loci	141
4.8. Accuracy and precision of estimates of effective population sizes of the descendant branches of the tree scaled by the mutation rate ($N_e^D \mu$) with 1000 base pair loci	142
4.9. Accuracy and precision of estimates of effective population sizes of the descendant branches of the tree scaled by the mutation rate ($N_e^D \mu$) with 500 base pair loci	143
4.10. Accuracy and precision of estimates of effective population sizes of the descendant branches of the tree scaled by the mutation rate ($N_e^D \mu$) with 250 base pair loci	144
4.11. Performance of <i>ecoevolity</i> with data sets simulated with unlinked characters	145

Chapter 1

Introduction

Speciation is the driving force behind the incredible diversity of life on Earth. By studying this process, we gain insights into the mechanisms that have shaped the natural world, enabling us to appreciate and understand this biodiversity. A fundamental aspect of speciation is the evolution of reproductive isolation. This phenomenon has puzzled and captivated evolutionary biologists since the field's inception (Mallet, 2008). Reproductive isolation was first viewed as incompatible with evolution by natural selection as it was inconceivable how natural selection might produce such an outcome (Mallet, 2008). It is now appreciated that reproductive isolation is in fact compatible with evolution by natural selection, but mysteries abound (Coyne & Orr, 2004). Why do organisms form discrete clusters instead of existing on a continuum? What evolutionary processes drive reproductive isolation? Which genes are involved and what are their functions under normal circumstances? What are the targets of selection that drive evolution of these genes? What is the role of gene flow in the speciation process? With increasingly powerful tools at their disposal, biologists are directing more attention than ever before into seeking answers to these questions.

Toads in the family Bufonidae have held a prominent place in the speciation literature (Blair, 1972). They have a number of qualities that make them attractive for furthering our understanding of the speciation process. Among these qualities is the ease with which the primary behavioral isolating mechanisms, spawning period and advertisement call, can be measured and quantified in order to understand the strength of prezygotic mating barriers and possible patterns consistent with reinforcement (Blair, 1974; Cocroft & Ryan, 1995; Kennedy, 1962). Researchers in the past were also drawn by the ease

with which they can be crossed in the laboratory (Blair, 1972). Spawning can be induced hormonally or performed in vitro, facilitating the planning and execution of experiments (Trudeau et al., 2010). The females of many species can produce thousands of offspring which are externally fertilized making a variety of embryological observations or manipulations possible (Blair, 1972). Many species pairs have proven to be reproductively compatible through laboratory crosses (Blair, 1972). This has provided an opportunity to investigate the tempo of the evolution of reproductive incompatibility and to understand the importance of pre-mating barriers (Fontenot et al., 2011; Malone & Fontenot, 2008; Sasa et al., 1998). Another attractive quality of Bufonidae is the existence of several known hybrid zones which provide useful opportunities for studying the evolution of reproductive isolation in a natural setting (Green, 1996; Van Riemsdijk et al., 2023).

Unlike many organisms which have been the subject of intensive study in the context of speciation, such as *Drosophila*, *Mus*, and *Heliconius*, most Bufonidae have homomorphic sex chromosomes (Blair, 1972). This is an interesting contrast in light of the apparent importance of sex chromosomes in the evolution of reproductive incompatibility and the role of heterogamety in explaining evolutionary patterns such as Haldane's rule, faster male evolution, and faster-X evolution (Delph & Demuth, 2016). Furthermore, there is evidence of sex chromosome turnovers within Bufonidae which presents an opportunity to study differences in the evolution of reproductive incompatibility among closely related species with different sex determination systems (Dufresnes et al., 2020; Stöck et al., 2011). All of these qualities, along with a near global distribution and large diversity of species (642 species; AmphibiaWeb, 2023) and ecological niches, make Bufonidae an excellent group to further our understanding of the evolution of reproductive incompatibility.

In the first chapter of my dissertation I investigate a putative hybrid zone between *Anaxyrus americanus* and *A. terrestris*, two species in the family Bufonidae. Hybrid zones are increasingly appreciated to be a widespread phenomenon in nature. One that can have important evolutionary consequences when it comes to the process of speciation (Moran et al., 2021). Hybrid zones also present a valuable opportunity to investigate reproductive

incompatibility (Rieseberg et al., 1999). The production of large numbers of recombinant offspring through multiple generations of backcrossing under natural conditions cannot be achieved through captive breeding for most organisms.

The only prior evidence of hybridization between *A. americanus* and *A. terrestris* comes from anecdotal reports and a single study of morphological variation across the contact zone between these two species in central Alabama (Mount, 1975; Weatherby, 1982). The amount of introgression, if any, within this putative hybrid zone is unknown. Using genome-wide data collected from a large sample across the hybrid zone, I characterize introgression between these two species for the first time. I find that introgression between them is extensive and I identify many candidate loci that may be involved in reproductive incompatibility. This study can serve as a guide to future studies in this system which could leverage quantitative measures of prezygotic isolation such as calls and breeding period, reference genomes, or crossing experiments paired with cutting edge genomic tools such as CRISPR-Cas9 to shed light on the process of speciation. In combination with other toad hybrid zones, there is a great deal we could learn about whether there are recurrent patterns in toad speciation, with their homomorphic sex chromosomes are a useful contrast against other taxa.

Hybrid zones have great potential for furthering our understanding of speciation. However, they provide only a snapshot in time. There is a great deal of historical context that is also important to understand. Questions such as, how long has it been since hybridizing species have diverged? What are the environmental factors that drive divergence between them? And, what are the lasting consequences of hybridization? In the second chapter of my dissertation, I investigate the evolutionary history of species within the genus *Anaxyrus* to attempt to answer these questions. To accomplish this, I infer the phylogenetic relationships among species in this genus from genome-wide sequence data and estimate the divergence times for nodes in the phylogenetic tree. I also test for a history of admixture to understand the importance of historical introgression among ancestral species during the evolutionary history of the genus.

To try to understand what factors might play a role in driving divergence between

populations and potentially result in speciation, I also investigate population structure within several species. The relationships and divergence-time estimates that I infer from the genomic data differ substantially from previous studies based on more limited data and methods (Fontenot et al., 2011; Graybeal, 1997; Masta et al., 2002; Portik et al., 2023; Pramuk et al., 2007; Pyron & Wiens, 2011). I also find evidence of previously unrecognized hybridization in the past and present between species of *Anaxyrus* which reinforces the increasingly appreciated recognition of gene flow as a common and important process during the diversification of organisms. My analysis of population structure shows strong population differentiation in one species which could be in the early stage of speciation. This chapter highlights the utility of *Anaxyrus* for understanding speciation as there is potentially hybridization occurring at multiple stages of the speciation process.

The inferences made about the evolutionary process in the previous two chapters rely heavily on a suite of computational methods developed for the task. All of these methods make assumptions about the processes that produce the data, i.e. DNA sequences, which are used as input. These are often simplifying assumptions made to achieve tractable models and computation, many of which are known to be violated. Many simplifying assumptions are sure to be violated and we know this to be the case for many of them. Other assumptions are made because they reflect our best set of beliefs about the evolutionary process or because work has not yet been done to incorporate additional complexity into the methods. Many of these are sure to be violated as well but are more challenging to recognize. Violations of assumptions may not be highly problematic (Oaks et al., 2020), but the impact of many violations have never been evaluated. In the third chapter of my dissertation, I investigate the impact of errors and biases that can arise through the collection and processing DNA sequence data. I find that these violations have a modest impact on inference. When clustering reads to construct an alignment, it is necessary to set a minimum similarity threshold that will very likely exclude variants from the alignment. In simulated data, I found this type of data acquisition bias had the effect of underestimating recent divergence times and underestimating all effective population sizes. This may be relevant for some of the very recent divergence times estimated for

the *Anaxyrus* phylogeny and suggests caution should be taken in interpreting these.

This dissertation greatly enhances our understanding of the evolutionary history in *Anaxyrus* and adds to a large body of research into speciation in Bufonidae that has been amassed over the past 60 years. This dissertation also provides important context for understanding this past work. Divergence time estimates give us an understanding of the tempo of diversification and for the evolution of reproductive incompatibility. They also give us some clues as to the drivers of diversification within *Anaxyrus*. I demonstrate that hybridization and introgression are important processes in the evolutionary history of *Anaxyrus* and provide confirmation of gene flow across two hybrid zones for the first time. Further analysis of these hybrid zones has promise for shedding light on the process of speciation generally. I also demonstrate why caution is necessary when interpreting the results of evolutionary inferences as the methods we rely on a suite of assumptions that may commonly be violated. This study lays a foundation for further advances in our understanding the process of speciation by taking advantage of many attractive qualities this system offers.

References

- AmphibiaWeb. (2023).
- Blair, W. F. (1972). *Evolution in the genus Bufo*. University of Texas Press.
- Blair, W. F. (1974). Character Displacement in Frogs. *American Zoologist*, 14(4), 1119–1125. <https://doi.org/10.1093/icb/14.4.1119>
- Cocroft, R. B., & Ryan, M. J. (1995). Patterns of advertisement call evolution in toads and chorus frogs. *Animal Behaviour*, 49(2), 283–303. <https://doi.org/10.1006/anbe.1995.0043>
- Coyne, J. A., & Orr, H. A. (2004). *Speciation*. Sinauer Associates.
- Delph, L. F., & Demuth, J. P. (2016). Haldane's Rule: Genetic Bases and Their Empirical Support. *Journal of Heredity*, 107(5), 383–391. <https://doi.org/10.1093/jhered/esw026>

- Dufresnes, C., Litvinchuk, S. N., Rozenblut-Kościsty, B., Rodrigues, N., Perrin, N., Crochet, P.-A., & Jeffries, D. L. (2020). Hybridization and introgression between toads with different sex chromosome systems. *Evolution Letters*, 4(5), 444–456. <https://doi.org/10.1002/evl3.191>
- Fontenot, B. E., Makowsky, R., & Chippindale, P. T. (2011). Nuclear–mitochondrial discordance and gene flow in a recent radiation of toads. *Molecular Phylogenetics and Evolution*, 59(1), 66–80. <https://doi.org/10.1016/j.ympev.2010.12.018>
- Graybeal, A. (1997). Phylogenetic relationships of bufonid frogs and tests of alternate macroevolutionary hypotheses characterizing their radiation. *Zoological Journal of the Linnean Society*, 119(3), 297–338. <https://doi.org/10.1111/j.1096-3642.1997.tb00139.x>
- Green, D. M. (1996). The bounds of species: Hybridization in the *Bufo americanus* group of North American toads. *Israel Journal of Zoology*, 42, 95–109.
- Kennedy, J. P. (1962). Spawning Season and Experimental Hybridization of the Houston Toad, *Bufo houstonensis*. *Herpetologica*, 17(4), 239–245.
- Mallet, J. (2008). Hybridization, ecological races and the nature of species: Empirical evidence for the ease of speciation. *Philosophical Transactions of the Royal Society B: Biological Sciences*, 363(1506), 2971–2986. <https://doi.org/10.1098/rstb.2008.0081>
- Malone, J. H., & Fontenot, B. E. (2008). Patterns of Reproductive Isolation in Toads (R. DeSalle, Ed.). *PLoS ONE*, 3(12), e3900. <https://doi.org/10.1371/journal.pone.0003900>
- Masta, S. E., Sullivan, B. K., Lamb, T., & Routman, E. J. (2002). Molecular systematics, hybridization, and phylogeography of the *Bufo americanus* complex in Eastern North America. *Molecular Phylogenetics and Evolution*, 24(2), 302–314. [https://doi.org/10.1016/S1055-7903\(02\)00216-6](https://doi.org/10.1016/S1055-7903(02)00216-6)
- Moran, B. M., Payne, C., Langdon, Q., Powell, D. L., Brandvain, Y., & Schumer, M. (2021). The genomic consequences of hybridization (P. J. Wittkopp, Ed.). *eLife*, 10, e69016. <https://doi.org/10.7554/eLife.69016>

- Mount, R. H. (1975). *The Reptiles and Amphibians of Alabama*. The University of Alabama Press.
- Oaks, J. R., L'Bahy, N., & Cobb, K. A. (2020). Insights from a general, full-likelihood Bayesian approach to inferring shared evolutionary events from genomic data: Inferring shared demographic events is challenging*. *Evolution*, 74(10), 2184–2206. <https://doi.org/10.1111/evo.14052>
- Portik, D. M., Streicher, J. W., & Wiens, J. J. (2023). Frog phylogeny: A time-calibrated, species-level tree based on hundreds of loci and 5,242 species. *Molecular Phylogenetics and Evolution*, 188, 107907. <https://doi.org/10.1016/j.ympev.2023.107907>
- Pramuk, J. B., Robertson, T., Sites, J. W., & Noonan, B. P. (2007). Around the world in 10 million years: Biogeography of the nearly cosmopolitan true toads (Anura: Bufonidae). *Global Ecology and Biogeography*, 0(0), 070817112457001–???. <https://doi.org/10.1111/j.1466-8238.2007.00348.x>
- Pyron, R. A., & Wiens, J. J. (2011). A large-scale phylogeny of Amphibia including over 2800 species, and a revised classification of extant frogs, salamanders, and caecilians. *Molecular Phylogenetics and Evolution*, 61(2), 543–583. <https://doi.org/10.1016/j.ympev.2011.06.012>
- Rieseberg, L. H., Whitton, J., & Gardner, K. (1999). Hybrid zones and the genetic architecture of a barrier to gene flow between two sunflower species. *Genetics*, 152(2), 713–727.
- Sasa, M. M., Chippindale, P. T., & Johnson, N. A. (1998). PATTERNS OF POSTZYGOTIC ISOLATION IN FROGS. *Evolution*, 52(6), 1811–1820. <https://doi.org/10.1111/j.1558-5646.1998.tb02258.x>
- Stöck, M., Croll, D., Dumas, Z., Biollay, S., Wang, J., & Perrin, N. (2011). A cryptic heterogametic transition revealed by sex-linked DNA markers in Palearctic green toads: Heterogametic transition in Bufonidae. *Journal of Evolutionary Biology*, 24(5), 1064–1070. <https://doi.org/10.1111/j.1420-9101.2011.02239.x>
- Trudeau, V. L., Somoza, G. M., Natale, G. S., Pauli, B., Wignall, J., Jackman, P., Doe, K., & Schueler, F. W. (2010). Hormonal induction of spawning in 4 species of frogs

by coinjection with a gonadotropin-releasing hormone agonist and a dopamine antagonist. *Reproductive Biology and Endocrinology*, 8(1), 36. <https://doi.org/10.1186/1477-7827-8-36>

- Van Riemsdijk, I., Arntzen, J. W., Bucciarelli, G. M., McCartney-Melstad, E., Rafačlović, M., Scott, P. A., Toffelmier, E., Shaffer, H. B., & Wielstra, B. (2023). Two transects reveal remarkable variation in gene flow on opposite ends of a European toad hybrid zone. *Heredity*. <https://doi.org/10.1038/s41437-023-00617-6>
- Weatherby, C. A. (1982). INTROGRESSION BETWEEN THE AMERICAN TOAD, BUFO AMERICANUS, AND THE SOUTHERN TOAD, B. TERRESTRIS, IN ALABAMA.

Chapter 2

Genomic Evidence for Hybridization and Introgression in a North American Toad (*Anaxyrus*) Hybrid Zone

2.1 Introduction

Speciation is the process by which genetic divergence leads to reproductive isolation between divergent lineages. It is a continuous process during which there may be ongoing gene flow or introgression via hybridization following a period of isolation and subsequent secondary contact (Mallet, 2008; Wu, 2001). Introgression is possible because genetic barriers to introgression that accumulate within the genome are a property of genomic regions rather than a property of the entirety of the genome (Gompert, Parchman, et al., 2012; Wu, 2001). Natural hybridization between divergent lineages has become increasingly appreciated as a widespread phenomenon in recent years (Mallet, 2005; Moran et al., 2021). It is a phenomenon that can have important evolutionary consequences. Hybridization can be a source of adaptive variation (Hedrick, 2013). It can also introduce deleterious genetic load which persists long term within a population (Moran et al., 2021). Hybridization can create conditions where selection favors the evolution of traits that enhance assortative mating and reduce the production of unfit hybrid offspring which drives further genetic divergence and reinforcement of reproductive barriers between lineages (Servedio & Noor, 2003). If hybrids do not suffer any negative fitness effects, hybridization could lead to the erosion of differences between divergent populations (Taylor et al., 2006), potentially resulting in populations that are genetically distinct from either parent species which can themselves eventually evolve reproductive

isolation from the parent species (Moran et al., 2021).

Aside from having important evolutionary consequences which need to be understood, hybridization is also an excellent opportunity to investigate the processes that result in the evolution of reproductive incompatibility and divergence between evolutionary lineages. Hybrid zones are particularly suitable for this due to the production of a large numbers of recombinant genomes carrying many possible combinations of genomic elements from parent species resulting from generations of backcrossing (Rieseberg et al., 1999). Generations of backcrossing and recombination make it possible to distinguish between the effects of closely linked genes (Rieseberg et al., 1999), and it is not feasible to achieve this experimentally in the vast majority of species (Rieseberg et al., 1999). Furthermore, the combination of genes produced are exposed to selection under natural conditions. This is important as the effect of hybrid incompatibilities can be dependent on environmental conditions and can only be fully understood in this context (Miller & Matute, 2016).

Despite being a fundamental evolutionary process, our understanding of speciation is far from complete (Butlin et al., 2011). Only a few loci, in a few species, have been pinpointed as the direct cause of reproductive incompatibility between species (Blackman, 2016; Nosil & Schlüter, 2011). Consequently, our understanding of the processes that drive the evolution of loci resulting in reproductive incompatibility is limited (Butlin et al., 2011). Studies of introgression within hybrid zones have identified highly variable rates of introgression among loci (Barton & Hewitt, 1985; Gompert et al., 2017). This heterogeneity can arise via genetic drift occurring within hybrid zones, but will also be caused by differences among loci in the strength of selection against them in a hybrid genomic background (Barton & Hewitt, 1985; Gompert et al., 2017). It has also been observed that the levels of genetic divergence between species are highly variable across the genome (Nosil et al., 2009). Much of this heterogeneity is the result of divergent selection acting on each species independently (Nosil et al., 2009). Regions with particularly high levels of divergence between closely related species have been coined "genomic islands of divergence" (Wolf & Ellegren, 2017). It is assumed, particularly in the case

of speciation with gene flow, that these genomic islands harbor genes that reduce interbreeding between species. When speciation occurs with gene flow, divergent selection can cause adaptive divergence in habitat use, phenology, or mating signals, and reduce the frequency or success of interspecific matings. When species diverge in geographic isolation, divergent selection and reproductive isolation could be decoupled and reproductive isolation is not the result of direct selection against of interspecific matings. Whether loci under divergent selection between two species also contribute to reproductive isolation has not been widely explored. A handful of studies have found evidence for a modest relationship between genetic divergence and selection against introgression (Gompert, Lucas, et al., 2012; Larson et al., 2013; Nikolakis et al., 2022; Parchman et al., 2013). How consistent and widespread this pattern is remains to be seen. At least one study has found no association (Jahner et al., 2021).

In this study I investigate hybridization between the American toad (*Anaxyrus americanus*) and Southern toad (*Anaxyrus terrestris*) at a suspected hybrid zone in the Southern United States to assess the extent of introgression between them and test for a relationship between introgression and genetic divergence. This suspected hybrid zone has not been investigated with genetic data previously but it bears many hallmarks of a tension zone (Barton & Hewitt, 1985). Under the tension zone model of hybridization, species boundaries are maintained by a balance between dispersal and selection against individuals carrying incompatible hybrid genotypes (Barton & Hewitt, 1985). The ranges of *A. americanus* and *A. terrestris* abut with an abrupt transition and no apparent overlap along a long contact zone which from Louisiana to Virginia. This contact zone closely corresponds with a prominent physiographic feature known as the "fall line" (Mount, 1975; Powell et al., 2016). The Fall line is the boundary between the Southern coastal plain to the South and the Appalachian Highlands to the North (Shankman & Hart, 2007). These regions differ in their underlying geology, topography, and elevation (Shankman & Hart, 2007). The distribution of *A. terrestris* is restricted to the coastal plain extending from the Mississippi River in the West to Virginia in the East (Fig. 2.4). The distribution of the American Toad encompasses nearly all of the Eastern North American with the ex-

ception of the Southern coastal plain (Fig. 2.4). Tension zones are expected to correspond with natural features that reduce dispersal or abundance (Barton, 1979). Such a sudden transition is difficult to explain if not the result of the processes characteristic of tension zones. For there to be no mutually hospitable areas permitting some range overlap is implausible without there being an extreme level of competition or extreme degree of adaptation by each species to their respective environments. The two species only differ slightly in male advertisement call, morphological appearance, and the timing of their spawn (Cocroft & Ryan, 1995; Mount, 1975; Weatherby, 1982). There is some overlap in the spawning period and male Bufonidae are famously indiscriminate in their choice of mates (Dorđević & Simović, 2014; Weatherby, 1982). They have also been shown to have a degree of reproductive compatibility through laboratory crossing experiments which produced viable F_2 offspring (Blair, 1963). Analysis of morphological variation in central Alabama by Weatherby (1982) suggests there has been introgression between them.

The "true toads" in the family Bufonidae, to which *A. americanus* and *A. terrestris* belong, have been a prominent group of organisms in the literature on hybridization. W.F. Blair and colleagues performed a remarkable 1,934 separate experimental crosses to quantify the degree of reproductive incompatibility between species pairs within this family (Blair, 1972; Malone & Fontenot, 2008). These experiments demonstrated a high degree of compatibility between some closely related species pairs in which hybrids were capable of producing viable backcross or F_2 hybrid offspring (Blair, 1963). Furthermore, numerous cases of natural hybridization among toad species have been reported with several apparent or clear hybrid zones (Colliard et al., 2010; Green, 1996; Van Riemsdijk et al., 2023; Weatherby, 1982). Despite the interest in and appreciation for hybridization in Bufonidae, only a small amount of work has been done to understand patterns of introgression within Bufonid hybrid zones. A clinal pattern of admixture at 26 allozyme loci has been shown within the *Anaxyrus americanus* X *Anaxyrus hemiophrys* hybrid zone in Ontario, Canada (Green, 1983). Almost no admixture was detected at 7 microsatellite loci within the suspected *Bufo siculus* X *Bufo balearicus* hybrid zone in Sicily, Italy (Colliard et al., 2010). The most comprehensive study of introgression within a Bufonidae

hybrid zone found significant levels of genome wide admixture, fitting a clinal pattern, at two separate transects at either end of the *Bufo bufo* x *Bufo spinosus* hybrid zone in Southern France (Van Riemsdijk et al., 2023).

The suspected *A. americanus*, *A. terrestris* hybrid zone has great potential to expand our understanding of speciation. This will be dependent on the degree of ongoing introgression, if any, between these species. In this study, I use genome-wide sequence data to characterize patterns of introgression within the hybrid zone using model-based inference of admixture proportions, Bayesian genomic cline analysis, and estimates of parental population differentiation. With these approaches, I specifically address the following questions: 1) Is there evidence of ongoing hybridization and admixture between the two species, 2) Do any loci have outstanding patterns of introgression consistent with them being linked to reproductive incompatibility, and 3) Is there any relationship between patterns of introgression and levels of genetic differentiation between parental lineages?

2.2 Methods

2.2.1 Sampling and DNA Isolation

I collected genetic samples from *A. americanus* and *A. terrestris* by driving roads during rainy nights between 2017 and 2020 in a region of central Alabama where hybridization has previously been inferred from the presence of morphological intermediate individuals (Weatherby, 1982). I euthanized individuals with immersion in buffered MS-222. I removed liver and/or toes and preserved them in 100% ethanol and fixed specimens with 10% Formalin solution. Genetic samples and formalin fixed specimens were deposited at the Auburn Museum of Natural History. Additional samples were also provided by museums (see Table 2.2).

I isolated DNA by lysing a small piece of liver or toe approximately the size of a grain of rice in 300 μ L of a solution of 10mM Tris-HCL, 10mM EDTA, 1% SDS (w/v), and nuclease free water along with 6 mg Proteinase K and incubating for 4-16 hours at 55°C. To purify the DNA and separate it from the lysis product, I mixed the lysis product

with a 2X volume of SPRI bead solution containing 1 mM EDTA, 10 mM Tris-HCl, 1 M NaCl, 0.275% Tween-20 (v/v), 18% PEG 8000 (w/v), 2% Sera-Mag SpeedBeads (GE Healthcare PN 65152105050250) (v/v), and nuclease free water. I then incubated the samples at room temperature for 5 minutes, placed the beads on a magnetic rack, and discarded the supernatant once the beads had collected on the side of the tube. I then performed two ethanol washes by adding 1 mL of 70% ETOH to the beads while still placed in the magnet stand and allowing it to stand for 5 minutes before removing and discarding the ethanol. After removing all ethanol from the second wash, I removed the tube from the magnet stand and allowed the sample to dry for 1 minute before thoroughly mixing the beads with 100 μ L of TLE solution containing 10 mM Tris-HCL, 0.1 mM EDTA, and nuclease free water. After allowing the bead mixture to stand at room temperature for 5 minutes, I returned the beads to the magnet stand, collected the TLE solution, and discarded the beads. I quantified DNA in the TLE solution with a Qubit fluorometer (Life Technologies, USA) and diluted samples with additional TLE solution to bring the concentration to 20 ng/ μ L.

2.2.2 RADseq Library Preparation

I prepared RADseq libraries using the 2RAD approach developed by Bayona-Vásquez et al. (2019). On 96 well plates, I ligated 100 ng of sample DNA in 15 μ L of a solution with 1X CutSmart Buffer (New England Biolabs, USA; NEB), 10 units of XbaI, 10 units of EcoRI, 0.33 μ M XbaI compatible adapter, 0.33 μ M EcoRI compatible adapter, and nuclease free water with a 1 hour incubation at 37°C. I then immediately added 5 μ L of a solution with 1X Ligase Buffer (NEB), 0.75 mM ATP (NEB), 100 units DNA Ligase (NEB), and nuclease free water and incubated at 22°C for 20 min and 37°C for 10 min for two cycles, followed by 80°C for 20 min to stop enzyme activity. For each 96 well plate, I pooled 10 μ L of each sample and split this pool equally between two microcentrifuge tubes. I purified each pool of libraries with a 1X volume of SpeedBead solution followed by two ethanol washes as described in the previous section except that the DNA was resuspended in 25 μ L of TLE solution and combined the two pools of cleaned ligation

product.

In order to be able to detect and remove PCR duplicates, I performed a single cycle of PCR with the iTru5-8N primer which adds a random 8 nucleotide barcode to each library construct. For each plate, I prepared four PCR reactions with a total volume of 50 μ L containing 1X Kapa Hifi Buffer (Kapa Biosystems, USA; Kapa), 0.3 μ M iTru5-8N Primer, 0.3 mM dNTP, 1 unit Kapa HiFi DNA Polymerase, 10 μ L of purified ligation product, and nuclease free water. I ran reactions through a single cycle of PCR on a thermocycler at 98°C for 2 min, 60°C for 30 s, and 72°C for 5 min. I pooled all of the PCR products for a plate into a single tube and purified the libraries with a 2X volume of SpeedBead solution as described above and resuspended in 25 μ L TLE. I added the remaining adapter and index sequences which were unique to each plate with four PCR reactions with a total volume of 50 μ L containing 1X Kapa Hifi (Kapa), 0.3 μ M iTru7 Primer, 0.3 μ M P5 Primer, 0.3 mM dNTP, 1 unit of Kapa Hifi DNA Polymerase (Kapa), 10 μ L purified iTru5-8N PCR product, and nuclease free water. I ran reactions on a thermocycler with an initial denaturation at 98°C for 2 min, followed by 6 cycles of 98°C for 20 s, 60°C for 15 s, 72°C for 30 s and a final extension of 72°C for 5 min. I pooled all of the PCR products for a plate into a single tube and purified the product with a 2X volume of SpeedBead solution as described above and resuspended in 45 μ L TLE.

I size selected the library DNA from each plate in the range of 450-650 base pairs using a BluePippin (Sage Science, USA) with a 1.5% dye free gel with internal R2 standards. To increase the final DNA concentrations, I prepared four PCR reactions for each plate with 1X Kapa Hifi (Kapa), 0.3 μ M P5 Primer, 0.3 μ M P7 Primer, 0.3 mM dNTP, 1 unit of Kapa HiFi DNA Polymerase (Kapa), 10 μ L size selected DNA, and nuclease free water and used the same thermocycling conditions as the previous (P5-iTru7) amplification. I pooled all of the PCR products for a plate into a single tube and purified the product with a 2X volume of SpeedBead solution as before and resuspended in 20 μ L TLE. I quantified the DNA concentration for each plate with a Qubit fluorometer (Life Technologies, USA) then pooled each plate in equimolar amounts relative to the number of samples on the plate and diluted the pooled DNA to 5 nM with TLE solution. The pooled libraries were

pooled with other projects and sequenced on an Illumina HiSeqX by Novogene (China) to obtain paired-end, 150 base-pair sequences.

2.2.3 Data Processing

I demultiplexed the iTru7 indexes using the *process_radtags* command from *Stacks* v2.6.4 (Rochette et al., 2019) and allowed for two mismatches for rescuing reads. To remove PCR duplicates, I used the *clone_filter* command from *Stacks*. I demultiplexed inline sample barcodes, trimmed adapter sequence, and filtered reads with low quality scores as well as reads with any uncalled bases using the *process_radtags* command again and allowed for the rescue of restriction site sequence as well as barcodes with up to two mismatches. I built alignments from the processed reads using the *Stacks* pipeline. I allowed for 14 mismatches between alleles within, as well as between individuals (M and n parameters). This is equivalent to a sequence similarity threshold of 90% for the 140 bp length of reads post trimming. I also allowed for up to 7 gaps between alleles within and between individuals. I used the *populations* command from *Stacks* to filter loci missing in more than 5% of individuals, filter all sites with minor allele counts less than 3, filter any individuals with more than 90% missing loci, and randomly sample a single SNP from each locus.

2.2.4 Genetic Clustering & Ancestry Proportions

To cluster individuals and characterize patterns of genetic differentiation and admixture between clusters, I used the Bayesian inference program *STRUCTURE* v2.3.4 (Pritchard et al., 2000) with *STRUCTURE*'s admixture model which returns an estimate of ancestry proportions for each sample. To evaluate the assumption that samples are best modeled as inheriting their genetic variation from the two groups corresponding to the species identification made in the field, I ran *STRUCTURE* under four different models, each with a different number of assumed clusters of individuals (K parameter) ranging from 1 to 4. For each value of K , I ran 20 independent runs for 100,000 total steps with the first 50,000 as burnin. I used the R package *POPHELP* v2.3.1 (Francis, 2017) to

combine iterations for each value of K and to select the model producing the largest ΔK which is the the model that has the greatest increase in likelihood score from the model with one fewer populations as described by (Evanno et al., 2005). I also examined genetic clustering and evidence of admixture using a non-parametric approach with a principal component analysis (PCA) implemented in the R package *adegenet* v2.1.10 (Jombart, 2008). I visualized the relationship between the first principal component axis and the estimated admixture proportion for each individual to check for agreement between the parametric *STRUCTURE* analysis and the non-parametric PCA analysis.

2.2.5 Genomic Cline Analysis

To investigate patterns of introgression across the hybrid zone I used the Bayesian genomic cline inference tool *BGC* v1.03 (Gompert & Buerkle, 2012) to infer parameters under a genomic cline model. A genomic cline model has two key parameters, denoted α and β , which describe introgression at each locus based on ancestry of individuals. The α parameter affects the cline center which is the increase (positive value) or decrease (negative value) in the probability from one species. The β parameter affects the cline rate which is the increase (positive value) or decrease (negative value) in the rate of transition from a low probability to a high probability of ancestry for one species. I classified a sample as being admixed if it had an inferred admixture proportion of $<95\%$ for one species under the model with a K of two in the *STRUCTURE* analysis. I used *VCFtools* v0.1.17 to filter all non-biallelic sites from the the VCF file produced by the *populations* command in *Stacks*. I converted the VCF formatted data into the *BGC* format using *bgc_utils* v0.1.0, a *Python* package that I developed for this project (github.com/kerrycobb/bgc_utils). I ran *BGC* with 5 independent chains, each for 1,000,000 steps and sampling every 1000. I visualized MCMC output to confirm patterns consistent with the chains converging on a shared stationary distribution, discarded samples prior to convergence, combined the independent chains, and identified outlier loci with *bgc_utils*.

A primary goal of *BGC* analysis is to identify loci which have exceptional patterns of introgression. These loci, or loci in close linkage to them, are expected to be enriched for

genetic regions affected by selection due to reproductive incompatibility between the two species. I identified loci with exceptional patterns of introgression using two approaches described by Gompert and Buerkle (2011). (1) If locus specific introgression differed from the genome-wide average, which I will refer to as "excess ancestry" following Gompert and Buerkle (2011). More specifically, I classified a locus as having excess ancestry if the 90% highest posterior density interval (HPDI) for the alpha or beta parameter did not cover zero. (2) If locus specific introgression is statistically unlikely relative to the genome-wide distribution of locus specific introgression which I will refer to as "outliers" following Gompert and Buerkle (2011). I classified a locus as an outlier if the median of the posterior sample for the α or β parameters for a locus were not contained in the interval from 0.05 to 0.95 of the cumulative probability density functions $Normal(0, \tau_\alpha)$ or $Normal(0, \tau_\beta)$ respectively, where τ_α and τ_β are the median values from the posterior sample for the conditional random effect priors on τ_α and τ_β . These conditional priors describe the genome-wide variation of locus specific α and β . I further classified outlier α parameter estimates for a locus based on whether the median of the posterior sample was positive or negative. Positive estimates of α mean there is a greater probability of *A. americanus* ancestry in individuals at the locus relative to their hybrid index whereas negative estimates of α mean there is a greater probability of *A. terrestris* ancestry.

2.2.6 Genetic differentiation and Introgression

To test for a relationship between patterns of introgression and genetic divergence, I used *VCFtools* to calculate the Weir and Cockerham (1984) F_{ST} between each species using only the samples inferred through the *STRUCTURE* analysis to have >95% ancestry for one species under the model with a K of two (Danecek et al., 2011). The Weir and Cockerham F_{ST} is calculated per-site and I calculated the per-site F_{ST} for the same sites as those used in the *BGC* analysis. To determine if patterns of introgression are correlated with population differentiation I performed a Pearson Correlation to test if F_{ST} correlates with either the α or β parameters. I ran the correlation test with the absolute value of the median of the posterior sample for the α parameter and the median

of the posterior sample for the β parameter. I also binned the F_{ST} estimates of loci based on their status as outliers for the α parameter in order to further test for a relationship between population differentiation and α . I categorized loci as positive α outliers, negative α outliers, and as α that are not outliers. I performed a Kruskal-Wallis test using *SciPy* v1.10.1 to test whether there were significant differences in values of F_{ST} at each locus between these groups (Virtanen et al., 2020). I then performed Mann-Whitney tests between all pairs of groups using *scikit-posthocs* to test which groups differ significantly from each other (github.com/maximtrp/scikit-posthocs).

2.3 Results

2.3.1 Sampling and Data Processing

I prepared reduced-representation sequencing libraries from 173 samples collected for this study (Table 2.1) and 19 samples available from existing collections (Table 2.2)). The *Stacks* pipeline assembled reads into 432,336 loci with a mean length of 253.31 bp. Prior to filtering the mean coverage per sample was 32X. After filtering loci missing from greater than 5% of samples, filtering sites with minor allele counts less than 3, filtering individuals with greater than 90% missing loci, and randomly sampling a single SNP from each locus, 1194 sites remained and 43 samples were excluded from further analyses leaving a total of 149. For the included samples, 56 had been identified as most closely resembling *A. americanus* and 93 had been identified as most closely resembling *A. terrestris*.

2.3.2 Genetic Clustering & Ancestry Proportions

A visual inspection of the *STRUCTURE* results shows that each iteration with same value for K converged on very similar results (Fig. 2.2). The *STRUCTURE* model with the largest ΔK was the model with a K of two (Fig. 2.1). Furthermore, individuals are inferred as having ancestry derived largely from only two ancestral groups even for K values of three and four. For these values of K , only a small amount of ancestry is

attributed to the third or fourth ancestral groups for any individual sample (Fig. 2.3). Using a 95% estimated ancestry proportion as a cutoff for considering individuals to have pure ancestry, 36 samples were classified as pure *A. americanus*, 75 as pure *A. terrestris*, and 38 as being admixed. The proportions of admixture among the samples shows a clear gradient between 0 and 1 which is consistent with many individuals being the product of advanced-generation hybrids beyond the F_1 generation. The transition of admixture proportions from one species to the other increase with distance from the locations of pure individuals with proportions closest to 0.5 being found in the center of this transition (Fig. 2.4).

2.3.3 Patterns of Introgression

Visualization of the MCMC output with trace plots and histograms of each parameter indicated that each of the five chains run in *BGC* converged on the same parameter space and that each chain quickly reached stationarity. I conservatively discarded the first 10% of samples as burnin. The median of the posterior sample for α , the cline center parameter, ranged from -0.525-0.494 across loci. The β parameter, the cline shape parameter, was less variable and ranged from -0.158-0.220 across loci. I identified 16 loci with excess ancestry for the α parameter relative to the genome wide average; i.e., the 90% HDPI does not cover 0. Of these, the median of the posterior sample for 5 of these loci was negative and for 11 loci was positive. Negative values represent a greater probability of *A. americanus* ancestry at a locus relative to the individual's hybrid index whereas positive values represent a greater probability of *A. terrestris* ancestry. I did not identify any loci for which the estimates of β were outliers relative to the genome-wide average. I identified 116 loci as outliers for the α parameter relative to the genome-wide distribution of locus specific introgression. Of these, the median of the posterior sample for 24 of these loci was negative and for 92 loci was positive (Fig. 2.5). I did not identify any loci for which the estimates of β were outliers relative to the genome-wide distribution of locus specific introgression. All 16 of the loci identified as having excess ancestry for the α parameter relative to the genome-wide average were also identified as

outliers relative to the genome-wide distribution of locus specific introgression.

2.3.4 Genomic Differentiation

Genetic differentiation between *A. americanus* and *A. terrestris* was highly variable among loci (Fig. 2.6). Locus-specific F_{ST} between non-admixed *A. americanus* and *A. terrestris* had a mean of 0.07. F_{ST} values for 249 loci were 0. Only a single locus had fixed differences between species with an F_{ST} of 1.0. There is little apparent relationship between α or β and F_{ST} except at that the highest α and β estimates have non-zero F_{ST} estimates (Fig. 2.7). The Pearson correlation test estimates a weak correlation between α and F_{ST} ($r=0.29$, $p=1.62e-23$) and between β and F_{ST} ($r=0.32$, $p = 8.28 \times 10^{-30}$). The result of the Kruskal-Wallis test are consistent with there being significant differences between the F_{ST} values of loci with outlier α estimates and non-outlier α estimates on average ($p = 1.32 \times 10^{-40}$) (Fig. 2.6). The results of the post hoc pairwise Mann-Whitney tests are consistent with both categories of loci with outlier α estimates having greater F_{ST} values on average than the non-outlier estimates of α . The difference between non-outlier loci and loci with greater probability of *A. americanus* ancestry was slightly higher ($p = 2.72 \times 10^{-38}$) than the difference between non-outlier loci and loci with greater *A. terrestris* ancestry ($p = 8.16 \times 10^{-6}$).

2.4 Discussion

2.4.1 Evidence for ongoing hybridization

With the genome-wide sequence data obtained in this study, I find evidence of substantial gene flow across the hybrid zone of these two species. The *STRUCTURE* analysis inferred 38 out of 149 samples as having a proportion of ancestry of at least 5% of sites attributable to admixture (Fig. 2.4). The admixture proportions inferred in the *STRUCTURE* analysis range from 0.05%-0.5% which is consistent with hybrids being viable, fertile, and capable of backcrossing over multiple generations (Fig. 2.4) (Slager et al., 2020). When backcrossing occurs over multiple generations in combination with migra-

tion of hybrid progeny and selection against introgressing alleles, a cline will form across the hybrid zone with introgressing alleles becoming more uncommon with distance from the cline center (Barton & Hewitt, 1985). The results of the *STRUCTURE* analysis are largely consistent with this. Inferred admixture coefficients are highest at the center of the hybrid zone and decrease and approach zero with distance from the center (Fig. 2.4).

Admixed samples were located quite far from the center of the hybrid zone. In fact samples with greater than 5% admixture proportions are located all the way at the Northeastern and Southwestern edges of the sampling area. The width of a hybrid zone is a product of the strength of selection for or against introgression and the average dispersal distance of individuals within their reproductive lifespan (Barton & Hewitt, 1985). Breden (1987) estimated that 27% of individual *A. fowleri* breed at non-natal breeding ponds with some dispersing more than 2 km. Female *A. americanus* can migrate more than 1 km between breeding sites and post-breeding locations (Forester et al., 2006). Invasive cane toads (*Rhinella marina*) in Australia are estimated to have expanded their range at a rate of 10-15 km per year shortly after their introduction although this rate slowed with time (Urban et al., 2008). The presence of samples with little to no admixture in close proximity to toads with high proportions of admixture shows that dispersal has an important roll in shaping the patterns of this hybrid zone. Individuals would be expected to appear more like their neighbors if dispersal rates and distances were very low. It is also likely that this hybrid zone may be more appropriately described as a mosaic hybrid zone rather than a more simple tension zone (Harrison, 1986). However, the sampling for this study is too sparse and irregular to definitively test this. Another possibility is that some of this inferred admixture is the result of a statistical artifact or due to error. *STRUCTURE* can only model admixture and not ancestral polymorphism which would be classified by the program as admixture (Pritchard et al., 2000). Some reassurance is provided by the result of the PCA which is largely consistent with the *STRUCTURE* results although it is possible that they could be affected by the same bias or error introduced in data collection and processing (Fig. 2.4).

The tension zone model of hybrid zones predicts that location of hybrid zones centers

will be dependent on the effects of selection along with population density and natural dispersal barriers (Barton, 1979). The *STRUCTURE* results show that in two areas, there is a clear transition from samples with primarily *A. americanus* ancestry to samples with primarily *A. terrestis* ancestry corresponding with the locations of streams and rivers. In the Northern part of the sampling area, transitions occur at the Coosa River and at Waxahatchee Creek (Fig. 2.4). In the Southern part, they occur at Sougahatchee Creek (Fig. 2.4). Clearly these are not impassable boundaries as there has been introgression beyond them. However, they likely reduce dispersal and as a result the center of the hybrid zone is caught in this location as described by Barton (1979).

2.4.2 Variability of introgression

There are two primary parameters of interest in a genomic cline model that can be interpreted in the evolutionary context of hybrid zones. The α parameter specifies the center of the cline and is dependent on the increase or decrease in the probability of locus-specific ancestry from one of the parental populations. The β parameter specifies the rate of change in probability of ancestry along the genome-wide admixture gradient. Extreme estimates of these parameters may be associated with loci that cause reproductive incompatibility between hybridizing species. The Bayesian genomic cline analysis of the genome-wide data in this study yielded extreme estimates for α at some sites. Sites were classified as having extreme values in two ways. First, sites could be classified as having excess ancestry if the HDPI of α or β does not cover zero and is therefore extreme relative to the genome-wide average of cline parameter estimates. Second, sites could be classified as being outliers if they are extreme relative to the genome-wide distribution of locus specific effects under the cline model. A greater number of sites qualified as outliers for estimates of α than qualified as having excess ancestry. There were 116 loci classified as outliers which make up 9.7% of the total number of sites. Of those, 16 were also classified as having excess ancestry making up 1.3% of all sites. This difference is consistent with other studies using both simulated and empirical data which typically find more outlier loci than excess ancestry loci (Gompert & Buerkle, 2012). Both of these methods

can produce false positives as these extreme values can be produced solely by genetic drift rather than by selection (Gompert & Buerkle, 2012). So not all sites with extreme estimates will be associated with incompatibility loci. The false positive rate is exacerbated when there are many loci with small effects on compatibility. However, these sites should be enriched for loci associated with modest to strong reproductive incompatibility and thus provide an upper estimate of the number of sites that are associated with these modest to strong barriers to gene flow (Gompert & Buerkle, 2012).

None of the estimates for β were classified as either outliers or as having excess ancestry. Simulations have demonstrated that the α parameter is more impacted by selection against hybrid genotypes than the β parameter (Gompert, Lucas, et al., 2012). Other studies have also found no extreme estimates of β (Gompert, Lucas, et al., 2012; Nikolakis et al., 2022). One possible interpretation of the absence of extreme values of β is that selection is only strong enough to have a significant impact on α but it is not strong enough to have a large impact on β . Unlike for α , there is not a strong relationship between locally positive selection favoring introgressed genotypes and β (Gompert, Lucas, et al., 2012). Therefore, some of the extreme values for α could be due to adaptive introgression which does not have much impact on estimates of β . This is plausible given the large extent of introgression which is potentially due to adaptive introgression. There is a negative relationship between β and dispersal rate (Gompert, Lucas, et al., 2012). It is also plausible that high dispersal rates, rather than selection is the cause of lower β values that do not reach the threshold to qualify as extreme.

Of the 9.7% of sites that qualified as α outliers, a substantially larger proportion had positive values which represent greater *A. americanus* ancestry than expected at those sites in admixed individuals. Negative α estimates represent a greater probability of *A. terrestris* ancestry at a site within admixed individuals. Sites with positive outlier estimates for α made up 7.7% of all sites whereas those with negative outlier estimates made up just 2%. This asymmetry suggests that introgression flows more in the direction of *A. americanus* than it does in the direction of *A. terrestris*. This result is consistent with a pattern evident upon visual inspection of the mapped *STRUCTURE* results.

Samples collected from sites adjacent to sites with admixed samples appear to have a greater proportion of *A. terrestoris* ancestry than *A. americanus* ancestry (Fig. 2.4). Taken together, these observations suggest that introgression at this hybrid zone is asymmetric (Yang et al., 2020). Asymmetries in introgression can arise for multiple reasons. There could be differences in mate choice which make females of one species more selective than females of the other (Baldassarre et al., 2014). There can also be species differences in dispersal tendencies. Reciprocal-cross differences in reproductive isolation, termed Darwin's Corollary, are very common (Turelli & Moyle, 2007). If one of the sexes is more prone to dispersal, introgression will flow more freely in one direction than it would in the other. It is possible that this observation is just an artifact of sampling. Particularly if this is a highly mosaic hybrid zone. However, many more samples with primarily *A. terrestoris* ancestry were collected than samples with primarily *A. americanus* ancestry.

2.4.3 Relationship between introgression and differentiation

Patterns of genetic differentiation and genomic introgression between *A. americanus* and *A. terrestoris* are consistent with the hypothesis that regions of the genome experiencing divergent selection also affect hybrid fitness. As predicted, there is a positive association between locus specific estimates of F_{ST} and both the absolute value of the α and the β parameter estimates. Although this correlation supports the hypothesis that introgression outliers are linked to loci under selection, the association is only a modest one. Despite this, it is notable all of the outlier α estimates as well as the highest β estimates have non-zero F_{ST} estimates. Whereas sites with lower α and β estimates span the entire range from zero to one. This is consistent with expectations of secondary contact where not all loci that have undergone genomic divergence will necessarily result in reproductive isolation. A tighter coupling of divergence and resistance to gene flow would be expected under a scenario of divergence with gene flow.

2.4.4 Conclusion

In conclusion, the genome-wide sequence data analysis conducted in this study has provided compelling evidence of significant gene flow across the hybrid zone of *A. americanus* and *A. terrestris*. The *STRUCTURE* analysis reveals that a substantial number of samples exhibit evidence of admixture, with the proportion of ancestry attributed to hybridization. These findings suggest that hybrids are not only viable and fertile but also capable of backcrossing over multiple generations. Furthermore, the spatial distribution of admixture coefficients suggests the formation of a cline, with the highest levels of admixture at the hybrid zone's center gradually diminishing with distance. Patterns in the distribution of admixture coefficients suggest a potentially important role for rivers as a partial barrier to dispersal. I found a weak relationship between loci with limited introgression and the degree of genetic divergence, measured with F_{ST} . This study demonstrates that introgression between *A. americanus* and *A. terrestris* is ongoing and can serve as a guide for future studies which could leverage quantitative measures of prezygotic isolation such as calls or spawning period, reference genomes, or crossing experiments paired with cutting edge genomic tools such as CRISPR-Cas9 to shed light on the process of speciation.

References

- Baldassarre, D. T., White, T. A., Karubian, J., & Webster, M. S. (2014). GENOMIC AND MORPHOLOGICAL ANALYSIS OF A SEMIPERMEABLE AVIAN HYBRID ZONE SUGGESTS ASYMMETRICAL INTROGRESSION OF A SEXUAL SIGNAL. *Evolution*, 68(9), 2644–2657. <https://doi.org/10.1111/evo.12457>
- Barton, N. H. (1979). The dynamics of hybrid zones. *Heredity*, 43(3), 341–359. <https://doi.org/10.1038/hdy.1979.87>
- Barton, N. H., & Hewitt, G. M. (1985). Analysis of Hybrid Zones. *Annual Review*, 16, 113–148.

- Bayona-Vásquez, N. J., Glenn, T. C., Kieran, T. J., Pierson, T. W., Hoffberg, S. L., Scott, P. A., Bentley, K. E., Finger, J. W., Louha, S., Troendle, N., Diaz-Jaimes, P., Mauricio, R., & Faircloth, B. C. (2019). Adapterama III: Quadruple-indexed, double/triple-enzyme RADseq libraries (2RAD/3RAD). *PeerJ*, 7, e7724. <https://doi.org/10.7717/peerj.7724>
- Blackman, B. (2016). Speciation Genes. *Encyclopedia of Evolutionary Biology* (pp. 166–175). Elsevier. <https://doi.org/10.1016/B978-0-12-800049-6.00066-4>
- Blair, W. F. (1963). Intragroup genetic compatibility in the *Bufo americanus* species group of toads. *The Texas Journal of Science*, 13, 15–34.
- Blair, W. F. (1972). *Evolution in the genus Bufo*. University of Texas Press.
- Breden, F. (1987). The Effect of Post-Metamorphic Dispersal on the Population Genetic Structure of Fowler's Toad, *Bufo woodhousei fowleri*. *Copeia*, 1987(2), 386–395. <https://doi.org/10.2307/1445775>
- Butlin, R., Debelle, A., Kerth, C., Snook, R. R., Beukeboom, L. W., RF, C. C., Diao, W., Maan, M. E., Paolucci, S., Weissing, F. J., et al. (2011). What do we need to know about speciation? *Trends in ecology & evolution*, 27(1), 27–39.
- Crocroft, R. B., & Ryan, M. J. (1995). Patterns of advertisement call evolution in toads and chorus frogs. *Animal Behaviour*, 49(2), 283–303. <https://doi.org/10.1006/anbe.1995.0043>
- Colliard, C., Sicilia, A., Turrisi, G. F., Arculeo, M., Perrin, N., & Stöck, M. (2010). Strong reproductive barriers in a narrow hybrid zone of West-Mediterranean green toads (*Bufo viridissubgroup*) with Plio-Pleistocene divergence. *BMC Evolutionary Biology*, 10(1), 232. <https://doi.org/10.1186/1471-2148-10-232>
- Danecek, P., Auton, A., Abecasis, G., Albers, C. A., Banks, E., DePristo, M. A., Handsaker, R. E., Lunter, G., Marth, G. T., Sherry, S. T., McVean, G., Durbin, R., & 1000 Genomes Project Analysis Group. (2011). The variant call format and VCFtools. *Bioinformatics*, 27(15), 2156–2158. <https://doi.org/10.1093/bioinformatics/btr330>

- Đorđević, S., & Simović, A. (2014). STRANGE AFFECTION: MALE BUFO BUFO (ANURA: BUFONIDAE) PASSIONATELY EMBRACING A BULGE OF MUD. *Ecologica Montenegrina*, 1(1), 15–17. <https://doi.org/10.37828/em.2014.1.4>
- Evanno, G., Regnaut, S., & Goudet, J. (2005). Detecting the number of clusters of individuals using the software structure: A simulation study. *Molecular Ecology*, 14(8), 2611–2620. <https://doi.org/10.1111/j.1365-294X.2005.02553.x>
- Forester, D. C., Snodgrass, J. W., Marsalek, K., & Lanham, Z. (2006). Post-Breeding Dispersal and Summer Home Range of Female American Toads (*Bufo americanus*). *Northeastern Naturalist*, 13(1), 59–72. [https://doi.org/10.1656/1092-6194\(2006\)13\[59:PDASHR\]2.0.CO;2](https://doi.org/10.1656/1092-6194(2006)13[59:PDASHR]2.0.CO;2)
- Francis, R. M. (2017). POPHELPER: An R package and web app to analyse and visualize population structure. *Molecular Ecology Resources*, 17(1), 27–32. <https://doi.org/10.1111/1755-0998.12509>
- Gompert, Z., & Buerkle, C. A. (2012). Bgc: Software for Bayesian estimation of genomic clines. *Molecular Ecology Resources*, 12(6), 1168–1176. <https://doi.org/10.1111/1755-0998.12009.x>
- Gompert, Z., & Buerkle, C. A. (2011). Bayesian estimation of genomic clines: BAYESIAN GENOMIC CLINES. *Molecular Ecology*, 20(10), 2111–2127. <https://doi.org/10.1111/j.1365-294X.2011.05074.x>
- Gompert, Z., Lucas, L. K., Nice, C. C., Fordyce, J. A., Forister, M. L., & Buerkle, C. A. (2012). GENOMIC REGIONS WITH A HISTORY OF DIVERGENT SELECTION AFFECT FITNESS OF HYBRIDS BETWEEN TWO BUTTERFLY SPECIES: GENOMICS OF SPECIATION. *Evolution*, 66(7), 2167–2181. <https://doi.org/10.1111/j.1558-5646.2012.01587.x>
- Gompert, Z., Mandeville, E. G., & Buerkle, C. A. (2017). Analysis of Population Genomic Data from Hybrid Zones. *Annual Review of Ecology, Evolution, and Systematics*, 48(1), 207–229. <https://doi.org/10.1146/annurev-ecolsys-110316-022652>

- Gompert, Z., Parchman, T. L., & Buerkle, C. A. (2012). Genomics of isolation in hybrids. *Philosophical Transactions of the Royal Society B: Biological Sciences*, 367(1587), 439–450. <https://doi.org/10.1098/rstb.2011.0196>
- Green, D. M. (1983). Allozyme Variation through a Clinal Hybrid Zone between the Toads *Bufo americanus* and *B. hemiophrys* in Southeastern Manitoba. *Herpetologica*, 39(1), 28–40.
- Green, D. M. (1996). The bounds of species: Hybridization in the *Bufo americanus* group of North American toads. *Israel Journal of Zoology*, 42, 95–109.
- Harrison, R. G. (1986). Pattern and process in a narrow hybrid zone. *Heredity*, 56(3), 337–349. <https://doi.org/10.1038/hdy.1986.55>
- Hedrick, P. W. (2013). Adaptive introgression in animals: Examples and comparison to new mutation and standing variation as sources of adaptive variation. *Molecular Ecology*, 22(18), 4606–4618. <https://doi.org/10.1111/mec.12415>
- Hunter, J. D. (2007). Matplotlib: A 2D Graphics Environment. *Computing in Science & Engineering*, 9(3), 90–95. <https://doi.org/10.1109/MCSE.2007.55>
- Jahner, J. P., Parchman, T. L., & Matocq, M. D. (2021). Multigenerational backcrossing and introgression between two woodrat species at an abrupt ecological transition. *Molecular Ecology*, 30(17), 4245–4258. <https://doi.org/10.1111/mec.16056>
- Jombart, T. (2008). Adegenet : A R package for the multivariate analysis of genetic markers. *Bioinformatics*, 24(11), 1403–1405. <https://doi.org/10.1093/bioinformatics/btn129>
- Larson, E. L., Andrés, J. A., Bogdanowicz, S. M., & Harrison, R. G. (2013). DIFFERENTIAL INTROGRESSION IN A MOSAIC HYBRID ZONE REVEALS CANDIDATE BARRIER GENES. *Evolution*, 67(12), 3653–3661. <https://doi.org/10.1111/evo.12205>
- Mallet, J. (2005). Hybridization as an invasion of the genome. *Trends in Ecology & Evolution*, 20(5), 229–237. <https://doi.org/10.1016/j.tree.2005.02.010>
- Mallet, J. (2008). Hybridization, ecological races and the nature of species: Empirical evidence for the ease of speciation. *Philosophical Transactions of the Royal Society*

B: Biological Sciences, 363(1506), 2971–2986. [https://doi.org/10.1098/rstb.2008.](https://doi.org/10.1098/rstb.2008.0081)

0081

Malone, J. H., & Fontenot, B. E. (2008). Patterns of Reproductive Isolation in Toads (R. DeSalle, Ed.). *PLoS ONE*, 3(12), e3900. <https://doi.org/10.1371/journal.pone.0003900>

Miller, C. J. J., & Matute, D. R. (2016). The Effect of Temperature on Drosophila Hybrid Fitness. *G3: Genes/Genomes/Genetics*, 7(2), 377–385. <https://doi.org/10.1534/g3.116.034926>

Moran, B. M., Payne, C., Langdon, Q., Powell, D. L., Brandvain, Y., & Schumer, M. (2021). The genomic consequences of hybridization (P. J. Wittkopp, Ed.). *eLife*, 10, e69016. <https://doi.org/10.7554/eLife.69016>

Mount, R. H. (1975). *The Reptiles and Amphibians of Alabama*. The University of Alabama Press.

Nikolakis, Z. L., Schield, D. R., Westfall, A. K., Perry, B. W., Ivey, K. N., Orton, R. W., Hales, N. R., Adams, R. H., Meik, J. M., Parker, J. M., Smith, C. F., Gompert, Z., Mackessy, S. P., & Castoe, T. A. (2022). Evidence that genomic incompatibilities and other multilocus processes impact hybrid fitness in a rattlesnake hybrid zone. *Evolution*, 76(11), 2513–2530. <https://doi.org/10.1111/evo.14612>

Nosil, P., Funk, D. J., & Ortiz-Barrientos, D. (2009). Divergent selection and heterogeneous genomic divergence. *Molecular Ecology*, 18(3), 375–402. <https://doi.org/10.1111/j.1365-294X.2008.03946.x>

Nosil, P., & Schlüter, D. (2011). The genes underlying the process of speciation. *Trends in Ecology & Evolution*, 26(4), 160–167. <https://doi.org/10.1016/j.tree.2011.01.001>

Parchman, T. L., Gompert, Z., Braun, M. J., Brumfield, R. T., McDonald, D. B., Uy, J. a. C., Zhang, G., Jarvis, E. D., Schlinger, B. A., & Buerkle, C. A. (2013). The genomic consequences of adaptive divergence and reproductive isolation between species of manakins. *Molecular Ecology*, 22(12), 3304–3317. <https://doi.org/10.1111/mec.12201>

- Powell, R., Conant, R., & Collins, J. T. (2016). *A Field Guide to Reptiles & Amphibians: Eastern and Central North America* (4th ed.). Houghton Mifflin Harcourt.
- Pritchard, J. K., Stephens, M., & Donnelly, P. (2000). Inference of Population Structure Using Multilocus Genotype Data. *Genetics*, 155(2), 945–959. <https://doi.org/10.1093/genetics/155.2.945>
- Rieseberg, L. H., Whitton, J., & Gardner, K. (1999). Hybrid zones and the genetic architecture of a barrier to gene flow between two sunflower species. *Genetics*, 152(2), 713–727.
- Rochette, N. C., Rivera-Colón, A. G., & Catchen, J. M. (2019). Stacks 2: Analytical methods for paired-end sequencing improve RADseq-based population genomics. *Molecular Ecology*, 28(21), 4737–4754. <https://doi.org/10.1111/mec.15253>
- Servedio, M. R., & Noor, M. A. (2003). The Role of Reinforcement in Speciation: Theory and Data. *Annual Review of Ecology, Evolution, and Systematics*, 34(1), 339–364. <https://doi.org/10.1146/annurev.ecolsys.34.011802.132412>
- Shankman, D., & Hart, J. L. (2007). The Fall Line: A Physiographic-Forest Vegetation Boundary. *Geographical Review*, 97(4), 502–519. <https://doi.org/10.1111/j.1931-0846.2007.tb00409.x>
- Slager, D. L., Epperly, K. L., Ha, R. R., Rohwer, S., Wood, C., Van Hemert, C., & Klicka, J. (2020). Cryptic and extensive hybridization between ancient lineages of American crows. *Molecular Ecology*, 29(5), 956–969. <https://doi.org/10.1111/mec.15377>
- Taylor, E. B., Boughman, J. W., Groenenboom, M., Sniatynski, M., Schluter, D., & Gow, J. L. (2006). Speciation in reverse: Morphological and genetic evidence of the collapse of a three-spined stickleback (*Gasterosteus aculeatus*) species pair. *Molecular Ecology*, 15(2), 343–355. <https://doi.org/10.1111/j.1365-294X.2005.02794.x>
- Turelli, M., & Moyle, L. C. (2007). Asymmetric Postmating Isolation: Darwin's Corollary to Haldane's Rule. *Genetics*, 176(2), 1059–1088. <https://doi.org/10.1534/genetics.106.065979>

- Urban, M. C., Phillips, B. L., Skelly, D. K., & Shine, R. (2008). A Toad More Traveled: The Heterogeneous Invasion Dynamics of Cane Toads in Australia. *The American Naturalist*, 171(3), E134–E148. <https://doi.org/10.1086/527494>
- Van Riemsdijk, I., Arntzen, J. W., Bucciarelli, G. M., McCartney-Melstad, E., Rafajlović, M., Scott, P. A., Toffelmier, E., Shaffer, H. B., & Wielstra, B. (2023). Two transects reveal remarkable variation in gene flow on opposite ends of a European toad hybrid zone. *Heredity*. <https://doi.org/10.1038/s41437-023-00617-6>
- Virtanen, P., Gommers, R., Oliphant, T. E., Haberland, M., Reddy, T., Cournapeau, D., Burovski, E., Peterson, P., Weckesser, W., Bright, J., van der Walt, S. J., Brett, M., Wilson, J., Millman, K. J., Mayorov, N., Nelson, A. R. J., Jones, E., Kern, R., Larson, E., ... SciPy 1.0 Contributors. (2020). SciPy 1.0: Fundamental algorithms for scientific computing in python. *Nature Methods*, 17, 261–272. <https://doi.org/10.1038/s41592-019-0686-2>
- Weatherby, C. A. (1982). INTROGRESSION BETWEEN THE AMERICAN TOAD, BUFO AMERICANUS, AND THE SOUTHERN TOAD, B. TERRESTRIS, IN ALABAMA.
- Weir, B. S., & Cockerham, C. C. (1984). Estimating F-Statistics for the Analysis of Population Structure. *Evolution*, 38(6), 1358–1370. <https://doi.org/10.2307/2408641>
- Wolf, J. B. W., & Ellegren, H. (2017). Making sense of genomic islands of differentiation in light of speciation. *Nature Reviews Genetics*, 18(2), 87–100. <https://doi.org/10.1038/nrg.2016.133>
- Wu, C.-I. (2001). The genic view of the process of speciation. *Journal of Evolutionary Biology*, 14(6), 851–865. <https://doi.org/10.1046/j.1420-9101.2001.00335.x>
- Yang, W., Feiner, N., Laakkonen, H., Sacchi, R., Zuffi, M. A. L., Scali, S., While, G. M., & Uller, T. (2020). Spatial variation in gene flow across a hybrid zone reveals causes of reproductive isolation and asymmetric introgression in wall lizards*. *Evolution*, 74(7), 1289–1300. <https://doi.org/10.1111/evo.14001>

2.5 Figures

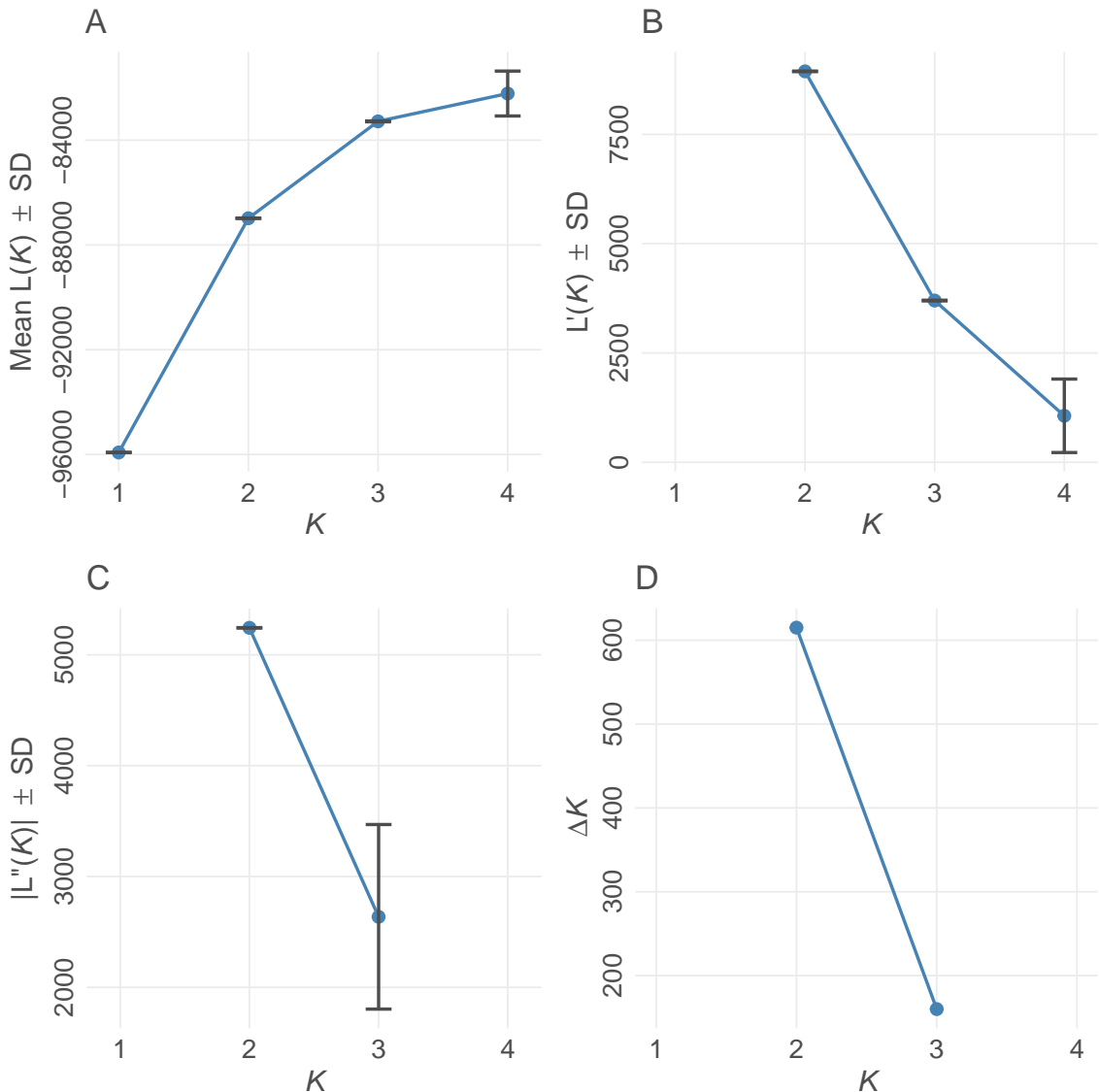


Figure 2.1. Evanno method for optimal value for K in *STRUCTURE* (Evanno et al., 2005). K refers to the number of populations for each of the different *STRUCTURE* models examined. (A) Mean estimated \ln probability of data over 10 iterations for each value of $K \pm SD$. (B) Rate of change of the likelihood distribution (mean $\pm SD$) (C) Absolute values of the second order rate of change of the likelihood distribution (mean $\pm SD$) (D) ΔK . The modal value of this distribution is considered the true value of K for the data. Plot created using *POPHELP* (Francis, 2017).

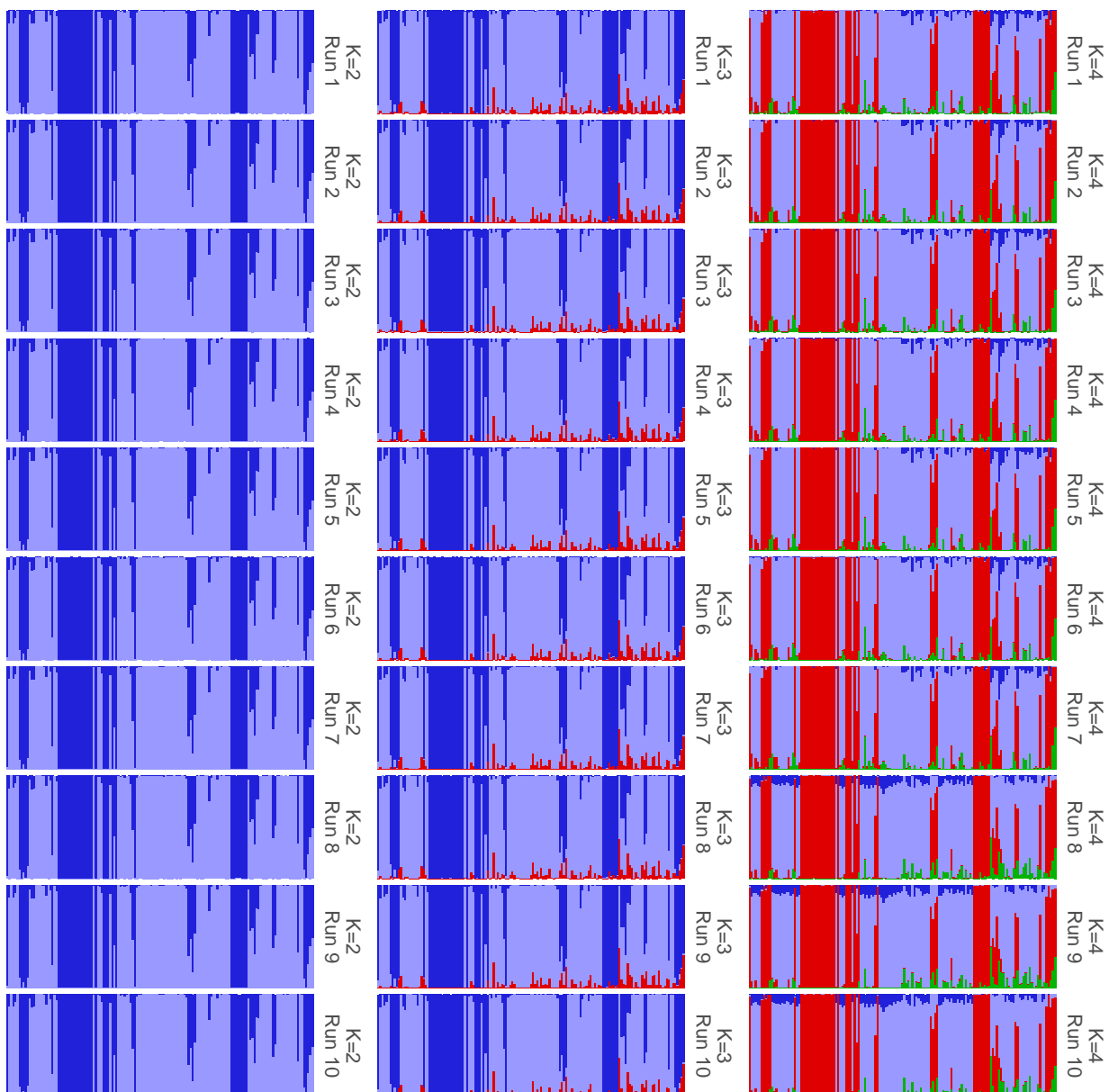


Figure 2.2. Results of each independent *STRUCTURE* run (rows) for each value of K (columns) showing convergence among runs with the same value for K . Plot was created with *POPHELPER* (Francis, 2017).

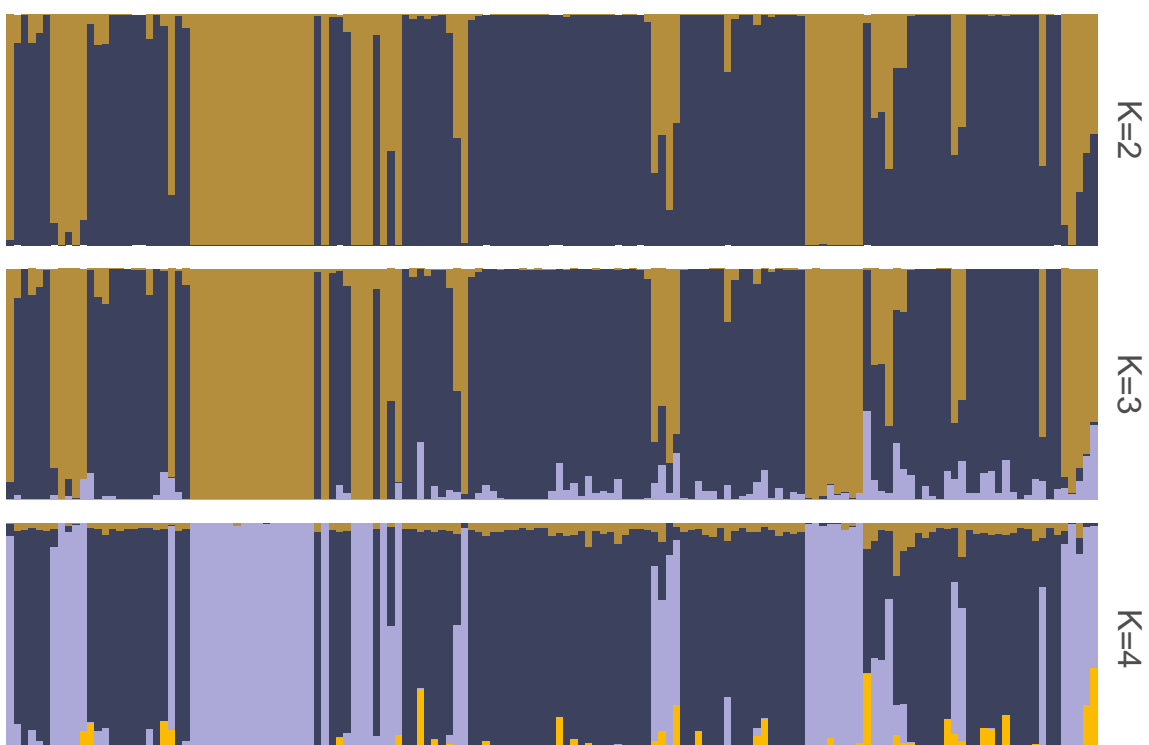


Figure 2.3. Summarized *STRUCTURE* results for each value of K. Ancestry proportions shown are the mean of ancestry proportions across all iterations. Summarization and plotting done using *POPHELP* (Francis, 2017).

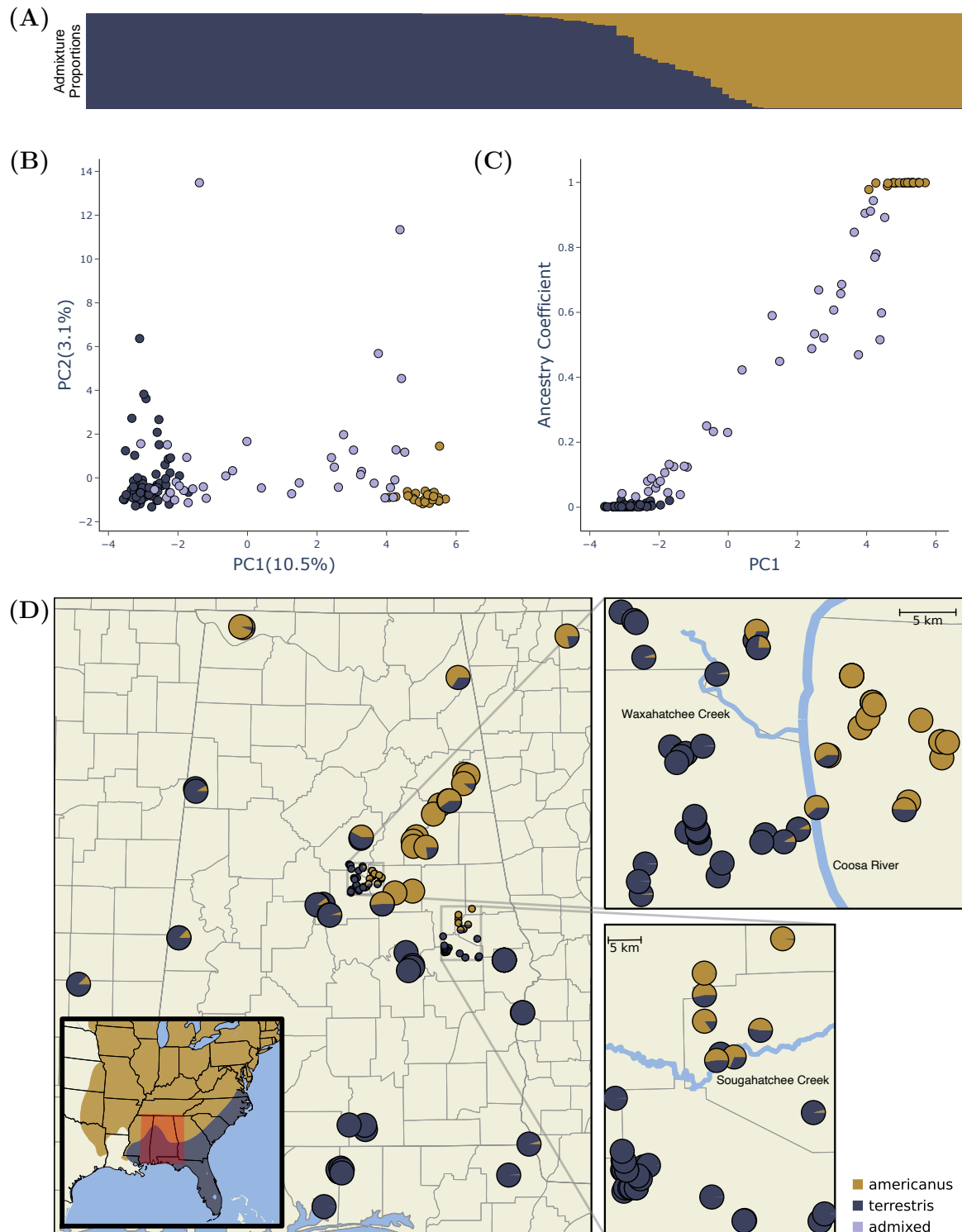


Figure 2.4. Genetic evidence of hybridization between *A. americanus* and *A. terrestris*. (A) Bar plot with the ancestry coefficients estimated with *STRUCTURE*. (B) Summary of population genetic structure based on the principal component axes one (PC1) and two (PC2). These axes explain 10.5% (PC1) and 3.1% (PC2) of the genetic variation among individuals. (C) Relationship between the first principal component axis and the admixture proportions estimated with *STRUCTURE*. (D) Sample map showing the sampling location and estimated ancestry coefficients of each sample. The inset map shows the approximate ranges of each species and the study area highlighted in red. Figure created using *POPHelper* (Francis, 2017) and *Matplotlib* (Hunter, 2007)

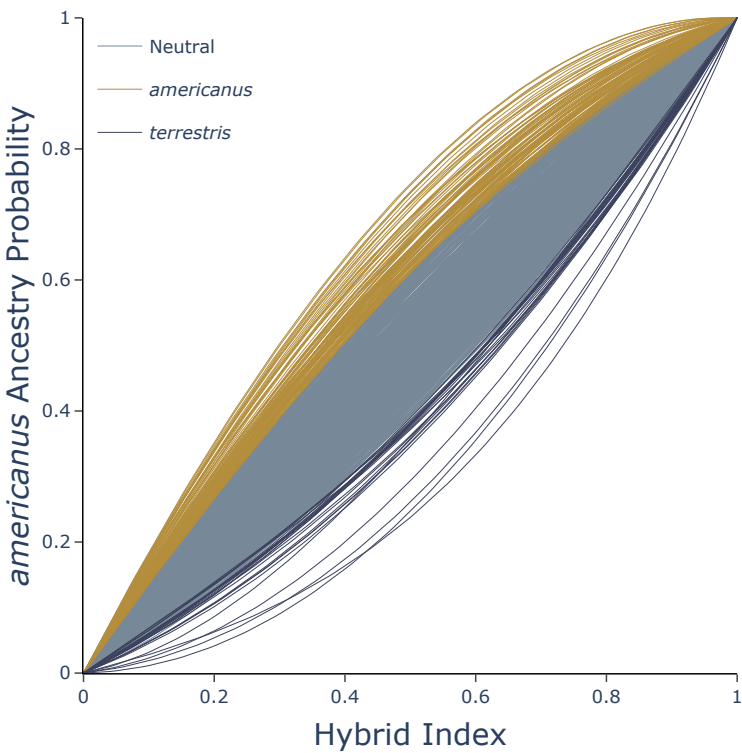


Figure 2.5. Shape of genomic clines estimated for each locus with *BGC*. Outliers are highlighted with yellow for loci that have greater *A. americanus* ancestry than expected and blue if loci have greater *A. terrestris* ancestry than expected.

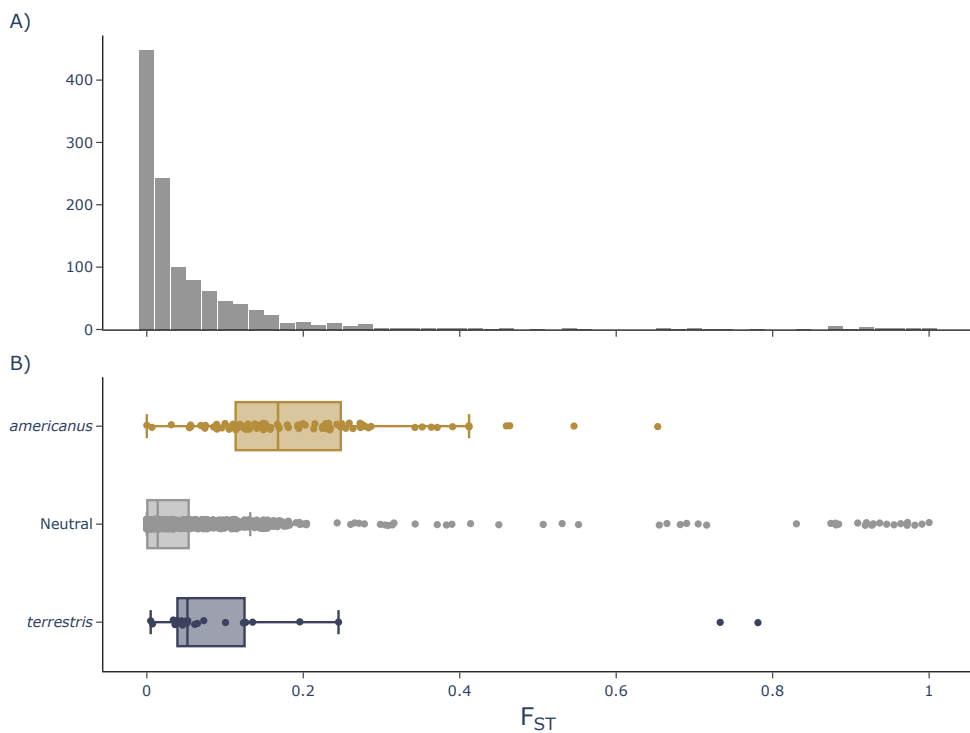


Figure 2.6. A) Distribution of per site F_{ST} estimates. B) Box plots showing the distribution and mean of F_{ST} for three categories of α estimates, outliers with greater than expected *A. americanus* ancestry (gold), outliers with greater than expected *A. terrestris* ancestry (violet), and non-outliers (gray).

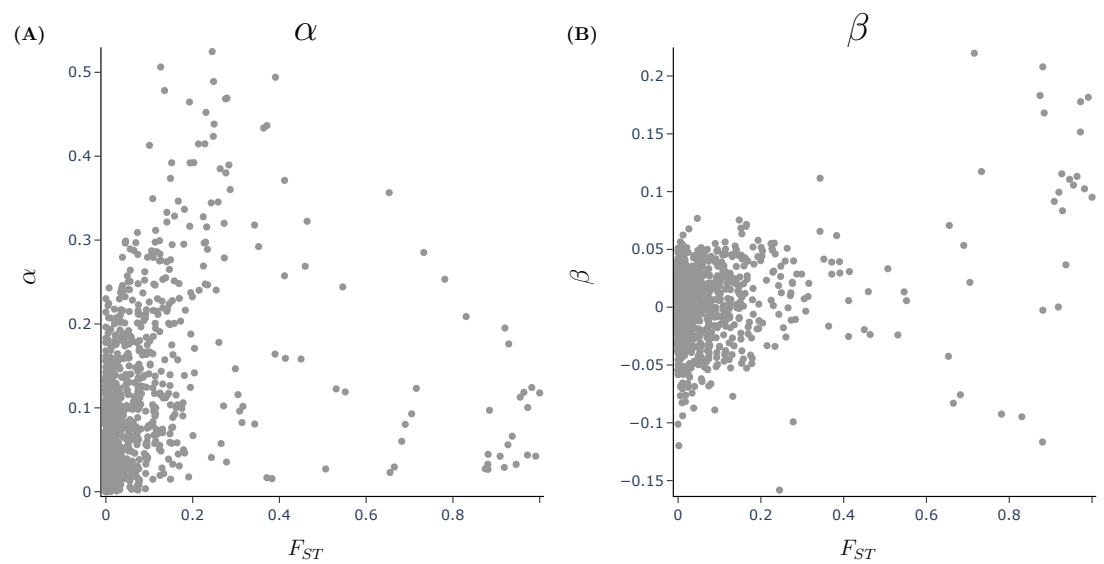


Figure 2.7. Relationship between genetic divergence measured with Weir and Cockerham, 1984 F_{ST} and BGC cline parameters A) α and B) β .

2.6 Tables

Table 2.1. Samples collected for this study

Sample ID	Species	Latitude	Longitude	Passed Filtering
KAC 016	<i>terrestris</i>	30.54819	-86.93067	X
KAC 038	<i>terrestris</i>	32.81470	-86.93968	X
KAC 039	<i>terrestris</i>	32.81094	-86.98967	X
KAC 040	<i>terrestris</i>	32.80985	-86.99795	X
KAC 042	<i>terrestris</i>	32.82406	-86.99314	
KAC 043	<i>terrestris</i>	32.82406	-86.99314	
KAC 044	<i>terrestris</i>	32.80450	-87.03078	
KAC 045	<i>terrestris</i>	32.76703	-87.07073	
KAC 046	<i>terrestris</i>	32.76592	-87.07184	
KAC 047	<i>terrestris</i>	32.78932	-86.90850	
KAC 048	<i>terrestris</i>	32.73575	-86.88149	X
KAC 049	<i>terrestris</i>	32.73291	-86.87707	X
KAC 050	<i>terrestris</i>	32.74822	-86.79806	
KAC 051	<i>terrestris</i>	32.78742	-86.75847	
KAC 052	<i>terrestris</i>	32.78044	-86.73877	
KAC 070	<i>americanus</i>	34.79963	-84.57678	X
KAC 071	<i>terrestris</i>	32.43478	-85.64630	
KAC 074	<i>terrestris</i>	30.77430	-85.22690	X
KAC 075	<i>terrestris</i>	32.94778	-86.63224	X
KAC 076	<i>terrestris</i>	32.94970	-86.52687	
KAC 077	<i>terrestris</i>	32.94970	-86.52687	
KAC 078	<i>americanus</i>	33.00267	-86.38960	X
KAC 079	<i>americanus</i>	33.01205	-86.47872	
KAC 080	<i>americanus</i>	33.04456	-86.45547	

Continued on next page

Table 2.1 – continued from previous page

Sample ID	Species	Latitude	Longitude	Passed Filtering
KAC 081	<i>americanus</i>	33.04456	-86.45547	X
KAC 082	<i>americanus</i>	33.04456	-86.45547	X
KAC 083	<i>americanus</i>	33.04456	-86.45547	X
KAC 084	<i>americanus</i>	33.04456	-86.45547	X
KAC 085	<i>americanus</i>	33.04456	-86.45547	
KAC 086	<i>americanus</i>	33.04456	-86.45547	X
KAC 087	<i>americanus</i>	33.01484	-86.39040	X
KAC 089	<i>americanus</i>	33.01484	-86.39040	X
KAC 090	<i>americanus</i>	33.06472	-86.47496	X
KAC 091	<i>americanus</i>	33.06472	-86.47496	X
KAC 092	<i>americanus</i>	33.06472	-86.47496	
KAC 093	<i>americanus</i>	33.06472	-86.47496	X
KAC 094	<i>americanus</i>	33.06472	-86.47496	X
KAC 095	<i>americanus</i>	33.06472	-86.47496	X
KAC 096	<i>americanus</i>	33.06472	-86.47496	X
KAC 097	<i>americanus</i>	33.06472	-86.47496	X
KAC 098	<i>americanus</i>	33.02572	-86.46711	X
KAC 099	<i>americanus</i>	33.02572	-86.46711	X
KAC 100	<i>terrestris</i>	32.92374	-86.67199	X
KAC 101	<i>americanus</i>	33.03283	-86.45975	X
KAC 102	<i>terrestris</i>	32.94544	-86.55777	X
KAC 103	<i>terrestris</i>	32.94947	-86.52630	X
KAC 104	<i>terrestris</i>	32.94947	-86.52630	X
KAC 105	<i>americanus</i>	33.04278	-86.45377	X
KAC 106	<i>americanus</i>	33.00464	-86.49692	X
KAC 107	<i>americanus</i>	33.01416	-86.38417	X

Continued on next page

Table 2.1 – continued from previous page

Sample ID	Species	Latitude	Longitude	Passed Filtering
KAC 108	<i>terrestris</i>	32.94013	-86.54004	X
KAC 109	<i>terrestris</i>	32.94173	-86.55787	
KAC 110	<i>americanus</i>	33.03099	-86.40941	X
KAC 111	<i>americanus</i>	33.00518	-86.49895	X
KAC 112	<i>terrestris</i>	32.95011	-86.53723	
KAC 113	<i>americanus</i>	33.00528	-86.38897	
KAC 114	<i>americanus</i>	33.01617	-86.40318	
KAC 115	<i>americanus</i>	32.98218	-86.40488	
KAC 116	<i>americanus</i>	32.96964	-86.42137	X
KAC 117	<i>terrestris</i>	32.97146	-86.52901	
KAC 121	<i>terrestris</i>	32.44120	-85.65386	X
KAC 122	<i>terrestris</i>	32.85411	-86.76619	
KAC 123	<i>terrestris</i>	32.90084	-86.67587	X
KAC 124	<i>terrestris</i>	32.91060	-86.67850	X
KAC 125	<i>terrestris</i>	32.91715	-86.68208	
KAC 126	<i>terrestris</i>	32.92717	-86.67407	
KAC 127	<i>terrestris</i>	32.97159	-86.62516	
KAC 128	<i>terrestris</i>	33.00585	-86.63703	
KAC 129	<i>terrestris</i>	33.00797	-86.64210	
KAC 130	<i>terrestris</i>	33.00818	-86.64333	
KAC 131	<i>terrestris</i>	33.01508	-86.64937	
KAC 132	<i>terrestris</i>	33.02034	-86.66651	
KAC 133	<i>terrestris</i>	33.01163	-86.64759	X
KAC 134	<i>terrestris</i>	33.00537	-86.63652	X
KAC 135	<i>terrestris</i>	33.00644	-86.63368	X
KAC 136	<i>terrestris</i>	33.00673	-86.63316	X

Continued on next page

Table 2.1 – continued from previous page

Sample ID	Species	Latitude	Longitude	Passed Filtering
KAC 138	<i>americanus</i>	32.70224	-85.66196	X
KAC 139	<i>americanus</i>	32.73042	-85.66173	X
KAC 140	<i>terrestris</i>	32.62553	-85.63684	X
KAC 141	<i>terrestris</i>	32.41032	-85.60107	X
KAC 142	<i>terrestris</i>	32.57011	-85.80888	X
KAC 143	<i>terrestris</i>	32.47773	-85.79824	X
KAC 144	<i>terrestris</i>	32.47707	-85.79577	X
KAC 145	<i>terrestris</i>	32.48128	-85.76354	X
KAC 146	<i>terrestris</i>	32.48291	-85.75622	X
KAC 147	<i>terrestris</i>	32.45001	-85.79652	X
KAC 148	<i>terrestris</i>	32.45420	-85.79408	X
KAC 149	<i>terrestris</i>	32.45449	-85.78664	X
KAC 150	<i>terrestris</i>	32.45449	-85.78664	X
KAC 151	<i>terrestris</i>	32.45451	-85.78416	X
KAC 152	<i>terrestris</i>	32.45423	-85.77634	X
KAC 153	<i>terrestris</i>	32.45423	-85.77634	X
KAC 154	<i>terrestris</i>	32.46574	-85.76977	X
KAC 155	<i>terrestris</i>	32.46961	-85.77369	X
KAC 156	<i>terrestris</i>	32.47709	-85.79175	X
KAC 158	<i>terrestris</i>	32.47709	-85.79175	X
KAC 159	<i>terrestris</i>	32.49000	-85.79741	X
KAC 160	<i>terrestris</i>	32.40809	-85.47857	X
KAC 161	<i>terrestris</i>	32.41744	-85.47117	X
KAC 162	<i>terrestris</i>	32.35417	-86.09838	X
KAC 163	<i>terrestris</i>	32.33994	-86.09946	X
KAC 164	<i>terrestris</i>	32.31562	-86.13789	X

Continued on next page

Table 2.1 – continued from previous page

Sample ID	Species	Latitude	Longitude	Passed Filtering
KAC 167	<i>terrestris</i>	33.06620	-86.60328	X
KAC 172	<i>americanus</i>	32.62171	-85.61467	X
KAC 173	<i>americanus</i>	32.61751	-85.64335	X
KAC 176	<i>americanus</i>	32.66836	-85.66233	X
KAC 177	<i>americanus</i>	32.65571	-85.57134	X
KAC 181	<i>terrestris</i>	32.38644	-85.23561	X
KAC 182	<i>terrestris</i>	32.38579	-85.23565	X
KAC 183	<i>terrestris</i>	32.38579	-85.23565	X
KAC 184	<i>terrestris</i>	32.38579	-85.23565	X
KAC 185	<i>terrestris</i>	32.38579	-85.23565	X
KAC 187	<i>americanus</i>	32.64548	-85.55135	
KAC 188	<i>terrestris</i>	32.40976	-85.60208	X
KAC 189	<i>terrestris</i>	33.09152	-86.56686	X
KAC 190	<i>terrestris</i>	33.11298	-86.69434	X
KAC 191	<i>terrestris</i>	33.10659	-86.68228	X
KAC 192	<i>terrestris</i>	33.10509	-86.68014	X
KAC 193	<i>terrestris</i>	33.07896	-86.67286	X
KAC 194	<i>terrestris</i>	32.93933	-86.62008	X
KAC 195	<i>terrestris</i>	32.94745	-86.62146	X
KAC 196	<i>terrestris</i>	32.94829	-86.62190	X
KAC 197	<i>terrestris</i>	32.94929	-86.62241	X
KAC 198	<i>terrestris</i>	32.95077	-86.62306	
KAC 199	<i>terrestris</i>	32.95794	-86.62477	X
KAC 200	<i>terrestris</i>	32.95940	-86.62489	X
KAC 205	<i>terrestris</i>	32.54852	-85.48692	X
KAC 206	<i>americanus</i>	33.30759	-86.58201	X

Continued on next page

Table 2.1 – continued from previous page

Sample ID	Species	Latitude	Longitude	Passed Filtering
KAC 207	<i>americanus</i>	33.31685	-86.57596	X
KAC 208	<i>americanus</i>	33.09829	-86.56529	X
KAC 209	<i>terrestris</i>	33.08600	-86.56394	X
KAC 210	<i>terrestris</i>	33.08600	-86.56394	X
KAC 211	<i>terrestris</i>	33.01464	-86.60995	
KAC 212	<i>terrestris</i>	33.01208	-86.61707	X
KAC 213	<i>terrestris</i>	33.00435	-86.63710	X
KAC 214	<i>terrestris</i>	32.99991	-86.64181	X
KAC 215	<i>terrestris</i>	32.99605	-86.64526	
KAC 216	<i>terrestris</i>	33.01346	-86.60960	
KAC 217	<i>terrestris</i>	32.91470	-86.60270	X
KAC 218	<i>terrestris</i>	32.92432	-86.59895	X
KAC 219	<i>terrestris</i>	32.93987	-86.56113	X
KAC 220	<i>americanus</i>	32.96579	-86.50892	X
KAC 221	<i>americanus</i>	32.96389	-86.42549	X
KAC 223	<i>terrestris</i>	32.53362	-85.79839	
KAC 224	<i>terrestris</i>	32.48869	-85.79555	X
KAC 225	<i>terrestris</i>	32.50159	-85.79860	X
KAC 230	<i>terrestris</i>	30.80933	-86.77686	X
KAC 232	<i>terrestris</i>	30.80922	-86.78994	X
KAC 233	<i>terrestris</i>	30.80922	-86.78994	X
KAC 234	<i>terrestris</i>	30.80922	-86.78994	X
KAC 236	<i>terrestris</i>	30.82632	-86.80258	X
KAC 237	<i>terrestris</i>	30.83733	-86.77630	X
KAC 238	<i>terrestris</i>	30.82433	-86.76284	X
KAC 239	<i>terrestris</i>	30.80162	-86.76659	X

Continued on next page

Table 2.1 – continued from previous page

Sample ID	Species	Latitude	Longitude	Passed Filtering
KAC 242	<i>americanus</i>	34.50446	-85.63768	X
KAC t1020	<i>terrestris</i>	31.10783	-86.62247	
KAC t1030	<i>terrestris</i>	31.99042	-85.07423	X
KAC t1040	<i>terrestris</i>	31.99016	-85.07046	X
KAC t2004	<i>americanus</i>	33.58295	-85.73524	X
KAC t2015	<i>americanus</i>	33.58435	-85.74064	X
KAC t2018-02-17-01	<i>americanus</i>	33.55274	-85.82913	X
KAC t2018-02-17-04	<i>americanus</i>	33.48548	-85.88857	X
KAC t2018-02-17-05	<i>americanus</i>	33.31649	-86.05293	X
KAC t2018-02-17-06	<i>americanus</i>	33.28443	-86.08443	X
KAC t2018-02-17-07	<i>americanus</i>	33.24576	-86.08168	X
KAC t2018-03-10-1	<i>americanus</i>	32.91057	-86.09272	X
KAC t2018-03-10-3	<i>americanus</i>	32.95104	-86.14539	
KAC t2018-03-10-4	<i>americanus</i>	32.89787	-86.26061	X
KAC t2018-03-10-5	<i>americanus</i>	32.81642	-86.38018	X
KAC t2019-08-25-1	<i>americanus</i>	34.21852	-87.36662	
KAC t2020	<i>americanus</i>	33.23853	-85.96270	X
KAC t2040	<i>americanus</i>	33.58295	-85.73539	X
KAC t2043	<i>americanus</i>	32.81642	-86.38018	X

Table 2.2. Samples loaned from museums

Sample ID	Species	Latitude	Longitude	Passed Filtering
AHT 1975	<i>americanus</i>	32.77356	-85.53325	X
AHT 2456	<i>terrestris</i>	32.19494	-89.23629	X
AHT 2885	<i>terrestris</i>	32.45090	-86.15934	X
AHT 3419	<i>terrestris</i>	33.67290	-88.16068	X
AHT 3421	<i>terrestris</i>	33.65420	-88.15580	X
AHT 3428	<i>terrestris</i>	31.12679	-86.54755	X
AHT 3459	<i>americanus</i>	34.88028	-87.71849	X
AHT 3460	<i>americanus</i>	33.78013	-85.58421	X
AHT 3461	<i>americanus</i>	34.88779	-87.74103	X
AHT 3462	<i>americanus</i>	33.77001	-85.55434	X
AHT 3463	<i>americanus</i>	33.71125	-85.59762	X
AHT 3813	<i>terrestris</i>	31.13854	-86.53906	
AHT 3833	<i>terrestris</i>	31.00422	-85.03427	X
AHT 3997	<i>terrestris</i>	32.55607	-88.29975	X
AHT 3998	<i>terrestris</i>	32.55607	-88.29975	X
AHT 5276	<i>terrestris</i>	31.55613	-86.82514	
AHT 5277	<i>terrestris</i>	31.15830	-86.55430	X
AHT 5278	<i>terrestris</i>	31.16105	-86.69868	X
UTEP 19947	<i>terrestris</i>	31.22432	-88.77548	

Chapter 3

Phylogenomic Insights Into the Evolutionary History of *Anaxyrus* Toads (Anura: Bufonidae)

3.1 Introduction

Many factors are hypothesized to be important in driving and shaping the diversification and evolutionary history of organisms. Chief among them is the interplay between climatic conditions and geologic processes (Hua & Wiens, 2013). Changes in these environmental variables can alter the distributions of organisms or alter the distribution of variation within species and as a result, change patterns of gene flow within a species (Coyne & Orr, 2004). Spatially separated populations may undergo genetic divergence from one another due to adaptive evolution in response to changing abiotic or biotic conditions or they might simply diverge via neutral evolution driven by the effects of drift (Coyne & Orr, 2004). Local adaptation in response to the environment may lead to assortative mating among populations of a species which in time could result in complete reproductive isolation (Mallet, 2008). Another important process, which itself will often be tied to environmental changes is hybridization. Environmental changes can reestablish migration between previously isolated populations resulting in hybridization and potentially introgression between species (Abbott et al., 2013). Understanding the interplay of all of these factors is critical for understanding the evolutionary history of organisms. A critical step to understanding these processes is obtaining an accurate phylogenetic reconstruction of organisms. Knowing the relationships among species and the timing of divergence between them, we can identify past events that have caused diversification. A

reconstruction of evolutionary relationships is also important for identifying signatures of introgression so we can understand its role in the diversification process.

The North American toads in the genus *Anaxyrus* are a group of organisms with a poorly understood evolutionary history, though not for lack of trying. Multiple studies of the evolutionary relationships among species in the genus have produced conflicting results (Fontenot et al., 2011; Graybeal, 1997; Masta et al., 2002; Portik et al., 2023; Pramuk et al., 2007; Pyron & Wiens, 2011). Particularly within the *americanus* group composed of *A. americanus*, *A. baxteri*, *A. fowleri*, *A. hemiophrys*, *A. houstonensis*, *A. terrestris*, and *A. woodhousii*. Two phylogenetic studies have inferred a paraphyletic relationship among different populations of *A. fowleri* making these trees inconsistent with the current taxonomy of *Anaxyrus* (Fontenot et al., 2011; Masta et al., 2002). The conflicting results produced by these studies could be due to methodological differences such as the species included, the number of individuals of each species sequenced, inference methods used, or the sequenced loci. But the differences in inferred relationships could also result from real biological processes. Incomplete lineage sorting is one potential source of discordance that arises from real biological processes and impacts phylogenetic inference (Kubatko & Degnan, 2007). Incomplete lineage sorting could also produce the paraphyletic relationship among *A. fowleri* populations.

Gene flow is another potential source of discordance among genes which could drive the differences in inferred relationships among studies using different loci and could also produce the pattern seen in *A. fowleri* (Degnan & Rosenberg, 2009). While incomplete lineage sorting is likely to have impacted patterns of genetic variation in *Anaxyrus*, gene flow due to hybridization is possible as well. There are numerous reports of natural hybridization between several different species of *Anaxyrus* (Green, 1996). A study of allozyme variation across a hybrid zone between *A. americanus* and *A. hemiophrys* revealed introgression taking place across a more than 50km wide hybrid zone (Green, 1983). Meacham (1962) presented compelling evidence on the basis of morphological variation for the existence of a hybrid zone between *A. fowleri* and *A. woodhousii* in East Texas, although this has never been investigated with genetic data. In the previous

chapter, I presented evidence for extensive hybridization between *A. americanus* and *A. terrestris*. Furthermore, numerous laboratory crosses have been performed between pairs of *Anaxyrus* species that occur in sympatry (Blair, 1963, 1972). Some of which produce viable and fertile backcross progeny (Blair, 1963, 1972). These studies suggest that gene flow could very well have played a role in shaping patterns of diversity in *Anaxyrus*. However, these studies provide only a snapshot in time with no indication of the long-term evolutionary consequences, if any. There are many potential lasting consequences of hybridization such as adaptive introgression, introgression of neutral genetic variation, reinforcement, lineage fusion, polyploidization, hybrid speciation, or transition to unisexual reproduction (Abbott et al., 2013). Inference of past introgression is an important starting point for exploring these outcomes, yet it remains a challenging problem. Inferring the structure of phylogenetic networks that incorporate inter-lineage gene flow is much more computationally demanding than inferring simpler bifurcating phylogenetic trees (Wen et al., 2018), and requires data from loci across the species' genomes. Advances in phylogenetic methods and sequencing technologies is making it feasible to investigate past gene flow.

Apart from the significant evolutionary implications of hybridization which need to be understood, this phenomenon also presents a valuable opportunity for investigating the mechanisms that drive divergence and the evolution of reproductive incompatibility (Rieseberg et al., 1999). Many generations of backcrossing within a hybrid zone will produce a large number of hybrid genotypes, allowing scientists to study the interplay between gene flow and natural selection under natural conditions (Rieseberg et al., 1999). In most species, it is not feasible to produce a large number of highly recombinant offspring in order to make such observations. The evolutionary history of hybridizing species provides context when studying contemporary hybrid zones, such as the phylogenetic relationships of hybridizing species, the amount of genetic divergence between them, the time since divergence, and the biogeographic processes driving initial divergence. This important context is currently missing for *Anaxyrus* which limits our understanding of hybridization within the genus.

Ultimately, changes in the environment are what drive speciation and hybridization and so it is important to identify these. To date, there have not been any studies conducted to understand how the environment has driven diversification in North American toads. North America has had a very complex geologic and climatic history (Lyman & Edwards, 2022), the effects of which are often clade specific (Nuñez et al., 2023). Large-scale environmental changes can cause multiple species to diverge (Oaks, 2019; Xue & Hickerson, 2015), and recent methods have been developed to infer the patterns of shared divergence times predicted by such processes (Oaks, 2019; Oaks et al., 2022). Present day population variation could also provide further understanding by revealing patterns of structure predicted by environmental factors that reduce gene flow.

In this study, I investigate the evolutionary history of North American toads in the genus *Anaxyrus* using genome-wide sequence data. For this, I obtained restriction enzyme-associated DNA sequence (RADseq) data from 12 species of *Anaxyrus*, including sampling that encompasses a large portion of the ranges of *A. americanus*, *A. fowleri*, *A. terrestris*, and *A. woodhousii*. With these genome-wide sequence data, I infer the phylogenetic relationships and divergence times among *Anaxyrus* species and test for patterns of shared divergences predicted by large-scale environmental changes. With these data I conduct the first inference of the evolutionary relationships among these species using genome-wide sequence data. I also test for the presence of shared divergence times which might suggest *Anaxyrus* diversification has been driven by the same environmental changes and also estimate the absolute timing of all divergences within the genus. With the robust estimate of phylogenetic relationships, I test for the presence of ongoing and historic introgression among *Anaxyrus* species. In order to identify the types of environmental factors that might have played a role in isolating populations that would eventually diverge as species, I investigate population structure within a subset of *Anaxyrus* species. Finally, I estimate proportions of admixture between *A. fowleri* and *A. woodhousii* to test the hypothesis that these species form a hybrid zone in the central United States where their ranges meet.

3.2 Methods

3.2.1 Sampling and DNA Isolation

I obtained tissue samples from museum collections as well as individuals that I collected from 2017 to 2020. I selected samples to represent as much of the range of each species of *Anaxyrus* as possible. I also included one *Incilius nebulifer* as an outgroup for phylogenetic analyses. I isolated sample DNA from liver or muscle tissue by lysing a piece approximately the size of a grain of rice in a 300 μL solution of 10mM Tris-HCL, 10mM EDTA, 1% SDS (w/v), 6 mg Proteinase K, and nuclease free water incubated for 4-12 hours at 55°C. To purify the DNA, I mixed the lysis solution with a 2X volume of SPRI bead solution containing 1 mM EDTA, 10 mM Tris-HCl, 1 M NaCl, 0.275% Tween-20 (v/v), 18% PEG 8000 (w/v), 2% Sera-Mag SpeedBeads (GE Healthcare PN 65152105050250) (v/v), and nuclease free water. I then incubated the samples at room temperature for 5 minutes, placed the beads on a magnetic rack, and discarded the supernatant after beads had collected on the side of the tube. I then performed two ethanol washes with 1 mL of 70% ETOH added to the beads while still placed in the magnet stand and allowed the sample to stand for 5 minutes before discarding the ethanol. After discarding all ethanol from the second wash, I removed the tube from the magnet stand and allowed the sample to dry for 1 minute. I then mixed the beads with 100 μL of TLE solution containing 10 mM Tris-HCL, 0.1 mm EDTA, and nuclease free water. After allowing this mixture to stand at room temperature for 5 minutes, I returned the beads to the magnet stand and separated the DNA solution from the beads. I quantified DNA with a Qubit fluorometer (Life Technologies, USA) and diluted samples with TLE solution to bring all sample concentrations to 20 ng/ μL .

3.2.2 RADseq Library Preparation

I prepared RADseq libraries using the 2RAD approach outlined by Bayona-Vásquez et al. (2019). On 96 well plates, I digested 100 ng of sample DNA in 15 μL of a solution

with 1X CutSmart Buffer (New England Biolabs, USA; NEB), 10 units of XbaI, 10 units of EcoRI, 0.33 μ M XbaI compatible adapter, 0.33 μ M EcoRI compatible adapter, and nuclease free water with a 1-hour incubation at 37°C. I ligated the adapter by adding 5 μ L of a solution with 1X Ligase Buffer (NEB), 0.75 mM ATP (NEB), 100 units DNA Ligase (NEB), and nuclease free water and incubated at 22°C for 20 min and 37°C for 10 min for two cycles, followed by 80°C for 20 min to stop enzyme activity. For each 96 well plate, I pooled 10 μ L of each sample and split this pool into equal volumes. I purified each pool of libraries with a 1X volume of SPRI bead solution followed by two ethanol washes as described in the previous section except that the DNA was resuspended in 25 μ L of TLE solution.

In order to be able to detect and remove PCR duplicates, I performed a single cycle of PCR with the iTru5-8N primer which adds a random 8 nucleotide barcode to each library construct. For each plate, I prepared four PCR reactions with a total volume of 50 μ L containing 1X Kapa Hifi Buffer (Kapa Biosystems, USA; Kapa), 0.3 μ M iTru5-8N Primer, 0.3 mM dNTP, 1 unit Kapa HiFi DNA Polymerase, 10 μ L of purified ligation product, and nuclease free water. I ran reactions through a single cycle of PCR on a thermocycler at 98°C for 2 min, 60°C for 30 s, and 72°C for 5 min. I pooled all of the PCR products for a plate into a single tube and purified the libraries with a 2X volume of SpeedBead solution as described before and resuspended in 25 μ L TLE. I added the remaining adapter and index sequences unique to each plate with four PCR reactions with a total volume of 50 μ L containing 1X Kapa Hifi (Kapa), 0.3 μ M iTru7 Primer, 0.3 μ M P5 Primer, 0.3 mM dNTP, 1 unit of Kapa Hifi DNA Polymerase (Kapa), 10 μ L purified iTru5-8N PCR product, and nuclease free water. I ran reactions on a thermocycler with an initial denaturation at 98°C for 2 min, followed by 6 cycles of 98°C for 20 s, 60°C for 15 s, 72°C for 30 s and a final extension of 72°C for 5 min. I pooled all of the PCR products for a plate into a single tube and purified the product with a 2X volume of SpeedBead solution as described before and resuspended in 45 μ L TLE.

I size selected the library DNA from each plate in the range of 450-650 base pairs using a BluePippin (Sage Science, USA) with a 1.5% dye free gel with internal R2 standards.

To increase the final DNA concentrations, I prepared four PCR reactions for each plate with 1X Kapa Hifi (Kapa), 0.3 μ M P5 Primer, 0.3 μ M P7 Primer, 0.3 mM dNTP, 1 unit of Kapa HiFi DNA Polymerase (Kapa), 10 μ L size selected DNA, and nuclease free water and used the same thermocycling conditions as the previous (P5-iTru7) amplification. I pooled all of the PCR products for a plate into a single volume and purified the product with a 2X SPRI bead solution as before and resuspended in 20 μ L TLE. I quantified the DNA concentration for each plate with a Qubit fluorometer (Life Technologies, USA) then pooled each plate in equimolar amounts relative to the number of samples on the plate and diluted the pooled DNA to 5 nM with TLE solution. These pooled libraries were pooled with other projects and sequenced on an Illumina HiSeqX by Novogene (China) to obtain paired end, 150 base pair sequences.

3.2.3 Phylogenetic Data Processing

To produce alignments for phylogenetic analysis, I first demultiplexed the iTru7 indexes (identifying the 96 well plates) using the *process_radtags* command from *Stacks* v2.6.4 (Rochette et al., 2019) and allowed for two mismatches for rescuing reads. I removed PCR duplicates using the *clone_filter* command from *Stacks*. To demultiplex individual samples I used *ipyrad* v0.9.90 and allowed for one mismatch for rescuing reads. I assembled and aligned reads with *ipyrad* using default parameters and a clustering threshold of 0.8. Using *ipyrad*, I filtered loci not present in at least 75% of samples and filtered samples with fewer than 200 loci.

3.2.4 Phylogenetic Inference

Maximum Likelihood

Phylogenetic methods that do not account for incomplete lineage sorting do not perform well with data impacted by this process (Degnan & Rosenberg, 2009). However, methods that do account for incomplete lineage sorting are far more computationally demanding. As a result, these methods cannot be performed with a large number of

samples. To identify potentially problematic samples due to data quality or misidentification, I estimated a maximum likelihood phylogeny of all the toad samples using the concatenated alignments of the RADseq loci. I conducted the maximum likelihood phylogenetic inference with *IQ-TREE* v1.6.12 (Nguyen et al., 2015) with the *ipyrad* alignment as input. I ran *IQ-TREE* with 1000 ultrafast bootstrap replicates (Hoang et al., 2018) under the GTR substitution model.

Multispecies Coalescent

In order to account for incomplete lineage sorting in the inference of phylogenetic relationships and to infer shared divergence times, I used the program *phycoeval* (Oaks et al., 2022). I selected a subset of up to four samples from each species due to infeasible run times for *phycoeval* with greater numbers of samples (see Table 3.1). I excluded sample 006 from consideration due to it having an anomalous position in the maximum likelihood tree. I used *ipyrad* to filter loci not present in at least 75% of samples. Using a custom script, I filtered the phylip alignment file produced by *ipyrad* to exclude sites with more than two characters and output the filtered alignment in nexus format with a biallelic character encoding. I ran *phycoeval* with:

- State frequencies fixed at 0.5.
- The mutation rate equal to one, making divergence times equal to expected substitutions per site.
- The prior for the root age exponentially distributed with a mean of 0.01.
- A single effective population size assumed to be shared across all branches of the tree.
- The prior on the effective population size gamma distributed with a shape of four and a mean of 0.0005.
- Five independent MCMC chains run for 10,000 generations, sampled every 10 generations.

- Each independent chain started with a comb tree topology.

I summarized the posterior sample of tree topologies and parameters using the *sumphycoeval* program packaged with *phycoeval* (Oaks et al., 2022). To assess convergence and mixing, I used *sumphycoeval* to calculate the potential scale reduction factor (PSRF) and the effective sample size (ESS). I discarded the first 100 samples from each chain as burnin. I used *sumphycoeval* to rescale the branch lengths of the maximum a posteriori (MAP) tree produced by *sumphycoeval* so that the posterior mean root age was 16.5 million years ago based on the estimate of Feng et al. (2017).

3.2.5 Introgression

In order to test for introgression between species of *Anaxyrus*, I used the program *dsuite* v0.5r50 (Malinsky et al., 2021) to compute the *f*-branch statistic for each pair of *Anaxyrus* species for which the statistic can be calculated (Malinsky et al., 2018; Reich et al., 2009). I used *ipyrad* to filter all loci that were not found in at least 50% of the samples that passed filtering and excluded sample 006 due to it's anomalous position in the maximum likelihood phylogeny. For the input tree topology required to run *dsuite*, I used the topology inferred by *phycoeval* and I specified *Incilius nebulifer* as the outgroup species. I ran the *dsuite* Dtrios command to compute Patterson's *f4*-ratio statistic for all possible trios with 20 block-jackknife replicates. I then ran the Fbranch command from *dsuite* to compute the *f*-branch statistics from the computed *f4*-ratio statistics. I plotted the *f*-branch statistics with *dtools* v0.1 which is packaged with the *dsuite* program (Malinsky et al., 2021).

3.2.6 Population Structure

For the investigation of population structure within *A. americanus*, *A. fowleri*, *A. terrestris*, and *A. woodhousii* as well as for the investigation of hybridization between *A. fowleri* and *A. woodhousii*, I processed reads and generated alignments using the *Stacks* pipeline. Starting from the decloning step of the data processing for the phylogenetic analyses, I demultiplexed individual samples using the *process_radtags* program

in *Stacks*. I also trimmed adapter sequence and filtered reads with low quality scores as well as reads with any uncalled bases with *process_radtags* and allowed for the rescue of restriction site sequence as well as barcodes with up to two mismatches. I allowed for 14 mismatches between alleles within, as well as between individuals (M and n parameters). This is equivalent to a sequence similarity threshold of 90% for the 140 bp length of reads post trimming. I also allowed for up to 7 gaps between alleles within and between individuals. I used the *populations* command from *Stacks* to filter loci missing in more than 5% of individuals, filter all sites with minor allele counts less than 3, filter any individuals with more than 90% missing loci, and randomly sample a single SNP from each locus to obtain independent un-linked SNPs.

I ran the program *STRUCTURE* v2.3.4 (Pritchard et al., 2000) with its admixture model for each species separately and with *A. fowleri* and *A. woodhousii* samples combined in order to cluster individuals and estimate their ancestry proportions. For the *STRUCTURE* analyses of individuals from a single species, I ran *STRUCTURE* under five different models, each assuming a different number of populations (K parameter) ranging from one to five. For the *STRUCTURE* analysis of the combined *A. fowleri* and *A. woodhousii* samples, I ran *STRUCTURE* under four different models with K ranging from one to four. For each analysis, I ran 10 independent runs of *STRUCTURE* for each value of K for a total of 100,000 steps and burnin of 50,000 for each run. I used the R package *POPHelper* v2.3.1 (Francis, 2017) to combine runs for each value of K and to select the model resulting in the largest ΔK , which is the the model that has the greatest increase in likelihood score from the previous model which assumed one less population as described by (Evanno et al., 2005). I also investigated population structure with a non-parametric approach, using principle component analysis (PCA) implemented in the R package *adegenet* v2.1.10 (Jombart, 2008).

3.3 Results

3.3.1 Assembly and alignment with *ipyrad*

A total of 436,265,266 reads were obtained for all samples. After filtering low quality reads and reads without restriction site sequence, 435,650,926 total reads remained for assembly. The number of filtered reads per individual was highly variable with a mean of 4,538,030 ($sd=3,619,076$). Prior to filtering there were 171,174 loci total loci which was reduced to 659 after filtering loci not present in at least 75% of samples and filtering samples which had fewer than 200 loci (see Table 3.1). Mean sequence read coverage of the loci passing filter was 54x. The final alignment contained a total of 184,453 sites and 20,361 SNPs with 14.96% of sites and 14.71% of SNPs missing.

3.3.2 Maximum Likelihood Phylogeny

The full majority rule consensus tree inferred by *IQ-TREE* is presented in Figs. 3.2 and 3.3. All species were inferred as a single monophyletic group with the exception of *A. fowleri*. A single *A. fowleri* sample (sample 006) does not form a monophyletic group with other *A. fowleri* samples but is instead sister to the branch containing *A. woodhousii* and *A. fowleri* samples (Figs. 3.2 and 3.3). A representation of the tree inferred by *IQ-TREE* with the tips within species-specific clades collapsed is presented in (Fig. 3.4). The base of each species-specific clade for which there are at least two representatives samples all have ultrafast bootstrap support values of 100% (Fig. 3.4). All branches basal to the species-specific clades have ultrafast bootstrap support values ranging from 70-100% with the majority being 100% (Fig. 3.4). The most basal internal branch of the tree, marking the split between most of *Anaxyrus* and *A. punctatus* along with the outgroup *Incilius nebulifer* has an ultrafast bootstrap support value of 99% (Fig. 3.4). The sister branch to *A. terrestris*, which contains the spurious *A. fowleri* sample (sample 006) and the clade containing *A. fowleri* and *A. woodhousii*, has an ultrafast bootstrap support value of 96% (Fig. 3.4). The lowest ultrafast bootstrap support value is found on the branch

sister to the *A. cognatus*/*A. speciosus* clade with a value of only 70% (Fig. 3.4).

3.3.3 Coalescent Phylogeny

The maximum a posteriori (MAP) tree inferred under the multispecies coalescent model using *phycoeval* has a topology that differs from the maximum likelihood topology inferred by *IQ-TREE* (Fig. 3.5). One major difference is that the *phycoeval* MAP tree has a multifurcation at the ancestral branch of the *A. quercicus*, *A. speciosus*/*A. cognatus*, and *A. americanus* group lineages (Fig. 3.5). However, this branch has a low posterior probability of 0.51 (Fig. 3.5). There are also differences in the relationships inferred within the *A. americanus* group, with *A. americanus* and *A. terrestris* inferred as sister to one another, and this pair inferred as sister to a clade containing *A. woodhousii* and *A. terrestris* (Fig. 3.5). The *A. hemiophrys* and *A. baxteri* clades are sister to the clade containing the aforementioned species (Fig. 3.5). With the exception of the single multifurcation, all branches in the MAP tree have posterior probabilities of 0.98 or more (Fig. 3.5) The number of divergence times with the highest approximate posterior probability (0.5) was 9 and thus the MAP tree does not have any shared divergence times among the 9 non-root nodes (Fig. 3.5). The 95% credible interval on the number of divergence times spanned 8-10 divergences. Most divergence events within *Anaxyrus* have occurred in the past 3.5 million years and all diversification within the *A. americanus* group is less than 2.5 million years old (Fig. 3.5).

3.3.4 Introgression

I used the program *dsuite* to compute the *f*-branch statistic which is an estimate of excess allele sharing between species pairs that is not due to incomplete lineage sorting. I used the species tree topology produced by *phycoeval* for estimating the *f*-branch statistics. The *f*-branch estimates for each species pair are presented with a heat map in Fig. 3.6. Most *f*-branch estimates produced by *dsuite* were zero or very near zero. Only 24 out of 112 *f*-branch estimates were greater than 0 and just 11 of those were greater than 0.05 (Fig. 3.6). *A. americanus* and *A. woodhousii* were associated with

the largest number of estimates greater than zero with nearly every pairwise comparison greater than 0 (Fig. 3.6). The highest *f*-branch statistic values are between *A. americanus* and two other species: *A. hemiophrys* (0.24) and *A. baxteri* (0.22) (Fig. 3.6). The values associated with *A. woodhousii* are appreciably lower with none exceeding 0.1 (Fig. 3.6). The highest being between *A. americanus* and *A. woodhousii* with a value of 0.098 (Fig. 3.6). The *A. woodhousii* *f*-branch values for *A. baxteri* and *A. hemiophrys* are 0.082 and 0.086, respectively (Fig. 3.6). The *f*-branch value between *A. woodhousii* and *A. microscaphus* is 0.05. Finally, the smallest *A. woodhousii* *f*-branch values are 0.023 and 0.029 for comparisons with *A. cognatus* and *A. speciosus*, respectively.

3.3.5 Population Structure

For the *STRUCTURE* analysis of each species and the analysis of the *A. fowleri* and *A. woodhousii* samples combined, a visual inspection of the 10 independent *STRUCTURE* runs performed for each value of K shows that each independent run converged on a nearly identical result for all runs for a given K value (Figs. 3.18–3.21). For the *A. americanus*, *A. fowleri*, *A. woodhousii*, and *A. fowleri + A. woodhousii* analyses, the *STRUCTURE* model with the highest ΔK was the model with a K of two. (Figs. 3.13, 3.14, 3.16 and 3.17). For the *A. terrestris* analysis, the *STRUCTURE* model with the highest ΔK was the model with a K of three (Fig. 3.15).

The *STRUCTURE* analysis with a K of two for *A. americanus* produced a western and eastern cluster of individuals with four admixed samples in the center of the species range (Fig. 3.7). There was a large increase in likelihood between the model with a K of two and the model with a K of three, although it was not large enough to be identified as the best model using the method described by Evanno et al. (2005). Therefore, I also present the *STRUCTURE* results for the model with a K of three (Fig. 3.8). The analysis performed with a K of three shows the same East/West division but also shows a gradient from North to South in the eastern half of the *A. americanus* range (Fig. 3.8). The PCA for *A. americanus* also shows three non-discrete groupings of individuals *A. americanus* samples, which more closely matches the *STRUCTURE* analysis with a K of three.

The ancestry coefficients inferred in the *STRUCTURE* analysis for *A. terrestris* fall into three categories. Individuals in the first category, which includes all but four individuals, have admixture proportions attributed to two different source populations (Population 1 and Population 2) with the majority of ancestry attributed to Population 1 (Fig. 3.9). The second category of individuals, which includes the two easternmost samples, have ancestry proportions attributed to Population 1 and a third population (Population 3) (Fig. 3.9). The third category, which includes the next easternmost sample (Sample 200), has ancestry proportions attributed to all three. These samples resemble the first category except that they have a small amount of ancestry attributable to population 3. The PCA result for *A. terrestris* is fairly consistent with the *STRUCTURE* results with most individuals clustering tightly together and three samples forming another cluster (Fig. 3.9).

The results of the *STRUCTURE* and PCA analyses with just *A. fowleri* and just *A. woodhousii* do not show any obvious population structure or spatial patterns in the distribution of genetic diversity (Figs. 3.10 and 3.11). Two *A. woodhousii* samples have ancestry coefficients of 1.0 for a separate population than the remaining samples (Fig. 3.10). However, when analyzing the *A. fowleri* and *A. woodhousii* samples together, these two samples have a high proportion of *A. fowleri* ancestry and are located in the center of the two ranges (Fig. 3.12). Several other samples in the combined *A. fowleri* and *A. woodhousii* analysis have mixed ancestry with a small proportion of *A. woodhousii* ancestry and these too are located in the center of the two ranges (Fig. 3.12). The PCA results are again consistent with the *STRUCTURE* results. The PCA plot has two tight clusters of samples corresponding to the respective species. Two samples are located right in the center of these two clusters along the first principal component axis which captures 42% of variation in the data (Fig. 3.12). Four other samples gravitate towards the center of the first principal component axis but cluster near the *A. fowleri* cluster of samples.

3.4 Discussion

3.4.1 Phylogenetic relationships

The maximum likelihood tree inferred by *IQ-TREE* (Figs. 3.2 and 3.4) differs from trees inferred in previous studies of the relationships among *Anaxyrus* (Fontenot et al., 2011; Graybeal, 1997; Masta et al., 2002; Portik et al., 2023; Pramuk et al., 2007; Pyron & Wiens, 2011). Even among these previous studies there has been a great deal of inconsistency in the inferred relationships except in the position of a few taxa. As in all previous studies, the maximum likelihood tree inferred in this study places *A. punctatus* sister to all other *Anaxyrus*. I also found the *americanus* group to be monophyletic and sister to *A. microscaphus* which is consistent with most previous studies. Two previous studies have inferred trees which do not place *A. fowleri* samples into a single monophyletic group (Fontenot et al., 2011; Masta et al., 2002). A single *A. fowleri* sample included in this study does not fall within a monophyletic group with the remaining *A. fowleri* samples, but is instead sister to the clade containing all *A. fowleri* and *A. woodhousii* samples (Fig. 3.4).

All of these studies have included different species, individuals, and loci, and also used different methods for alignment and phylogenetic inference. These differences in study design could result in the observed topology differences. The choice of locus in particular has a high likelihood of being the cause of these differences. Due to incomplete lineage sorting, the true histories of each gene may in fact differ from one another and not reflect the history of the species (Kingman, 1982). The practice of concatenating multiple loci, as all previous studies of *Anaxyrus* evolutionary relationships have done, can produce erroneous trees with high statistical support (Kubatko & Degnan, 2007). Despite the inappropriateness of concatenated analysis with genome-wide data, it was reassuring to find that all but one individual clustered with members of its own species in my analysis. In my experience, *Anaxyrus* can be challenging to identify, particularly in a preserved state. The maximum likelihood tree does not suggest that any samples in the dataset

have been misidentified, which could be problematic for other analyses.

To account for incomplete lineage sorting, I also inferred phylogenetic relationships among *Anaxyrus* species using the multispecies coalescent method *phycoeval*. Due to increased computational demands, I used a subset of the individuals for the *phycoeval* analysis. The topology of the *phycoeval* tree is different from the maximum-likelihood tree inferred in this study, as well as trees from previous studies (Fig. 3.5) (Fontenot et al., 2011; Graybeal, 1997; Masta et al., 2002; Portik et al., 2023; Pramuk et al., 2007; Pyron & Wiens, 2011). Unlike in any previous study or in the maximum-likelihood tree, *A. americanus* and *A. terrestris* are placed sister to one another, whereas in all other trees, *A. americanus* has had closer affinity to the *A. hemiophrys/A. baxteri* clade (Fig. 3.4) (Portik et al., 2023; Pyron & Wiens, 2011). In the *phycoeval* tree, the *A. hemiophrys/A. baxteri* clade is instead sister to the *A. americanus/A. fowleri/A. terrestris/A. woodhousii* clade. The sister relationship between *A. fowleri* and *A. woodhousii* is also different than previous estimates as well as the maximum-likelihood tree.

An unusual feature of *phycoeval* is that it can allow for multifurcations in inferred topologies (Oaks et al., 2022), which proved to be relevant in this study as the inferred tree included one multifurcation at the ancestral node of *A. quercicus*, the *A. cognatus/A. speciosus* clade, and the *americanus* group. Previous studies have produced trees with short internode branches at this part of the tree as did the maximum likelihood analysis in this study. Most phylogenetic methods only model bifurcating relationships and would force any true multifurcation into a series of bifurcating nodes with estimated branch lengths in between. In the *phycoeval* tree, the posterior probability of this split is low (0.51), but it is clear these three lineages diverged over a short period of time, if not simultaneously (Fig. 3.5).

3.4.2 Divergence Time

Only three previous studies have produced estimates for the age of *Anaxyrus* or any of its members (Feng et al., 2017; Frazão et al., 2015; Portik et al., 2023). The Frazão et al. (2015) phylogeny places *Anaxyrus* sister to the genus *Rhinella* rather than *Incilius* which

is not supported by most recent studies making their approximately 23 mya estimate for the origin of *Anaxyrus* questionable (Feng et al., 2017; Portik et al., 2023; Pyron & Wiens, 2011). Portik et al. (2023) estimate the split between *Anaxyrus* and *Incilius* to be 20.3 mya (95% HPD: 17.8-22.5), whereas Feng et al. (2017) estimate an earlier age of 16.5 mya (95% CI: 14.0-19.4). The dataset from Feng et al. (2017) included near complete coverage from 95 nuclear loci, whereas the Portik et al. (2023) has a higher degree of missing data (95%) and includes both mitochondrial as well as nuclear loci. For these reasons, I consider the Feng et al. (2017) estimate to be the most reliable and chose it for rescaling the branch lengths of the *phycoeval* tree.

I did not include any *Anaxyrus* taxa from within the *boreas* group which form a clade sister to all other *Anaxyrus*. As a result, the scaled *phycoeval* tree does not provide a point estimate for the time since the most recent common ancestor (MRCA) of all extant *Anaxyrus*. However, the interval between 11.9 mya when *A. punctatus* diverged from other *Anaxyrus* and 16.5 mya when *Anaxyrus* split from *Incilius* in the *phycoeval* tree is consistent with the 12.3 mya time since the MRCA of *Anaxyrus* estimated by Feng et al. (2017). The root age of the scaled *phycoeval* tree puts the divergence time between *Anaxyrus* and *Incilius* in the early part of the Miocene epoch. My results suggest a mid-Miocene divergence between *A. punctatus* and the rest of *Anaxyrus*, when precipitation and temperature declined and grasslands expanded in the North American interior (Morales-García et al., 2020). The timing of the multifurcation of the *A. quercicus*, *A. cognatus/A. speciosus*, and *americanus* group lineages coincides with a previously identified shift in the ecomorphology of ungulate mammals inhabiting North America (Morales-García et al., 2020). My results suggest that the *americanus* group diversified during the Pleistocene, a period marked by repeated glacial cycles that transformed the climate and geography of North America (Holman, 1995) Surprisingly, there is no evidence from the *phycoeval* analysis that any single one of these cycles was a driver of multiple diversification events and instead indicates that each event occurred independently during this period of *Anaxyrus* evolution. However, shared divergences could be masked by extinctions or biased divergence-time estimates due to gene flow.

3.4.3 Hybridization

There are numerous reports of hybridization among many different pairs of *Anaxyrus* species. However, the consequences of this hybridization are largely unknown. Using the *f*-branch test, I found support for a modest level of introgression among several species pairs which have been previously reported to hybridize, most of which presently exist in sympatry with one another. The highest *f*-branch statistics were calculated between *A. americanus* and *A. hemiophrys* and between *A. americanus* and *A. baxteri* with values of 0.24 and 0.22, respectively (Fig. 3.6). A hybrid zone is known to exist between *A. americanus* and *A. hemiophrys*, Green (1983) reported clinal variation of allozyme alleles at five different loci across an approximately 100 km transect in southeastern Manitoba, Canada. The steep cline observed by Green (1983) over a relatively short distance suggests that reproductive isolation between these species is quite high. It is possible that introgression is occurring beyond this narrow hybrid zone, but I was unable to test this given that the location of my sample of *A. hemiophrys* is in close proximity to the range of *A. americanus* (Fig. 3.1) (Conant & Collins, 1998).

Interestingly, there is also a high *f*-branch score between *A. americanus* and *A. baxteri* which are allopatric to one another. It is possible that introgression from *A. americanus* occurred before the divergence of *A. hemiophrys* and *A. baxteri*, causing high *f*-branch scores in comparisons with both species. Such ancestral introgression can cause elevated *f*-branch values associated with descending branches (Malinsky et al., 2021). This scenario is plausible as *A. baxteri* is believed to be a relic of a more southerly distribution of *A. hemiophrys* during a recent Pleistocene glacial period (Henrich, 1968). Unfortunately, it is not possible to directly test for this scenario with *dsuite* due to limitations of the *f*-branch test and without wider sampling from the range of *A. hemiophrys* (Malinsky et al., 2021).

Several other *f*-branch tests returned non-zero values, albeit much smaller. More than half of the *A. woodhousii* *f*-branch statistics were greater than zero (Fig. 3.6). Hybridization between all of these species is plausible as *A. woodhousii* occurs in sym-

patry at some part of its range with nearly all of them, and contemporary hybridization involving *A. woodhousii* has been reported with *A. americanus*, *A. cognatus*, *A. microscaphus*, and *A. speciosus* (Sullivan, 1986). There is presently little to no overlap between *A. woodhousii* and *A. hemiophrys*, but there could have been in the recent past due to Pleistocene glaciation pushing the range of *A. hemiophrys* further south (Henrich, 1968). The two non-zero *f*-branch values for *A. quercicus* with *A. punctatus* and *A. speciosus* are perplexing. The distribution of *A. quercicus* is confined to the pine woodlands of the Southeastern United States, whereas the other two species are found in the short arid grasslands and deserts of the Southwest (Conant & Collins, 1998). The *f*-branch statistic for the comparison between *A. punctatus* and the common ancestor of *A. speciosus* and *A. cognatus* is more plausible given their broadly overlapping distributions in the present day (Conant & Collins, 1998).

Unfortunately there were several ancestral and extant *Anaxyrus* species for which the *f*-branch test could not be performed. Therefore the *f*-branch test does not give a comprehensive picture of introgression within the genus. There may be introgression that is all together un-detectable with this method and missing pairs of ancestral species create limits on identifying precisely when introgression has occurred (Malinsky et al., 2021). Regardless of these limitations, results presented here are consistent with introgression being an important factor in the evolutionary history of *Anaxyrus*.

The d-statistic class of methods for detecting introgression are not able to test for introgression between sister species, and could not shed any light on putative hybridization between *A. fowleri* and *A. woodhousii* (Meacham, 1962). In order to test for admixture between *A. fowleri* and *A. woodhousii*, I used the program *STRUCTURE* and PCA analysis. The results of the *STRUCTURE* and PCA analyses are consistent with the existence of a hybrid zone between these two species (Fig. 3.12). Two *A. woodhousii* samples, one from Arkansas and the other from Texas, have large proportions of inferred ancestry from *A. fowleri* (Fig. 3.12). Several *A. fowleri* samples have large admixture proportions from *A. woodhousii* as well. The transition of ancestry proportions generally forms a steady East-West gradient (Fig. 3.12). The PCA results largely corroborate

the results of the *STRUCTURE* analysis, with *A. woodhousii* samples clustered tightly together, most *A. fowleri* samples clustering tightly with a few deviating toward the center of the first principal component axis, and finally two samples right in the center of the first principal component axis (Fig. 3.12). These results suggest the hybrid zone between *A. fowleri* and *A. woodhousii* is quite wide, possibly on the order of hundreds of kilometers (Fig. 3.12).

This brings the number of *Anaxyrus* hybrid zones where gene flow is supported by genetic evidence to three along with the *A. americanus/A. terrestris* and *A. americanus/A. hemiophrys* hybrid zones. Based on the *phycoeval* phylogeny, all of these species emerged within the past 2.5 million years, which provides important context this important context sheds light on the tempo of diversification within *Anaxyrus*. The sister species pairs *A. fowleri/A. woodhousii* and *A. americanus/A. terrestris* diverged only 0.7 and 1.0 mya, respectively (Fig. 3.5). Within this timeframe neither of these species pairs has evolved a degree of reproductive isolation and/or character displacement that permits them to exist in sympatry with one another. Introgression between these two pairs of recently diverged species extends a long distance, whereas the introgression between the older diverging species *A. americanus* and *A. hemiophrys* appears to be more limited (Green, 1983). Despite having more recent divergence times, *A. fowleri* occurs in sympatry across a large area with both *A. americanus* and *A. terrestris*, and *A. woodhousii* overlaps significantly with *A. americanus* (Conant & Collins, 1998). This is likely possible due to a higher degree of reproductive isolation that has evolved between these species pairs in the form of differences in advertisement call and timing of reproduction (Blair, 1974). Why more recently diverged species exist in sympatry and have evolved pre-zygotic isolating mechanisms, whereas *A. americanus* and *A. hemiophrys* with much greater time since divergence do not, is interesting. Perhaps they have recently come into secondary contact and have not had sufficient time to evolve pre-zygotic barriers to reproduction. This would lend support to reinforcement being the driving force behind the evolution of pre-zygotic isolation in these taxa.

3.4.4 Population Structure

An examination of population structure can potentially provide clues about the environmental factors that have shaped the evolutionary history of a species, because population divergence is an early stage along the speciation continuum (Mallet, 2008). The geographic barriers that result in the reduction of gene flow within species could be the same types of barriers that have resulted in past speciation events involving a species or its close relatives. In my analysis of population structure in *A. americanus*, *A. fowleri*, *A. terrestris*, and *A. woodhousii*, none of the *STRUCTURE* analyses show evidence consistent with a complete cessation of gene flow between any populations within species Figs. 3.8–3.11.

The most abrupt transitions in admixture coefficients are seen within *A. americanus*. I will focus the discussion of the *STRUCTURE* results for *A. americanus* on the analysis run with a K=3, despite it producing a likelihood that was only marginally better than the model with K=2 (Fig. 3.13). The results from the K=3 correspond well with the results of the PCA, make sense in a geographic context, and still show a stark transition of admixture coefficients from East to West as seen in the analysis with K=2 (Figs. 3.7 and 3.8). The *STRUCTURE* analysis for *A. americanus* reveals a fairly abrupt transition from East to West beginning at the Mississippi River (Fig. 3.8). All samples West of the Mississippi River have an admixture coefficient of one for the Western cluster of samples. This cluster of individuals has a range that loosely corresponds with a proposed subspecies, *A. anaxyrus charlesmithi*, which was said to exist in parts of Oklahoma, Arkansas, Missouri, and along the margins of some bordering states (Bragg, 1954). This sudden transition associated with a prominent geographic feature may represent an early stage in the process of speciation. An important caveat to consider in the interpretation of the *STRUCTURE* results is that *STRUCTURE* does not account for the spatial distribution of samples and models populations as panmictic. This assumption is almost certainly violated by *A. americanus* with isolation by distance having an effect on patterns of genetic variation that are not accounted for by *STRUCTURE*.

East of the Mississippi River, admixture coefficients associated with this cluster shrink with increasing distance from the river. In the Southeastern direction, the admixture coefficients associated with samples at the most Southeastern extent increase to one along this axis. In the Northeastern direction the transition is more gradual, from samples with a fairly balanced proportion of admixture from all three clusters to samples with a mixture of Northeastern and Southeastern ancestry, to finally a single sample with an admixture coefficient of one for the cluster of samples associated with this direction. Samples in the Eastern part of the *A. americanus* range appear to only vary with distance from one another and do not have any patterns of variation that are associated with any geographic feature, as they do in the West.

The *STRUCTURE* results for *A. fowleri*, *A. terrestris*, and *A. woodhousii* show very little, if any, differentiation within species. Among these three species, *A. terrestris* shows the greatest level of differentiation, with eastern samples having ancestry attributed to a population not represented in any of the western samples (Fig. 3.9). It is difficult to interpret this result with the extent and size of the current dataset, but it suggests there may be a gradient of genetic variation across the range of *A. terrestris*, much like *A. americanus*. Sampling from a greater extent of the *A. terrestris* range may shed light on this.

The PCA for *A. fowleri* shows one tightly clustered group with 4 samples that stand out from the rest (Fig. 3.10). These same samples were inferred as having a proportion of *A. woodhousii* ancestry in the combined *A. fowleri* and *A. woodhousii* *STRUCTURE* analysis (Fig. 3.12). The same four samples inferred as having *A. woodhousii* ancestry have the highest proportion of ancestry from the secondary population in the *A. fowleri* *STRUCTURE* analysis (Fig. 3.10). Apart from these individuals, the admixture proportions are highly uniform across the range of *A. fowleri* (Fig. 3.10).

Based on morphological differentiation, Shannon and Lowe (1955) described the subspecies, *A. woodhousii australis*, distributed across the southern parts of Arizona and New Mexico. Masta et al. (2003) found two divergent clades of *A. woodhousii* in a phylogeny inferred from a single mitochondrial locus. The distribution of samples from one of these

clades closely matched the distribution of *A. woodhousii australis*, although there was overlap with the distribution of samples from the other clade Masta et al. (2003) and Shannon and Lowe (1955). My sampling of *A. woodhousii* may no be adequate to detect population structure consistent with previous findings, however, I did include one sample from Southwest New Mexico and the STRUCTURE analysis did not differentiate it from the other samples Fig. 3.11. However, the sampling does include one sample from Southwest New Mexico and the *STRUCTURE* analysis does not differentiate it from other samples (Fig. 3.1). There are two samples assigned to a different population, however these are the same two samples found to be highly admixed with *A. fowleri*.

3.4.5 Conclusion

As the first investigation of the evolutionary history of *Anaxyrus* using genome-wide data, this study provides valuable insights into the complex evolutionary history of the genus and underscores the need for comprehensive sampling and rigorous analyses to better understand the dynamics of species relationships and diversification within this genus. Using methods that appropriately model incomplete lineage sorting in combination with genome-wide data, I inferred different evolutionary relationships and divergence time estimates compared to past studies using more limited datasets and methods. I found genetic structure within some species of *Anaxyrus*, which could indicate that these populations are at early stages of speciation. I also found evidence for ancient and ongoing gene flow among species within the genus which adds to the mounting evidence that diversification does not always proceed in a tree-like fashion. This study is the first to provide genetic evidence of hybridization between *A. fowleri* and *A. woodhousii*, which brings the total number of hybrid zones to three. These findings provide context for the evolution of reproductive isolation within *Anaxyrus* and highlight the promise of this genus in furthering our understanding of speciation.

References

- Abbott, R., Albach, D., Ansell, S., Arntzen, J. W., Baird, S. J. E., Bierne, N., Boughman, J., Brelandsford, A., Buerkle, C. A., Buggs, R., Butlin, R. K., Dieckmann, U., Eroukhmanoff, F., Grill, A., Cahan, S. H., Hermansen, J. S., Hewitt, G., Hudson, A. G., Jiggins, C., ... Zinner, D. (2013). Hybridization and speciation. *Journal of Evolutionary Biology*, 26(2), 229–246. <https://doi.org/10.1111/j.1420-9101.2012.02599.x>
- Bayona-Vásquez, N. J., Glenn, T. C., Kieran, T. J., Pierson, T. W., Hoffberg, S. L., Scott, P. A., Bentley, K. E., Finger, J. W., Louha, S., Troendle, N., Diaz-Jaimes, P., Mauricio, R., & Faircloth, B. C. (2019). Adapterama III: Quadruple-indexed, double/triple-enzyme RADseq libraries (2RAD/3RAD). *PeerJ*, 7, e7724. <https://doi.org/10.7717/peerj.7724>
- Blair, W. F. (1963). Intragroup genetic compatibility in the *Bufo americanus* species group of toads. *The Texas Journal of Science*, 13, 15–34.
- Blair, W. F. (1972). *Evolution in the genus Bufo*. University of Texas Press.
- Blair, W. F. (1974). Character Displacement in Frogs. *American Zoologist*, 14(4), 1119–1125. <https://doi.org/10.1093/icb/14.4.1119>
- Bragg, A. N. (1954). *Bufo terrestris charlesmithi*, a new subspecies from Oklahoma. *The Wasmann Journal of Biology*, 12, 245–254.
- Conant, R., & Collins, ___. (1998). *Reptiles and amphibians: Eastern/Central North America* (3rd ed.). Houghton Mifflin Co., Boston, MA.
- Coyne, J. A., & Orr, H. A. (2004). *Speciation*. Sinauer Associates.
- Degnan, J. H., & Rosenberg, N. A. (2009). Gene tree discordance, phylogenetic inference and the multispecies coalescent. *Trends in Ecology & Evolution*, 24(6), 332–340. <https://doi.org/10.1016/j.tree.2009.01.009>
- Evanno, G., Regnaut, S., & Goudet, J. (2005). Detecting the number of clusters of individuals using the software structure: A simulation study. *Molecular Ecology*, 14(8), 2611–2620. <https://doi.org/10.1111/j.1365-294X.2005.02553.x>

- Feng, Y.-J., Blackburn, D. C., Liang, D., Hillis, D. M., Wake, D. B., Cannatella, D. C., & Zhang, P. (2017). Phylogenomics reveals rapid, simultaneous diversification of three major clades of Gondwanan frogs at the Cretaceous–Paleogene boundary. *Proceedings of the National Academy of Sciences*, 114(29). <https://doi.org/10.1073/pnas.1704632114>
- Fontenot, B. E., Makowsky, R., & Chippindale, P. T. (2011). Nuclear–mitochondrial discordance and gene flow in a recent radiation of toads. *Molecular Phylogenetics and Evolution*, 59(1), 66–80. <https://doi.org/10.1016/j.ympev.2010.12.018>
- Francis, R. M. (2017). POPHELPER: An R package and web app to analyse and visualize population structure. *Molecular Ecology Resources*, 17(1), 27–32. <https://doi.org/10.1111/1755-0998.12509>
- Frazão, A., da Silva, H. R., & Russo, C. A. d. M. (2015). The Gondwana Breakup and the History of the Atlantic and Indian Oceans Unveils Two New Clades for Early Neobatrachian Diversification. *PLOS ONE*, 10(11), e0143926. <https://doi.org/10.1371/journal.pone.0143926>
- Graybeal, A. (1997). Phylogenetic relationships of bufonid frogs and tests of alternate macroevolutionary hypotheses characterizing their radiation. *Zoological Journal of the Linnean Society*, 119(3), 297–338. <https://doi.org/10.1111/j.1096-3642.1997.tb00139.x>
- Green, D. M. (1983). Allozyme Variation through a Clinal Hybrid Zone between the Toads *Bufo americanus* and *B. hemiophrys* in Southeastern Manitoba. *Herpetologica*, 39(1), 28–40.
- Green, D. M. (1996). The bounds of species: Hybridization in the *Bufo americanus* group of North American toads. *Israel Journal of Zoology*, 42, 95–109.
- Henrich, T. W. (1968). Morphological Evidence of Secondary Intergradation between *Bufo hemiophrys* Cope and *Bufo americanus* Holbrook in Eastern South Dakota. *Herpetologica*, 24(1), 1–13.

- Hoang, D. T., Chernomor, O., von Haeseler, A., Minh, B. Q., & Vinh, L. S. (2018). UFBoot2: Improving the Ultrafast Bootstrap Approximation. *Molecular Biology and Evolution*, 35(2), 518–522. <https://doi.org/10.1093/molbev/msx281>
- Holman, J. A. (1995). *Pleistocene Amphibians and Reptiles in North America*. Oxford University Press.
- Hua, X., & Wiens, J. J. (2013). How Does Climate Influence Speciation? *The American Naturalist*, 182(1), 1–12. <https://doi.org/10.1086/670690>
- Huerta-Cepas, J., Serra, F., & Bork, P. (2016). ETE 3: Reconstruction, Analysis, and Visualization of Phylogenomic Data. *Molecular Biology and Evolution*, 33(6), 1635–1638. <https://doi.org/10.1093/molbev/msw046>
- Jombart, T. (2008). Adegenet : A R package for the multivariate analysis of genetic markers. *Bioinformatics*, 24(11), 1403–1405. <https://doi.org/10.1093/bioinformatics/btn129>
- Kingman, J. (1982). The coalescent. *Stochastic Processes and their Applications*, 13(3), 235–248. [https://doi.org/10.1016/0304-4149\(82\)90011-4](https://doi.org/10.1016/0304-4149(82)90011-4)
- Kubatko, L. S., & Degnan, J. H. (2007). Inconsistency of Phylogenetic Estimates from Concatenated Data under Coalescence (T. Collins, Ed.). *Systematic Biology*, 56(1), 17–24. <https://doi.org/10.1080/10635150601146041>
- Lyman, R. A., & Edwards, C. E. (2022). Revisiting the comparative phylogeography of unglaciated eastern North America: 15 years of patterns and progress. *Ecology and Evolution*, 12(4), e8827. <https://doi.org/10.1002/ece3.8827>
- Malinsky, M., Matschiner, M., & Svardal, H. (2021). Dsuite - Fast D-statistics and related admixture evidence from VCF files. *Molecular Ecology Resources*, 21(2), 584–595. <https://doi.org/10.1111/1755-0998.13265>
- Malinsky, M., Svardal, H., Tyers, A. M., Miska, E. A., Genner, M. J., Turner, G. F., & Durbin, R. (2018). Whole-genome sequences of Malawi cichlids reveal multiple radiations interconnected by gene flow. *Nature Ecology & Evolution*, 2(12), 1940–1955. <https://doi.org/10.1038/s41559-018-0717-x>

- Mallet, J. (2008). Hybridization, ecological races and the nature of species: Empirical evidence for the ease of speciation. *Philosophical Transactions of the Royal Society B: Biological Sciences*, 363(1506), 2971–2986. <https://doi.org/10.1098/rstb.2008.0081>
- Masta, S. E., Laurent, N. M., & Routman, E. J. (2003). Population genetic structure of the toad *Bufo woodhousii* : An empirical assessment of the effects of haplotype extinction on nested cladistic analysis. *Molecular Ecology*, 12(6), 1541–1554. <https://doi.org/10.1046/j.1365-294X.2003.01829.x>
- Masta, S. E., Sullivan, B. K., Lamb, T., & Routman, E. J. (2002). Molecular systematics, hybridization, and phylogeography of the *Bufo americanus* complex in Eastern North America. *Molecular Phylogenetics and Evolution*, 24(2), 302–314. [https://doi.org/10.1016/S1055-7903\(02\)00216-6](https://doi.org/10.1016/S1055-7903(02)00216-6)
- Meacham, W. R. (1962). Factors Affecting Secondary Intergradation Between Two Allopatic Populations in the *Bufo Woodhousei* Complex. *American Midland Naturalist*, 67(2), 282. <https://doi.org/10.2307/2422709>
- Morales-García, N. M., Säilä, L. K., & Janis, C. M. (2020). The Neogene Savannas of North America: A Retrospective Analysis on Artiodactyl Faunas. *Frontiers in Earth Science*, 8.
- Nguyen, L.-T., Schmidt, H. A., von Haeseler, A., & Minh, B. Q. (2015). IQ-TREE: A Fast and Effective Stochastic Algorithm for Estimating Maximum-Likelihood Phylogenies. *Molecular Biology and Evolution*, 32(1), 268–274. <https://doi.org/10.1093/molbev/msu300>
- Nuñez, L. P., Gray, L. N., Weisrock, D. W., & Burbrink, F. T. (2023). The phylogenomic and biogeographic history of the gartersnakes, watersnakes, and allies (Natricidae: Thamnophiini). *Molecular Phylogenetics and Evolution*, 186, 107844. <https://doi.org/10.1016/j.ympev.2023.107844>
- Oaks, J. R. (2019). Full Bayesian Comparative Phylogeography from Genomic Data (L. Kubatko, Ed.). *Systematic Biology*, 68(3), 371–395. <https://doi.org/10.1093/sysbio/syy063>

- Oaks, J. R., Wood, P. L., Siler, C. D., & Brown, R. M. (2022). Generalizing Bayesian phylogenetics to infer shared evolutionary events. *Proceedings of the National Academy of Sciences*, 119(29), e2121036119. <https://doi.org/10.1073/pnas.2121036119>
- Portik, D. M., Streicher, J. W., & Wiens, J. J. (2023). Frog phylogeny: A time-calibrated, species-level tree based on hundreds of loci and 5,242 species. *Molecular Phylogenetics and Evolution*, 188, 107907. <https://doi.org/10.1016/j.ympev.2023.107907>
- Pramuk, J. B., Robertson, T., Sites, J. W., & Noonan, B. P. (2007). Around the world in 10 million years: Biogeography of the nearly cosmopolitan true toads (Anura: Bufonidae). *Global Ecology and Biogeography*, 0(0), 070817112457001–???. <https://doi.org/10.1111/j.1466-8238.2007.00348.x>
- Pritchard, J. K., Stephens, M., & Donnelly, P. (2000). Inference of Population Structure Using Multilocus Genotype Data. *Genetics*, 155(2), 945–959. <https://doi.org/10.1093/genetics/155.2.945>
- Pyron, R. A., & Wiens, J. J. (2011). A large-scale phylogeny of Amphibia including over 2800 species, and a revised classification of extant frogs, salamanders, and caecilians. *Molecular Phylogenetics and Evolution*, 61(2), 543–583. <https://doi.org/10.1016/j.ympev.2011.06.012>
- Reich, D., Thangaraj, K., Patterson, N., Price, A. L., & Singh, L. (2009). Reconstructing Indian population history. *Nature*, 461(7263), 489–494. <https://doi.org/10.1038/nature08365>
- Rieseberg, L. H., Whitton, J., & Gardner, K. (1999). Hybrid zones and the genetic architecture of a barrier to gene flow between two sunflower species. *Genetics*, 152(2), 713–727.
- Rochette, N. C., Rivera-Colón, A. G., & Catchen, J. M. (2019). Stacks 2: Analytical methods for paired-end sequencing improve RADseq-based population genomics. *Molecular Ecology*, 28(21), 4737–4754. <https://doi.org/10.1111/mec.15253>
- Shannon, F. A., & Lowe, F. A. (1955). A new subspecies of *Bufo woodhousei* from the inland Southwest. *Herpetologica*, 11, 185–190.

- Sullivan, B. K. (1986). Hybridization between the Toads *Bufo microscaphus* and *Bufo woodhousei* in Arizona: Morphological Variation. *Journal of Herpetology*, 20(1), 11–21. <https://doi.org/10.2307/1564120>
- Wang, L.-G., Lam, T. T.-Y., Xu, S., Dai, Z., Zhou, L., Feng, T., Guo, P., Dunn, C. W., Jones, B. R., Bradley, T., Zhu, H., Guan, Y., Jiang, Y., & Yu, G. (2020). Treeio: An R Package for Phylogenetic Tree Input and Output with Richly Annotated and Associated Data. *Molecular Biology and Evolution*, 37(2), 599–603. <https://doi.org/10.1093/molbev/msz240>
- Wen, D., Yu, Y., Zhu, J., & Nakhleh, L. (2018). Inferring Phylogenetic Networks Using PhyloNet. *Systematic Biology*, 67(4), 735–740. <https://doi.org/10.1093/sysbio/syy015>
- Wickam, H. (2016). Ggplot2: Elegant graphics for data analysis. *Springer-Verlag*. Accessed March, 16, 2021.
- Xue, A. T., & Hickerson, M. J. (2015). The aggregate site frequency spectrum for comparative population genomic inference. *Molecular Ecology*, 24(24), 6223–6240. <https://doi.org/10.1111/mec.13447>
- Yu, G., Smith, D. K., Zhu, H., Guan, Y., & Lam, T. T.-Y. (2017). Ggtree: An r package for visualization and annotation of phylogenetic trees with their covariates and other associated data. *Methods in Ecology and Evolution*, 8(1), 28–36. <https://doi.org/10.1111/2041-210X.12628>

3.5 Figures

Sampling Distribution

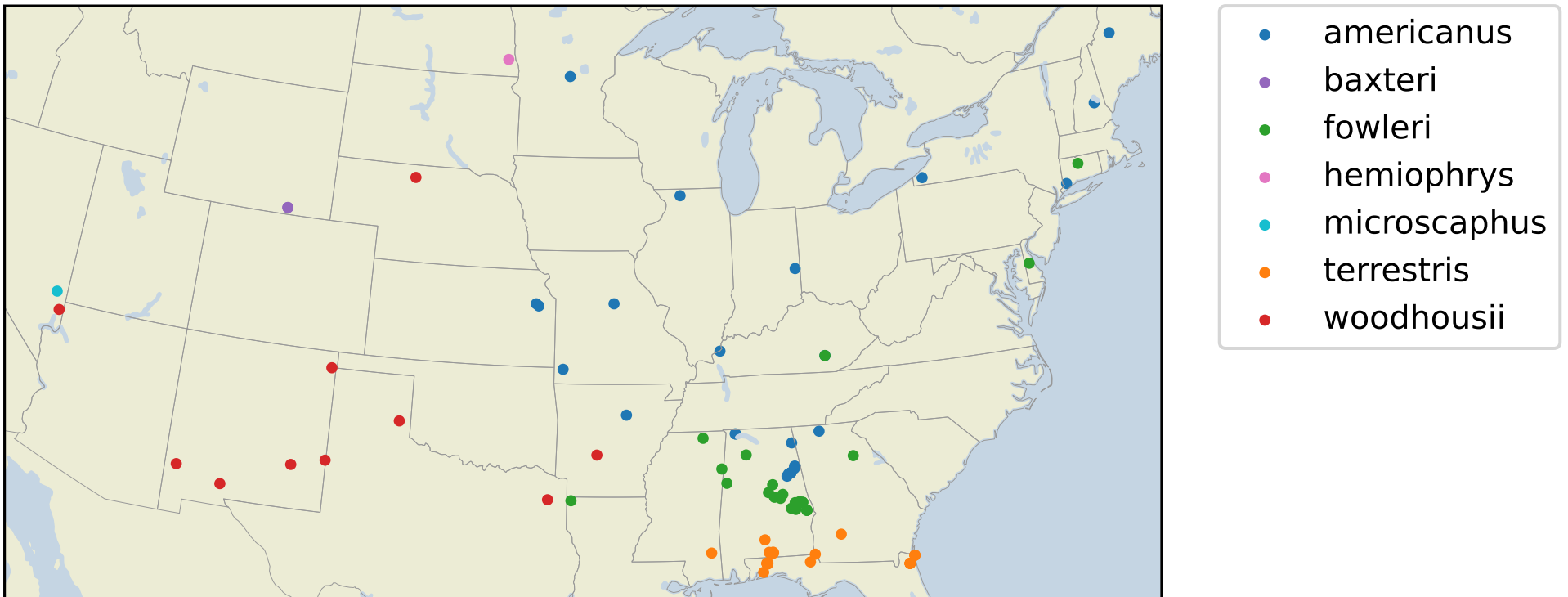


Figure 3.1. Map showing the distribution of the *americanus* group samples sequenced for this study.

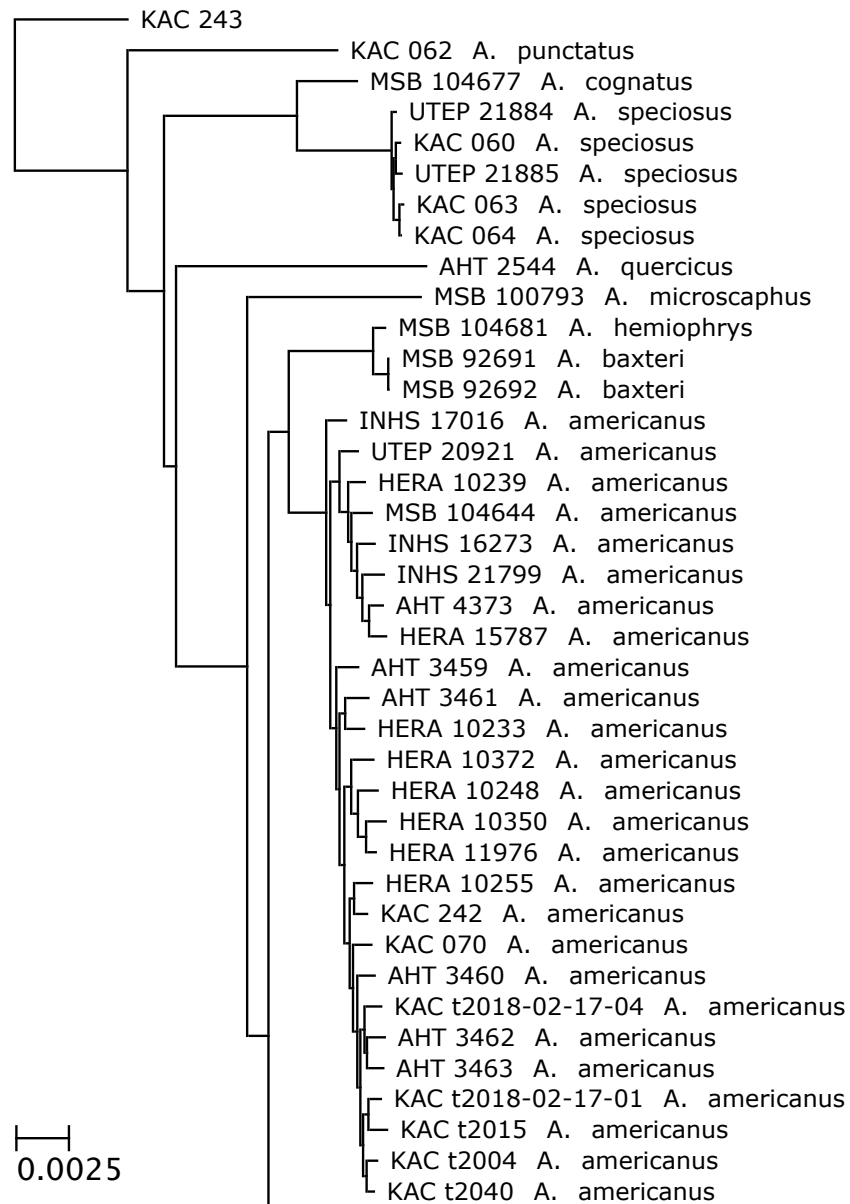


Figure 3.2. Part of maximum likelihood phylogeny inferred with *IQ-TREE*. The values associated with nodes are the ultra fast bootstrap support values rounded down to the nearest whole number. The tree was plotted using ETE 3.1.2 (Huerta-Cepas et al., 2016).

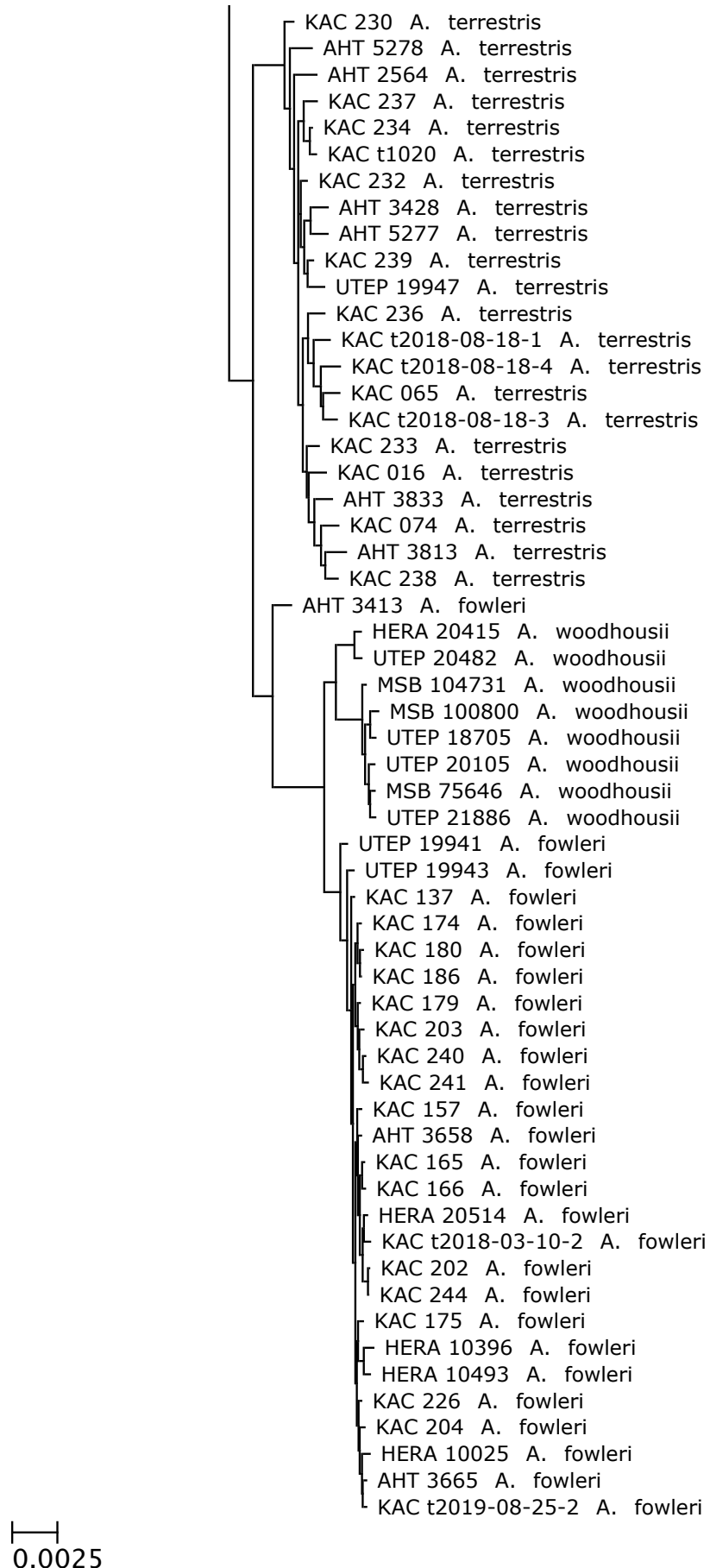


Figure 3.3. Part of maximum likelihood phylogeny inferred with *IQ-TREE*. Continued from Fig. 3.2.

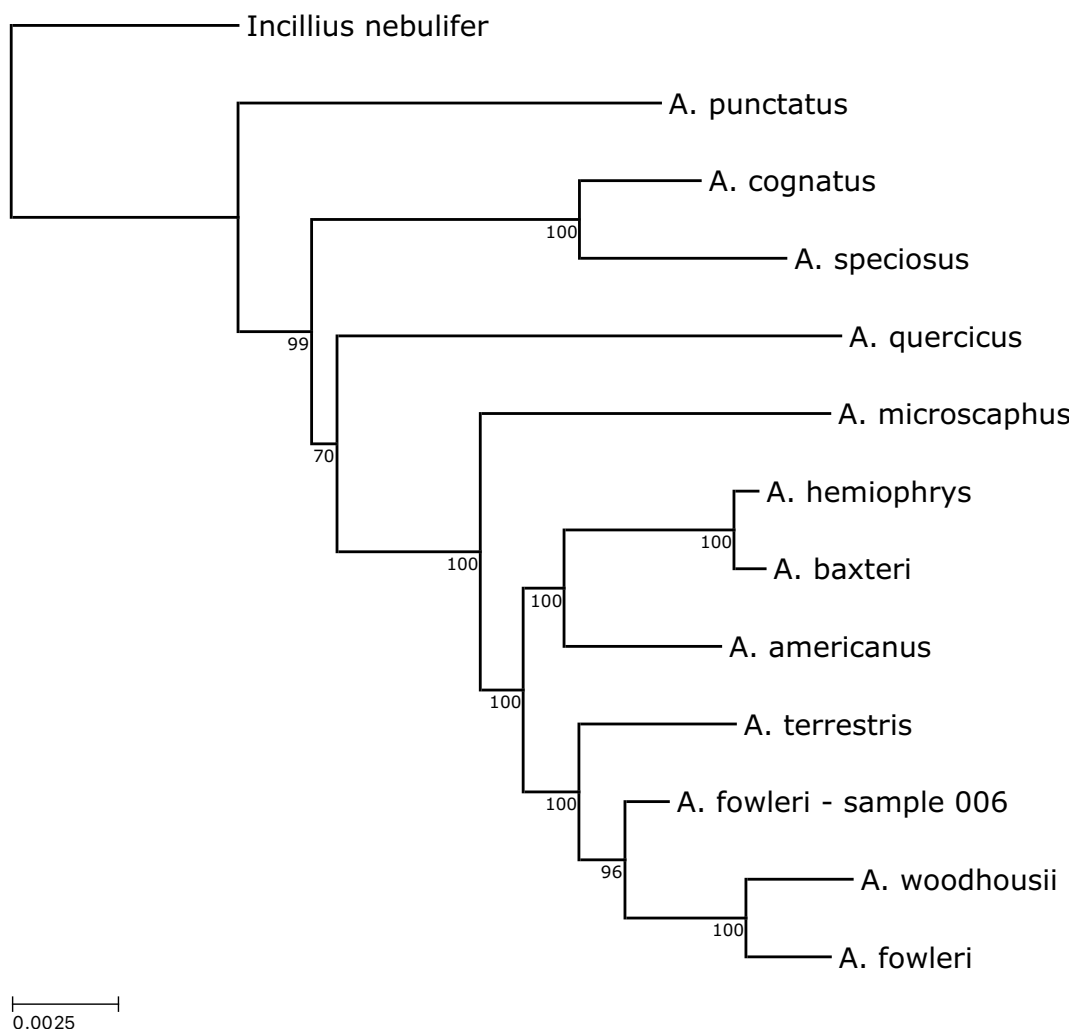


Figure 3.4. Maximum likelihood phylogeny inferred with *IQ-TREE* with clades for each species collapsed. The values associated with nodes are the ultra fast bootstrap support values rounded down to the nearest whole number. The tree was plotted using ETE 3.1.2 (Huerta-Cepas et al., 2016).

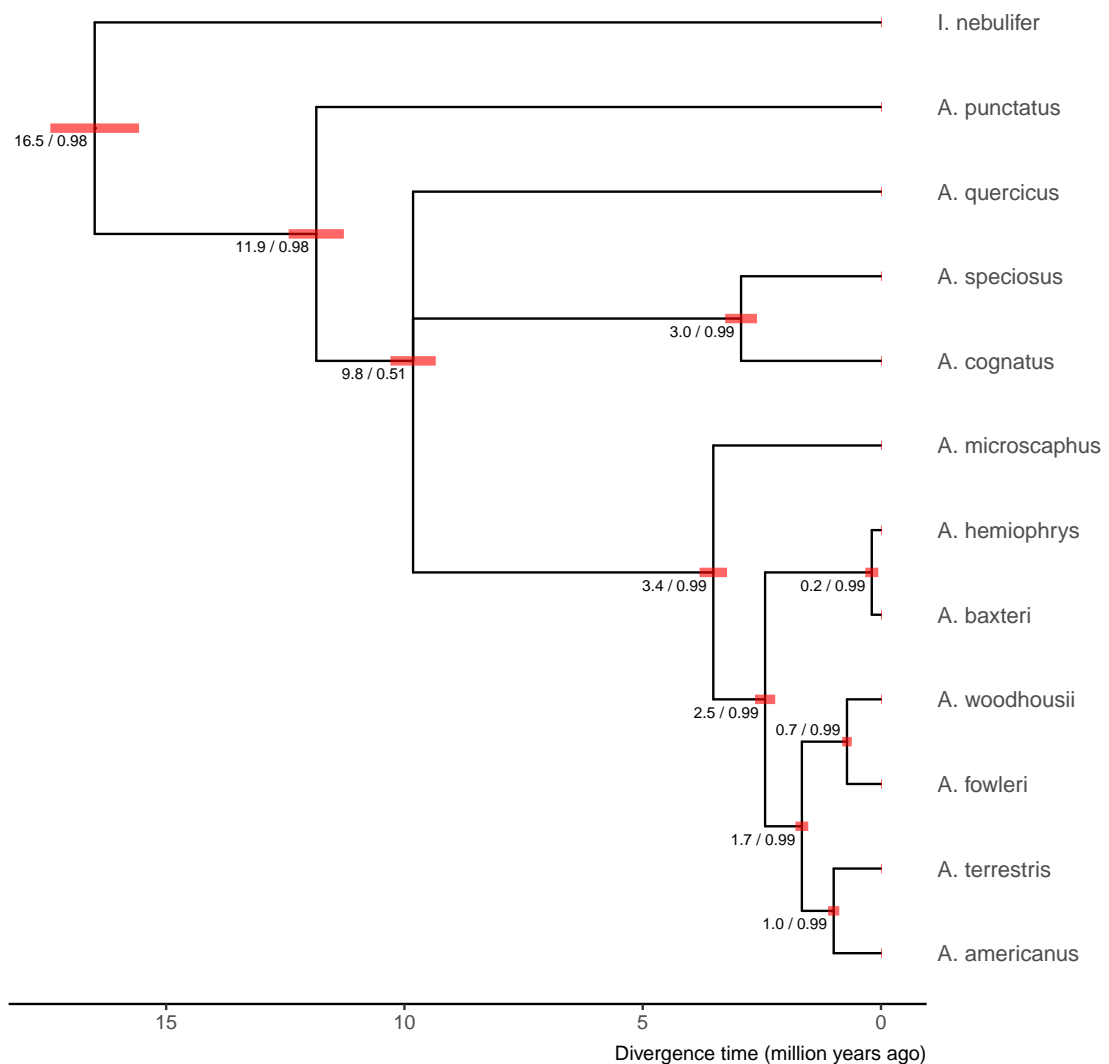


Figure 3.5. The maximum a posteriori tree inferred under a multispecies coalescent model by *phycoeval*. Branch lengths are rescaled from expected substitutions per site to millions of years using a secondary time calibration (*Materials and Methods*). Numbers displayed at each node are the mean posterior node age followed by the approximate posterior probability of the node rounded down to the nearest hundredth. Red bars show the 95% HPDI for the scaled node age at each node. Created using ggplot2 (Wickam, 2016), ggtree (Yu et al., 2017), and treeio (Wang et al., 2020).

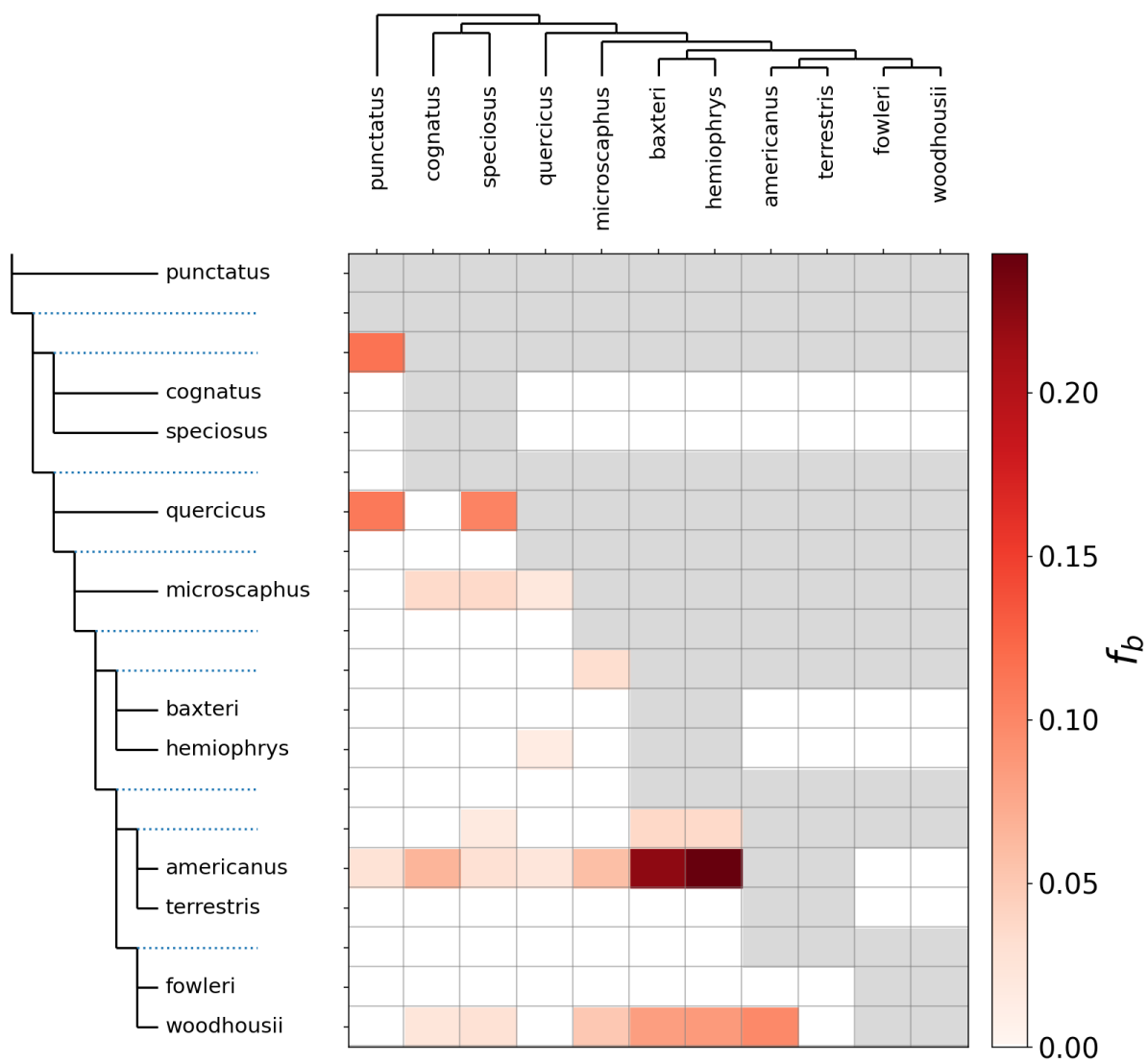


Figure 3.6. Heatmap showing the value of the f -branch statistic computed for each possible pair of *Anaxyrus* species. The f -branch statistic indicates the proportion of excess allele sharing between a species on the x-axis and branch on the y-axis (relative to its sister branch). Excess allele sharing between species indicates possible gene flow between them. Grey boxes indicate that pairs cannot be tested by Dsuite for the given tree topology.

A. americanus Population Structure, K=2

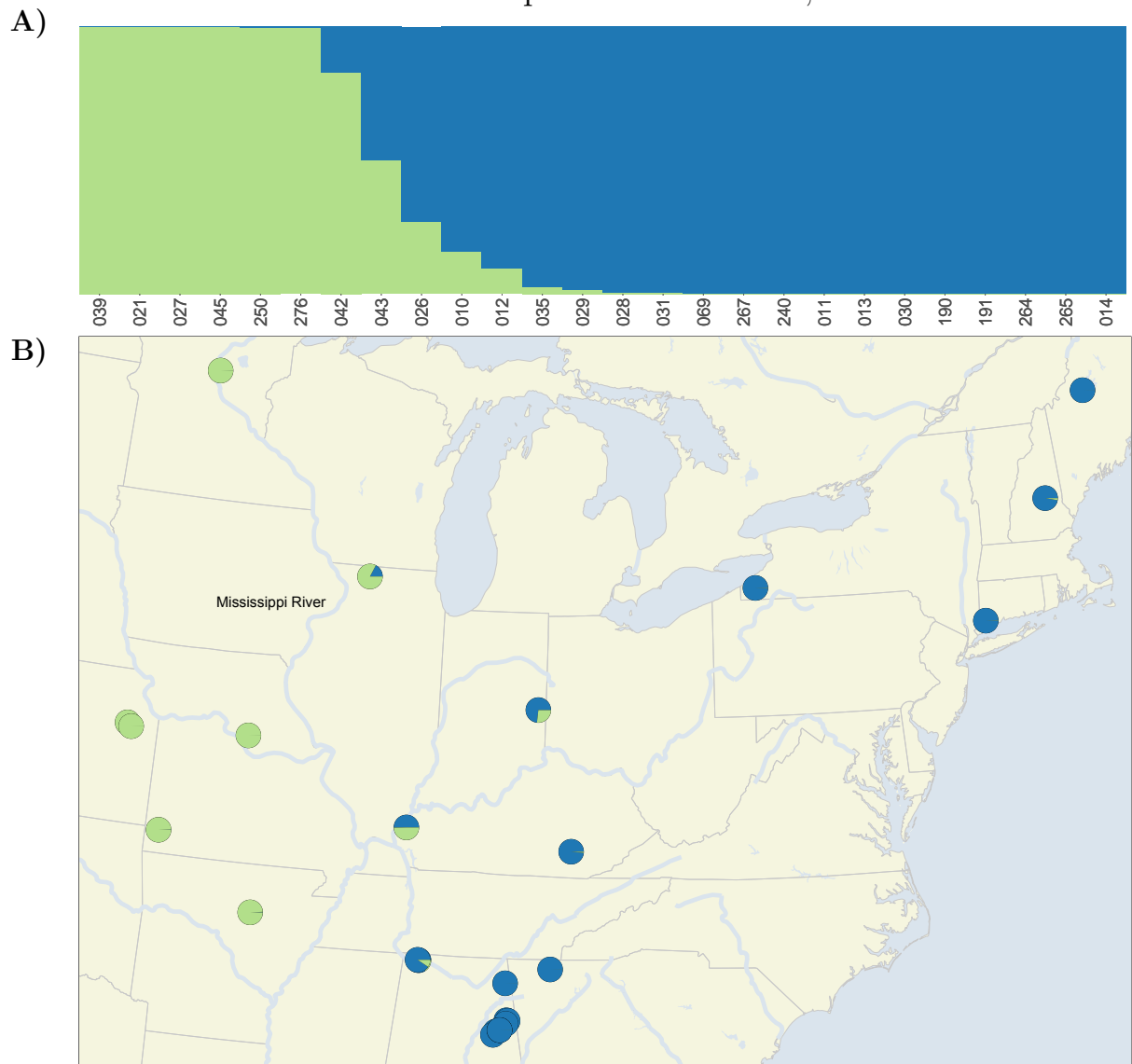


Figure 3.7. *A. americanus* population structure with K=2. A) Barplot with admixture coefficients from the *STRUCTURE* analysis with K=2. B) Sample map with pie chart markers showing the sampling location and estimated ancestry coefficients of *A. americanus* samples.

A. americanus Population Structure, K=3

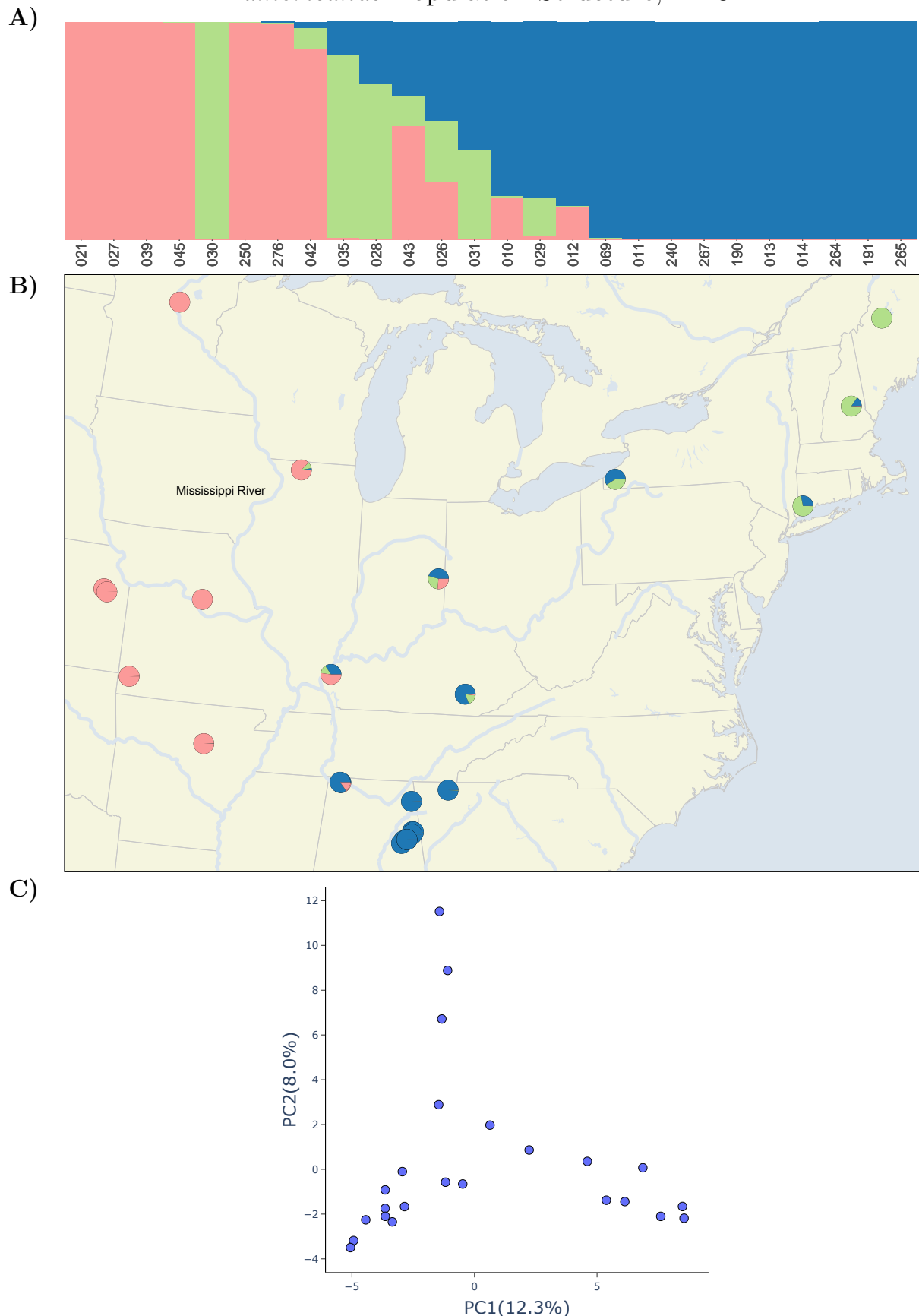


Figure 3.8. *A. americanus* population structure with K=3. A) Barplot with admixture coefficients from the *STRUCTURE* analysis with K=3. B) Sample map with pie chart markers showing the sampling location and estimated ancestry coefficients of *A. americanus* samples. C) Plot showing principal component one and two from the PCA performed on SNP data.

A. terrestris Population Structure

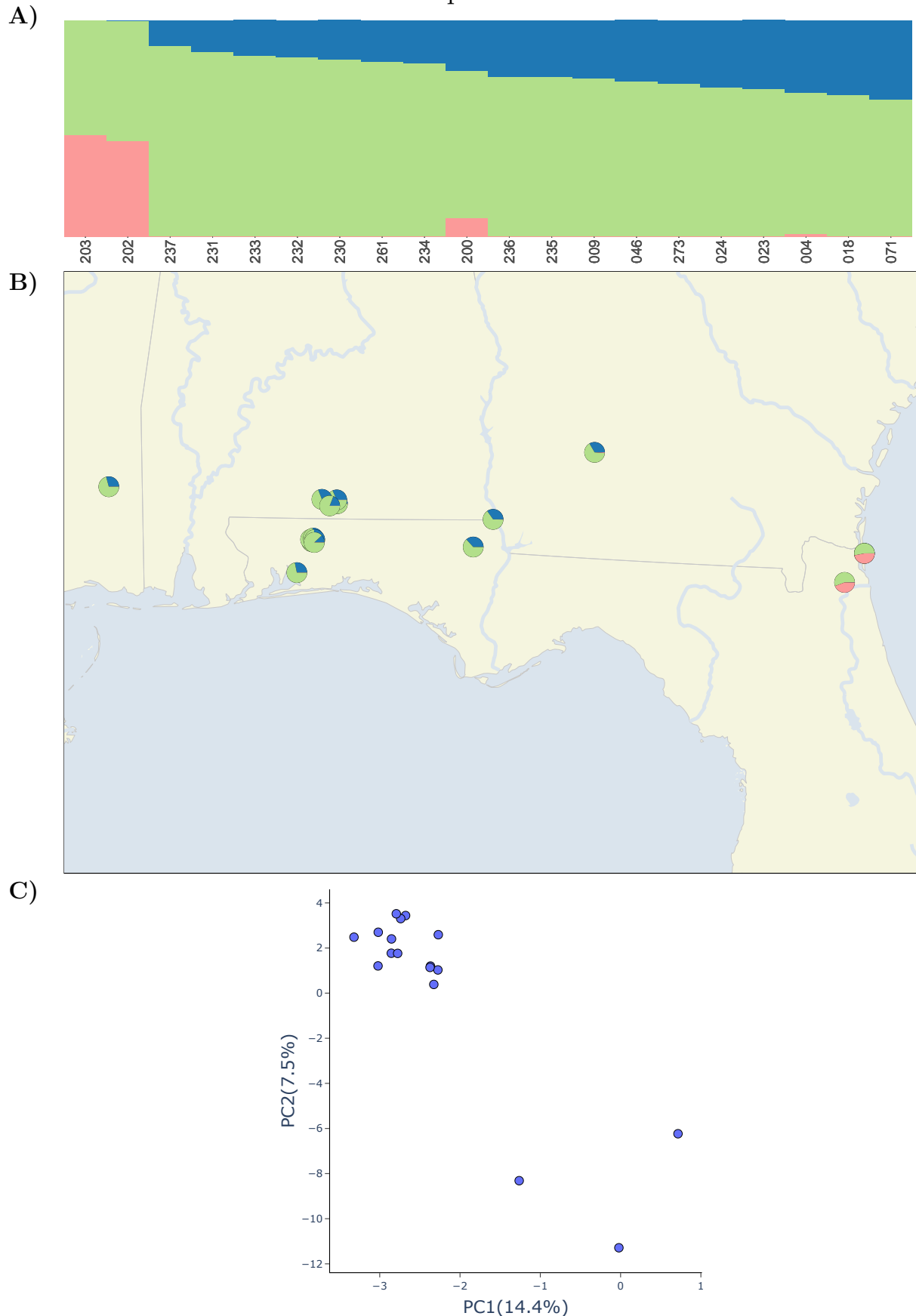


Figure 3.9. *A. terrestris* population structure. A) Barplot with admixture coefficients from the *STRUCTURE* analysis with K=2. B) Sample map with pie chart markers showing the sampling location and estimated ancestry coefficients of *A. terrestris* samples. C) Plot showing principal component one and two from the PCA performed on SNP data.

A. fowleri Population Structure

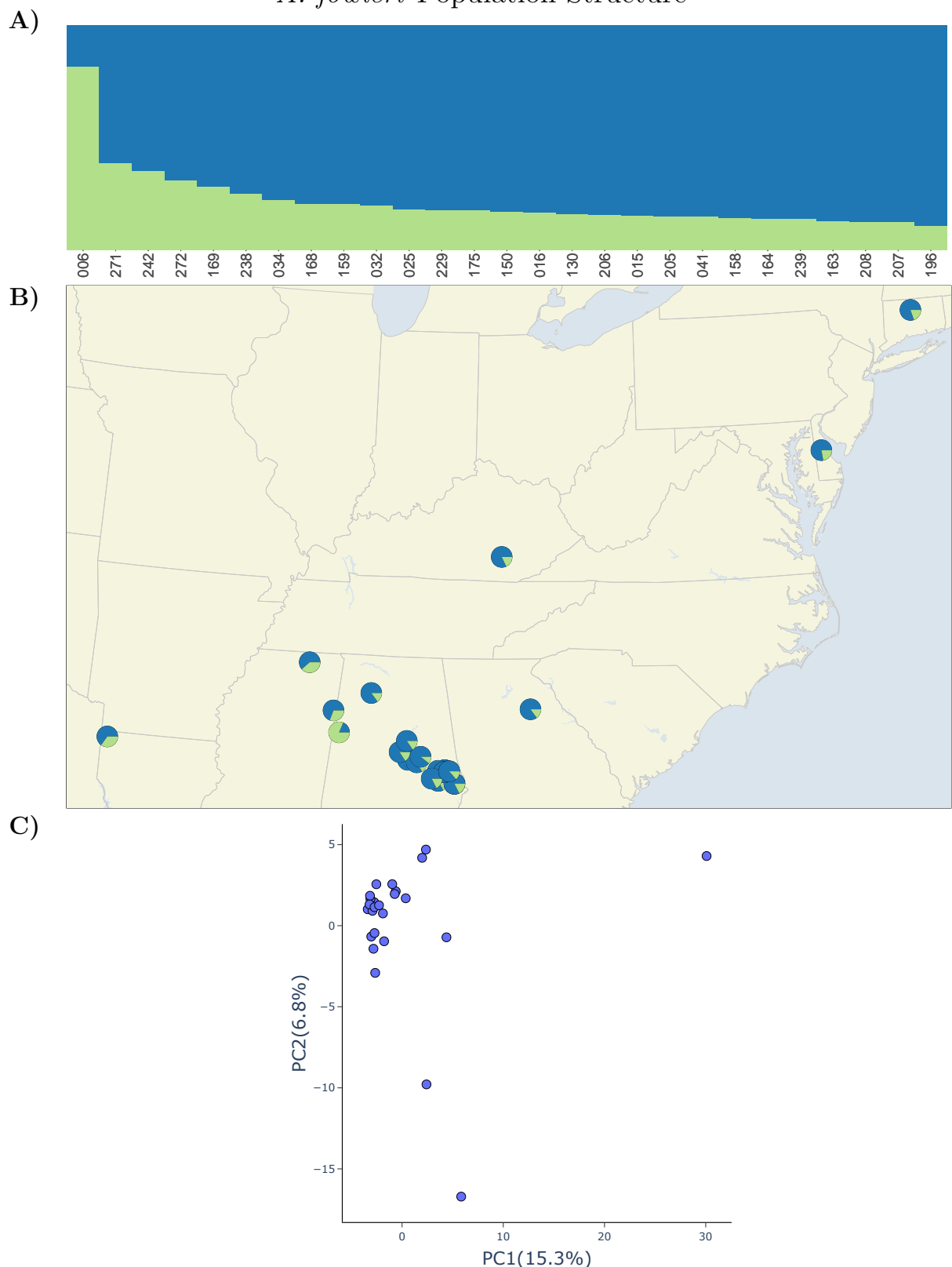


Figure 3.10. *A. fowleri* population structure. A) Barplot with admixture coefficients from the *STRUCTURE* analysis with $K=2$. B) Sample map with pie chart markers showing the sampling location and estimated ancestry coefficients of *A. fowleri* samples. C) Plot showing principal component one and two from the PCA performed on SNP data.

A. woodhousii Population Structure

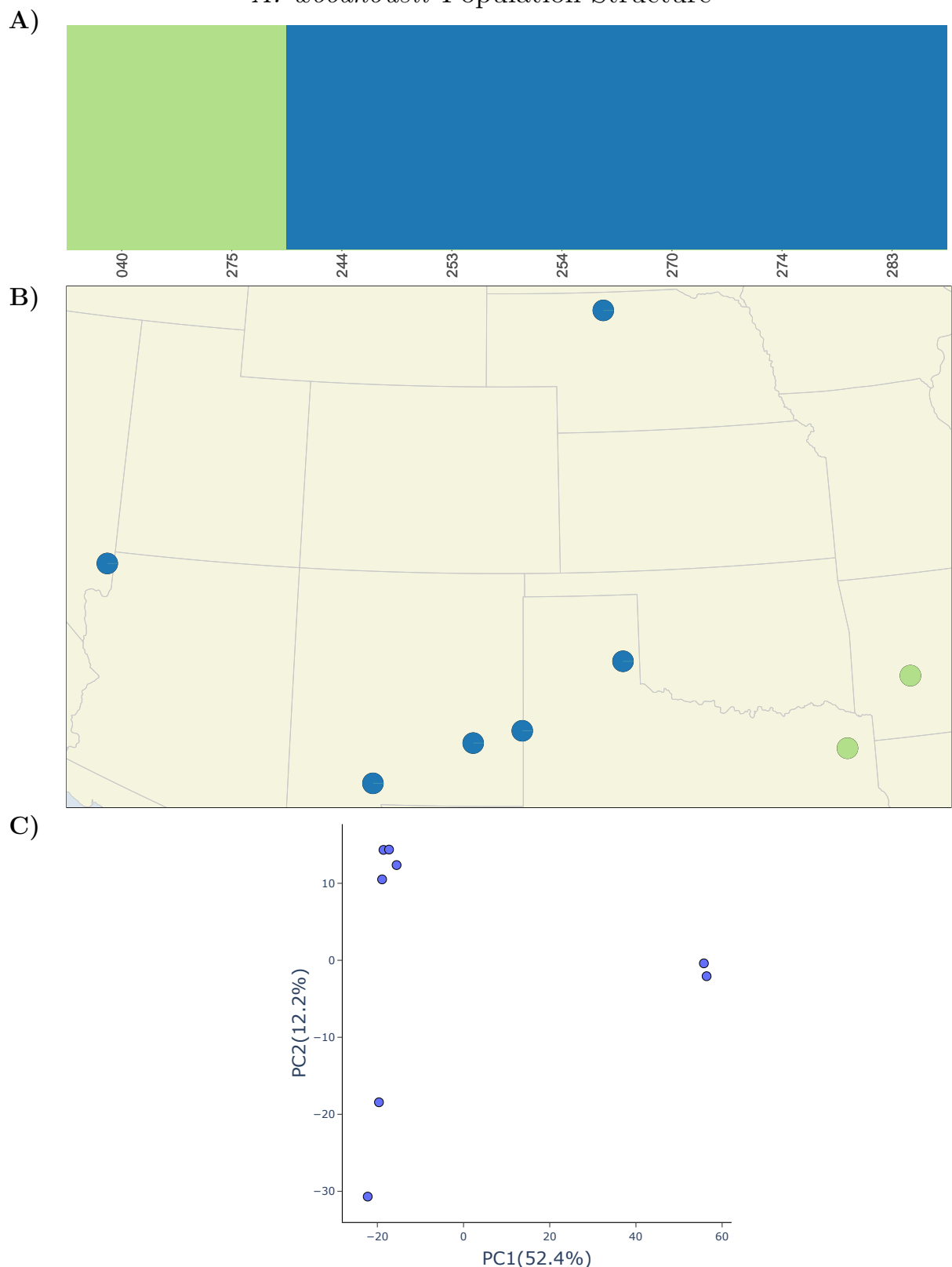
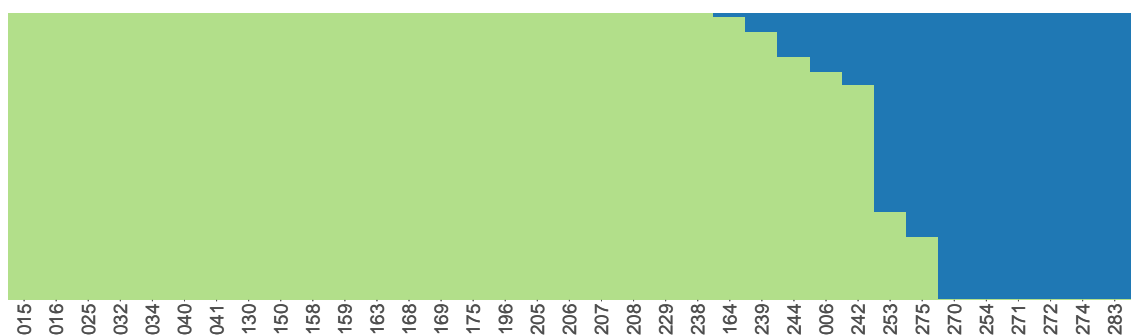


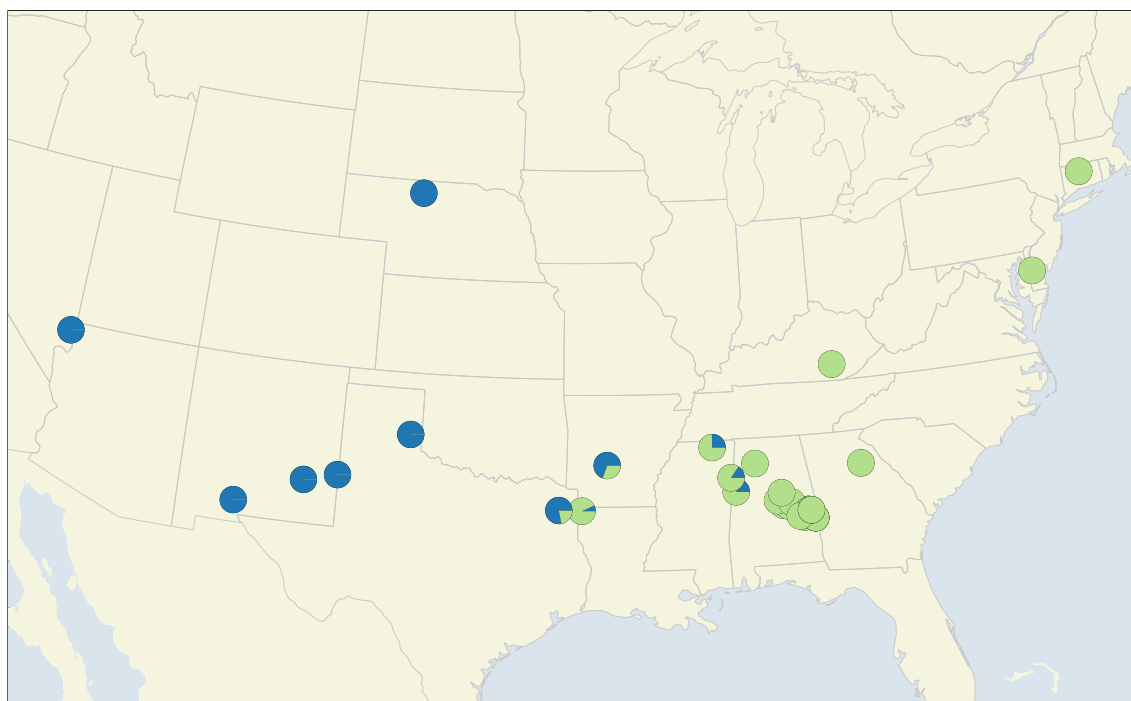
Figure 3.11. *A. woodhousii* population structure. A) Barplot with admixture coefficients from the STRUCTURE analysis with K=2. B) Sample map with pie chart markers showing the sampling location and estimated ancestry coefficients of *A. woodhousii* samples. C) Plot showing principal component one and two from the PCA performed on SNP data.

A. fowleri + A. woodhousii Population Structure

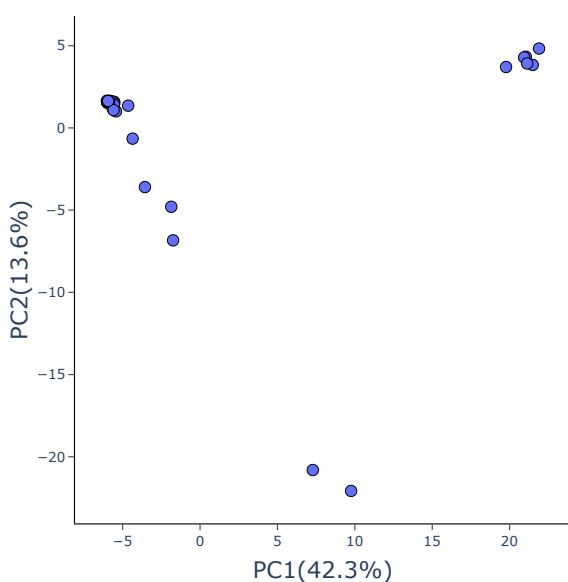
A)



B)



C)



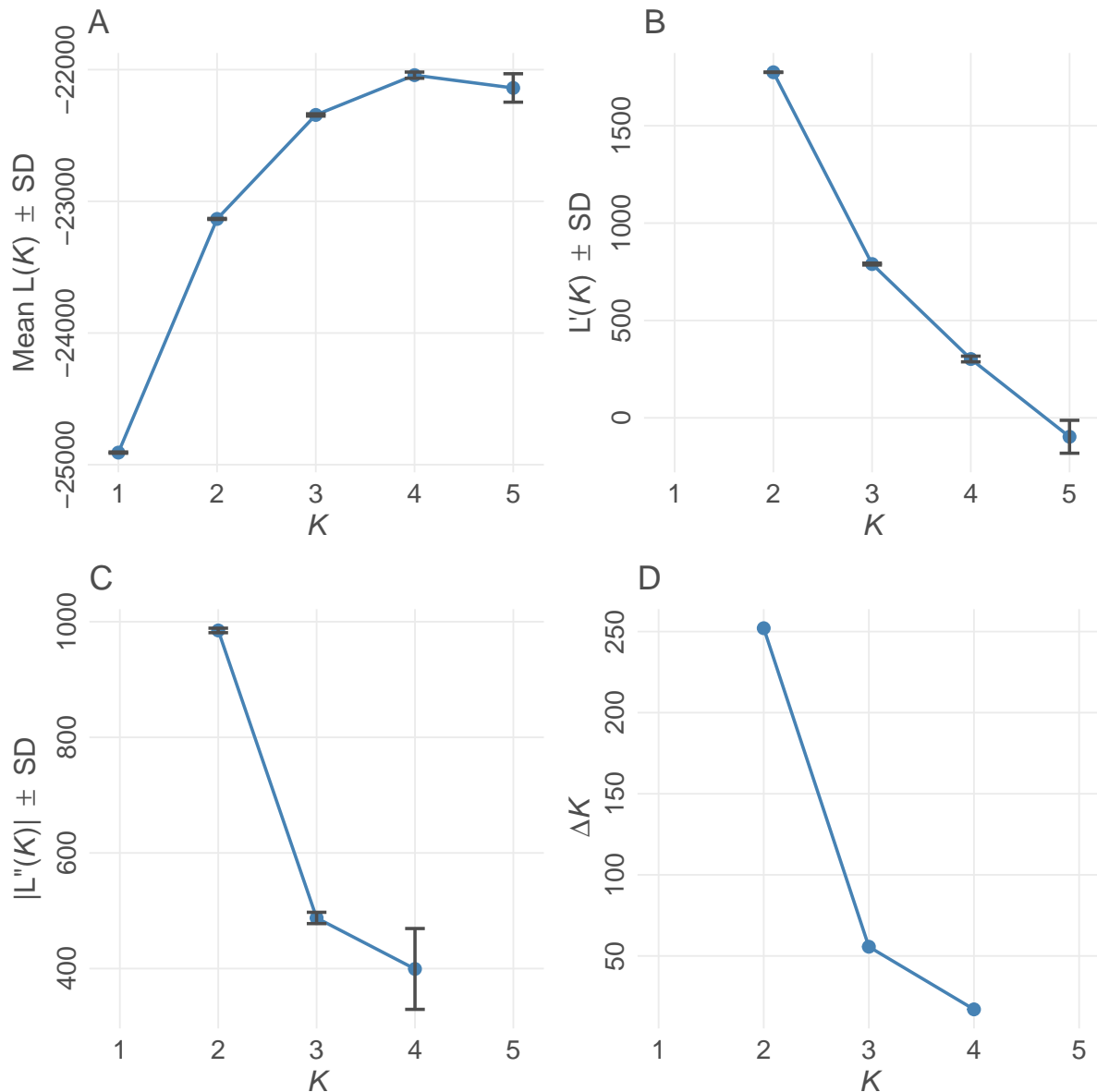


Figure 3.13. Evanno method for optimal value of K among *A. americanus* *STRUCTURE* analyses (Evanno et al., 2005). The following caption applies to all Evanno figures that follow. K refers to the number of populations for each of the different *STRUCTURE* models examined. (A) Mean estimated \ln probability of data over 10 runs for each value of K . (B) Rate of change of the likelihood distribution (C) Mean absolute values of the second order rate of change of the likelihood distribution (mean $\pm SD$) (D) The rate of change of the likelihood of data between successive K values (ΔK). The modal value of this distribution is considered the true value of K for the data. Plot created using *POPHELP* (Francis, 2017).

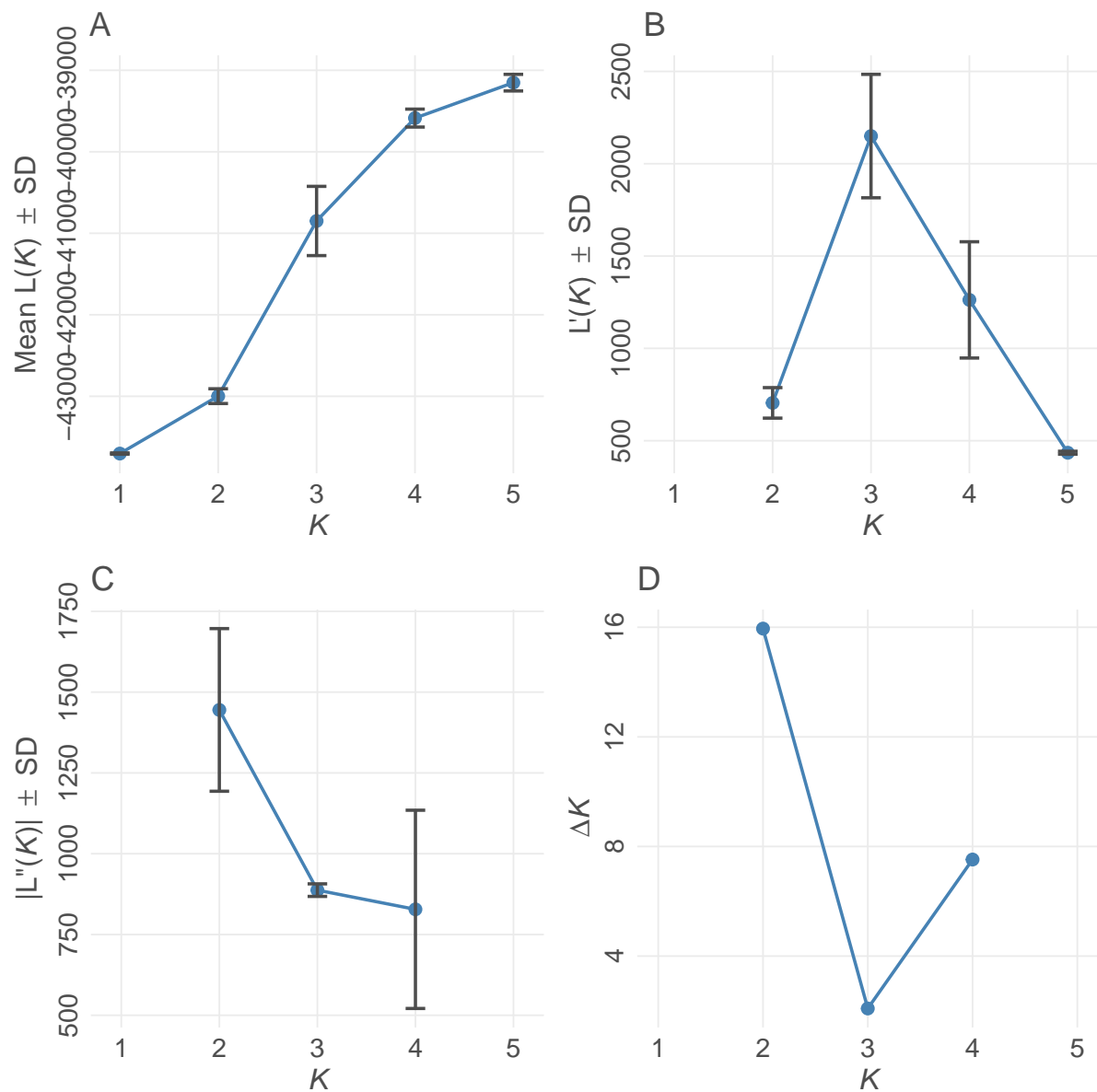


Figure 3.14. Evanno method for optimal value of K in *A. fowleri* STRUCTURE analysis (Evanno et al., 2005). See Fig. 3.13 for full figure caption.

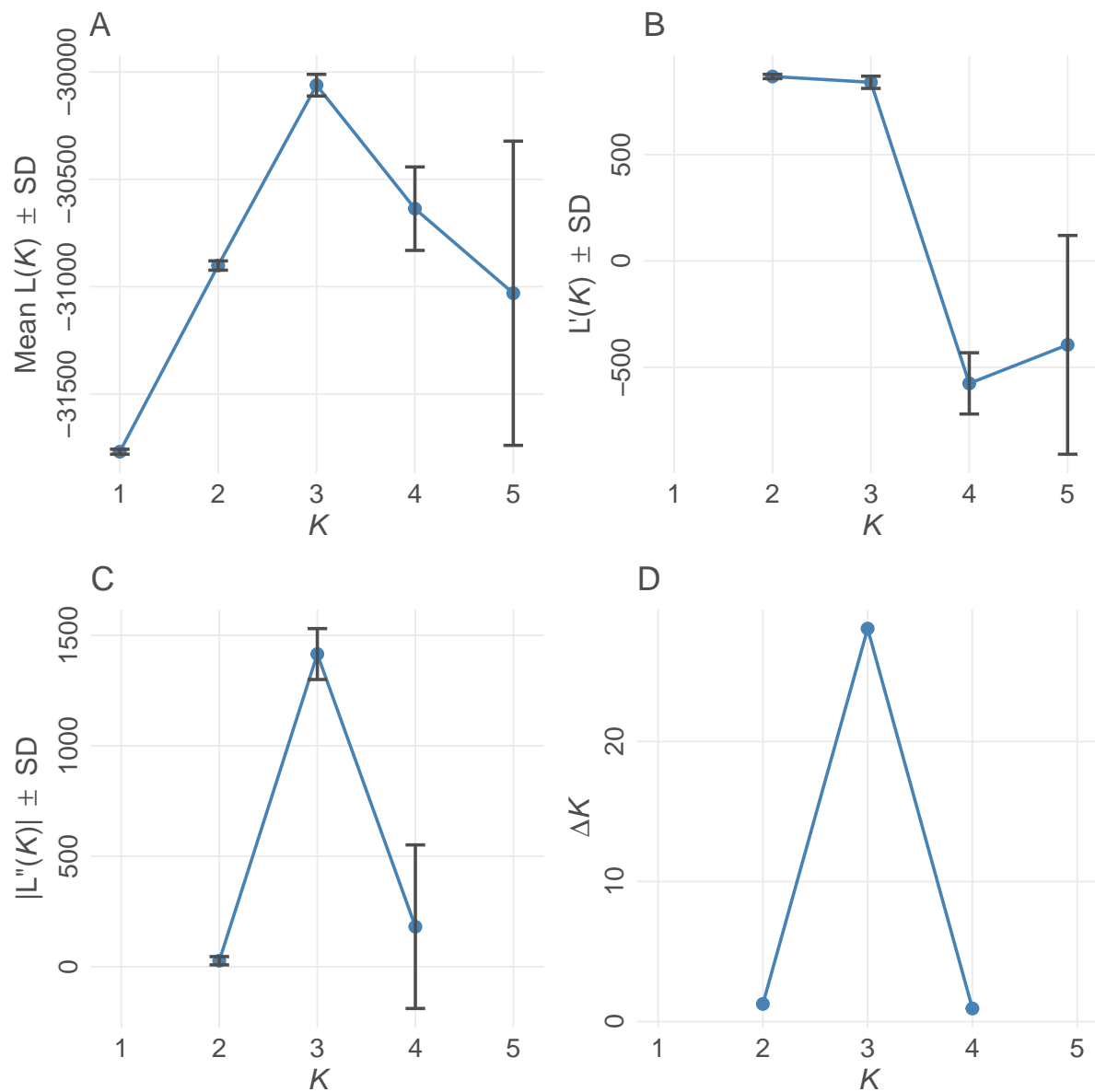


Figure 3.15. Evanno method for optimal value of K in *A. terrestris* STRUCTURE analysis (Evanno et al., 2005). See Fig. 3.13 for full figure caption.

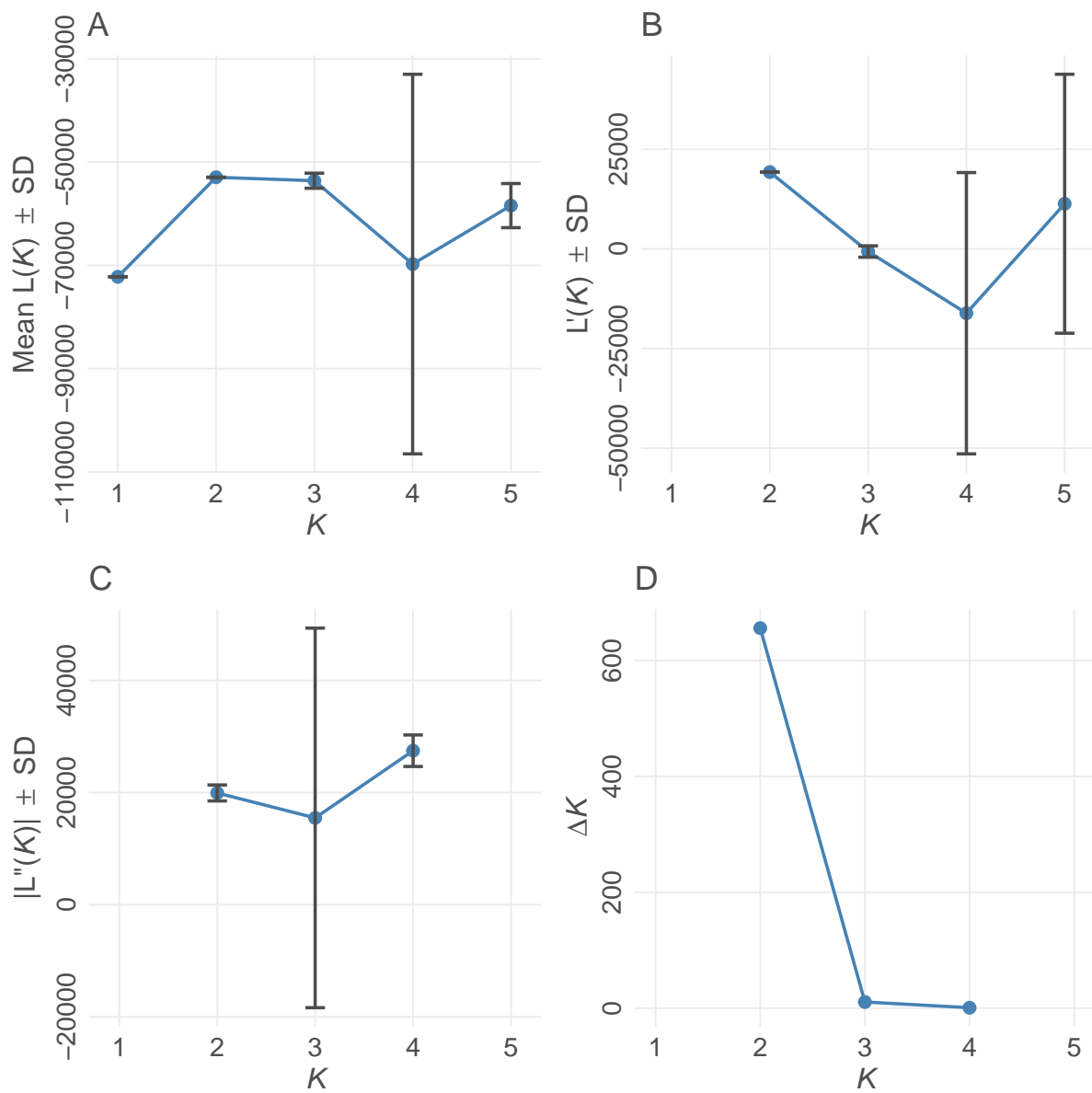


Figure 3.16. Evanno method for optimal value of K in *A. woodhousii* STRUCTURE analysis (Evanno et al., 2005). See Fig. 3.13 for full figure caption.

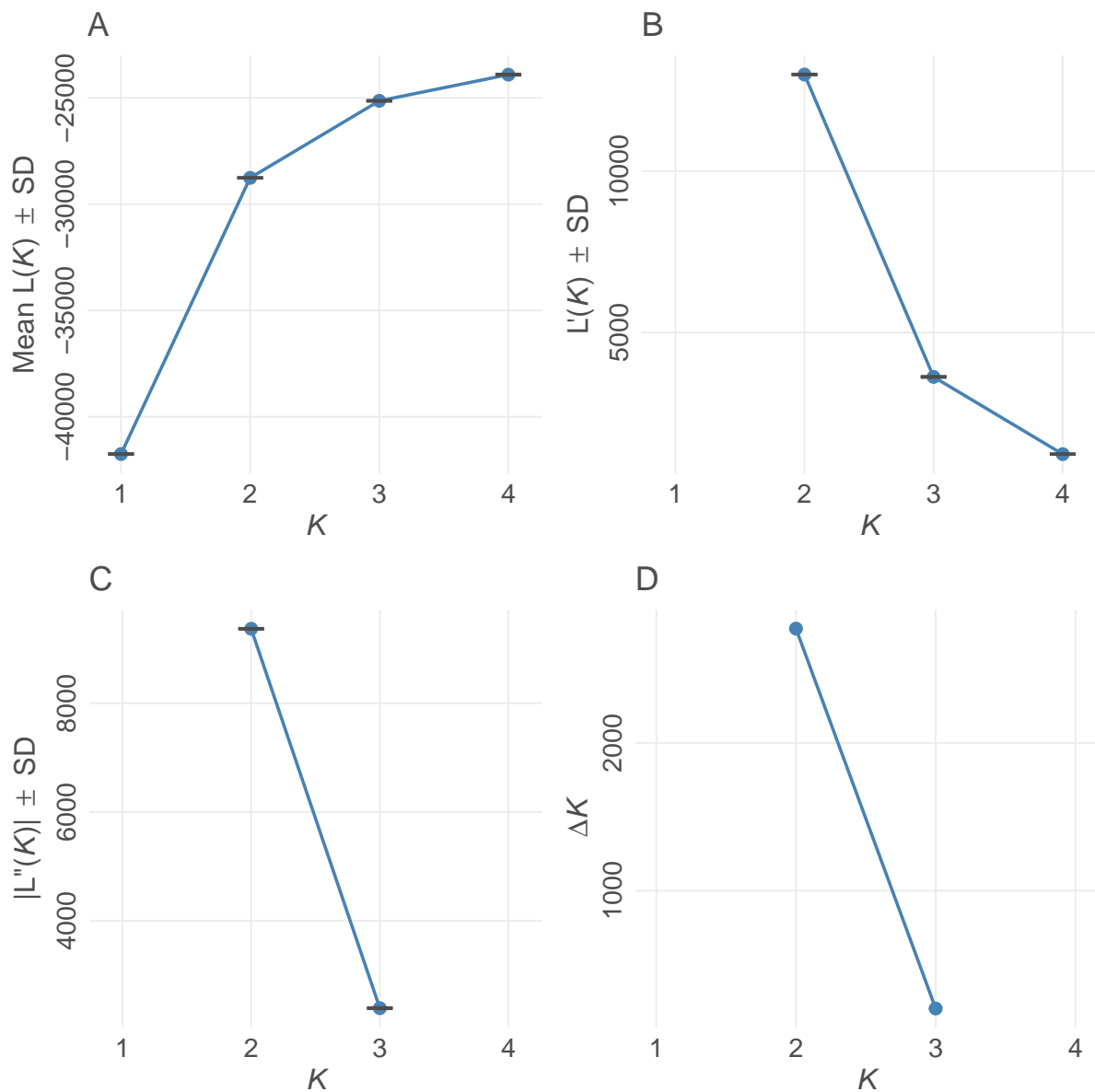


Figure 3.17. Evanno method for optimal value of K in the combined *A. fowleri* and *A. woodhousii* STRUCTURE analysis (Evanno et al., 2005). See Fig. 3.13 for full figure caption.

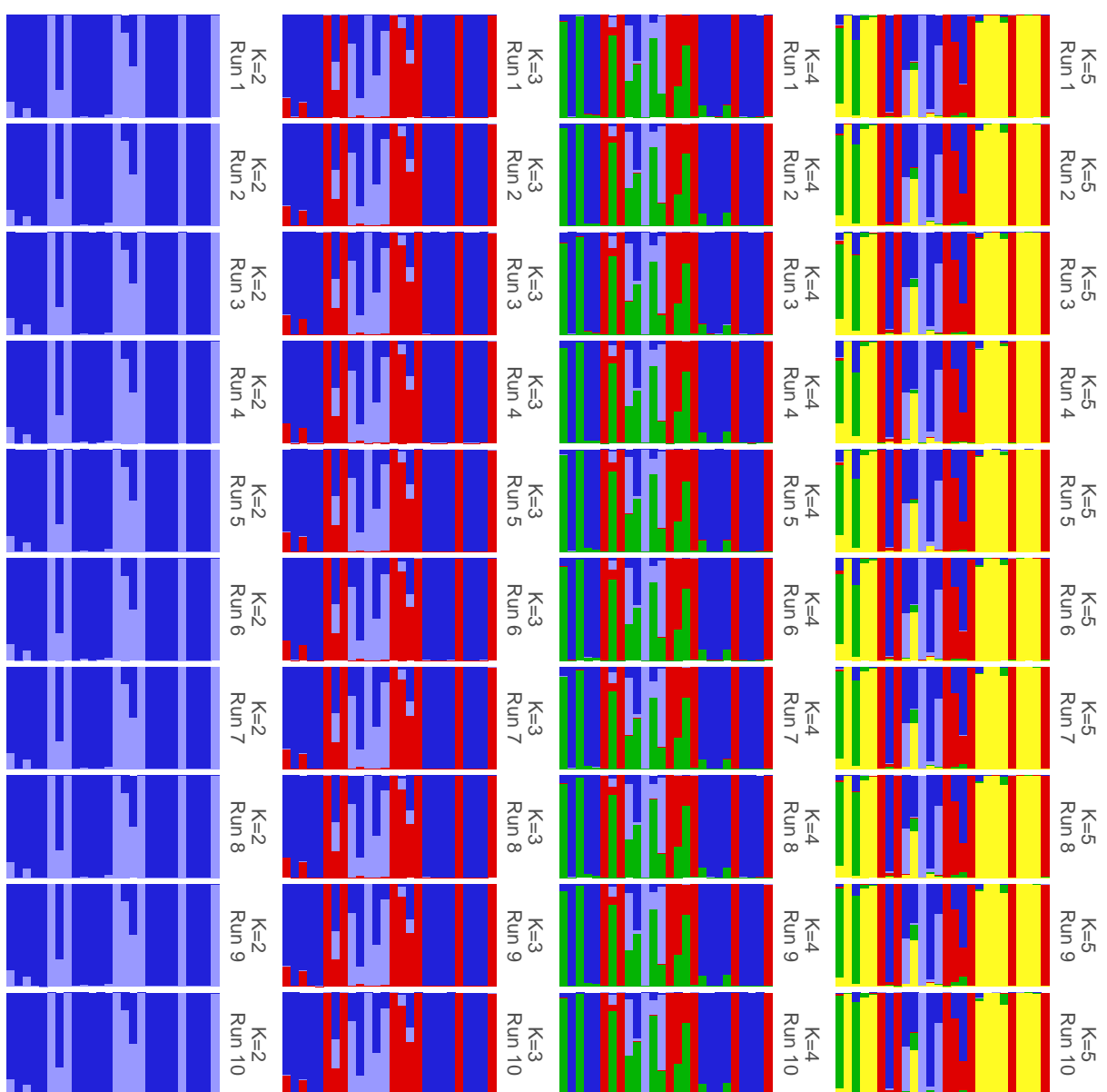


Figure 3.18. Results of each independent *A. americanus* STRUCTURE run (rows) for each value of K (columns) showing convergence among runs with the same value for K. Plot was created with POPHELPER (Francis, 2017).

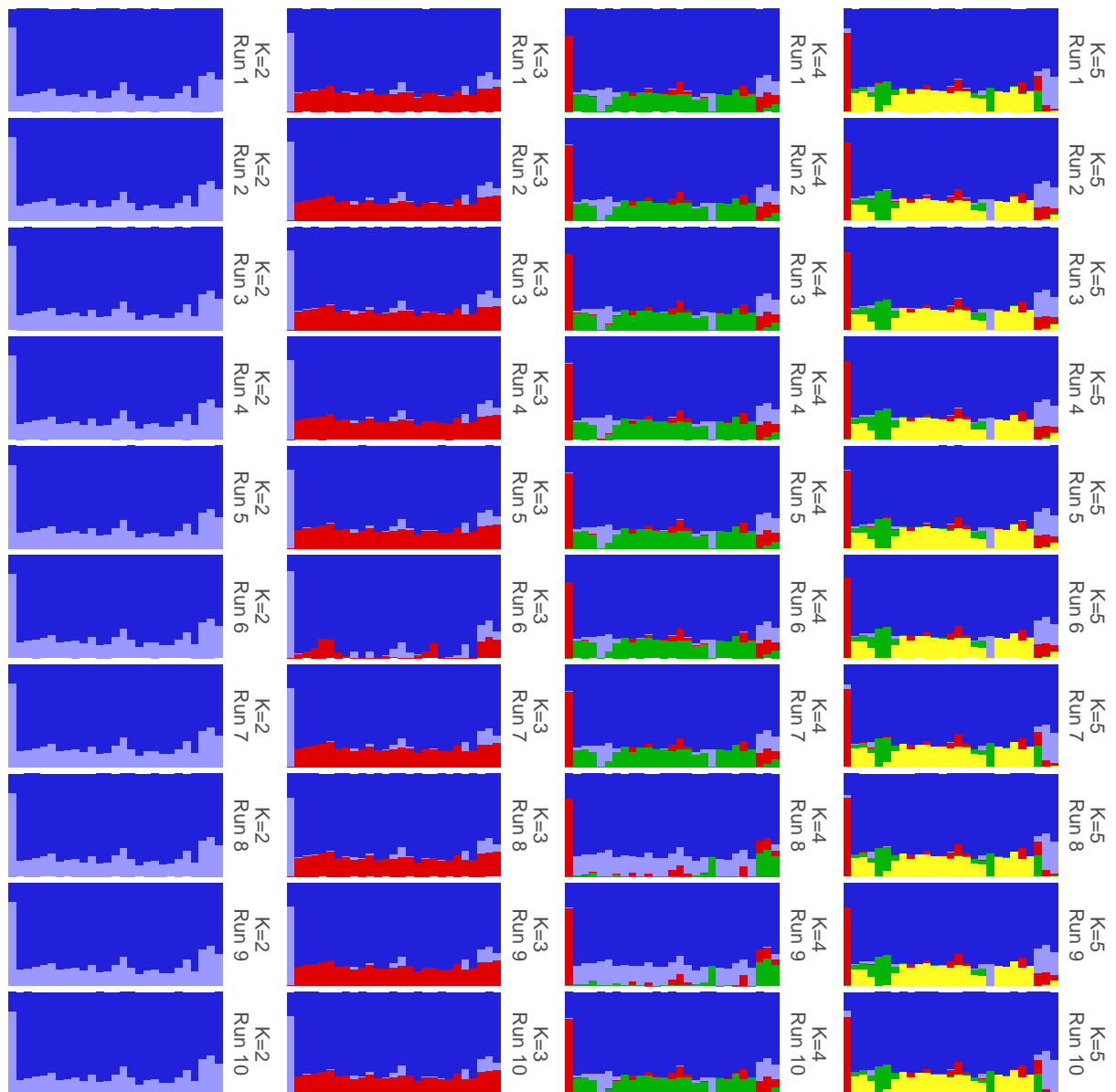


Figure 3.19. Results of each independent *A. fowleri* *STRUCTURE* run (rows) for each value of K (columns) showing convergence among runs with the same value for K . Plot was created with *POPHELPER* (Francis, 2017).

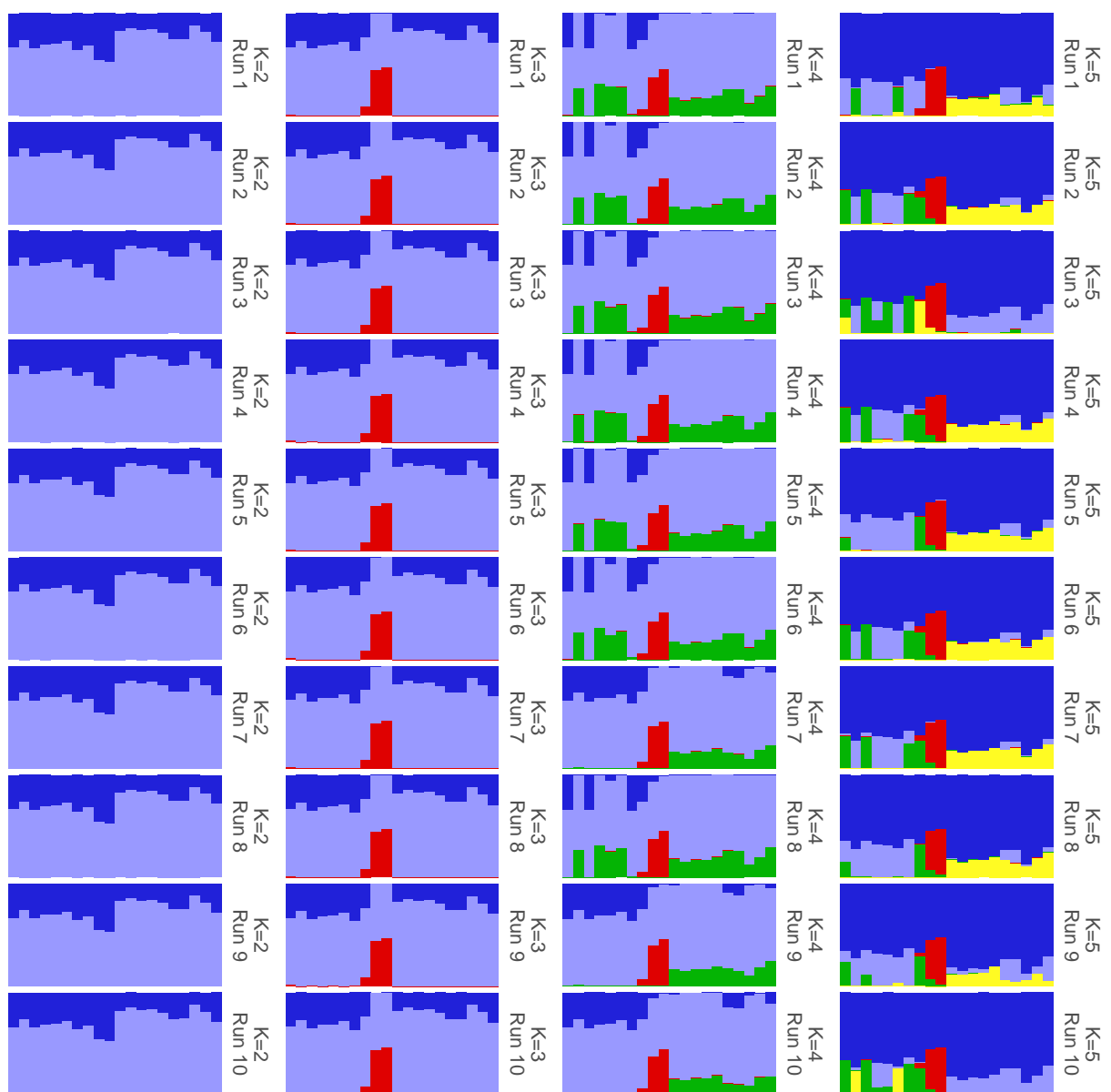


Figure 3.20. Results of each independent *A. terrestris* *STRUCTURE* run (rows) for each value of K (columns) showing convergence among runs with the same value for K . Plot was created with *POPHELPER* (Francis, 2017).

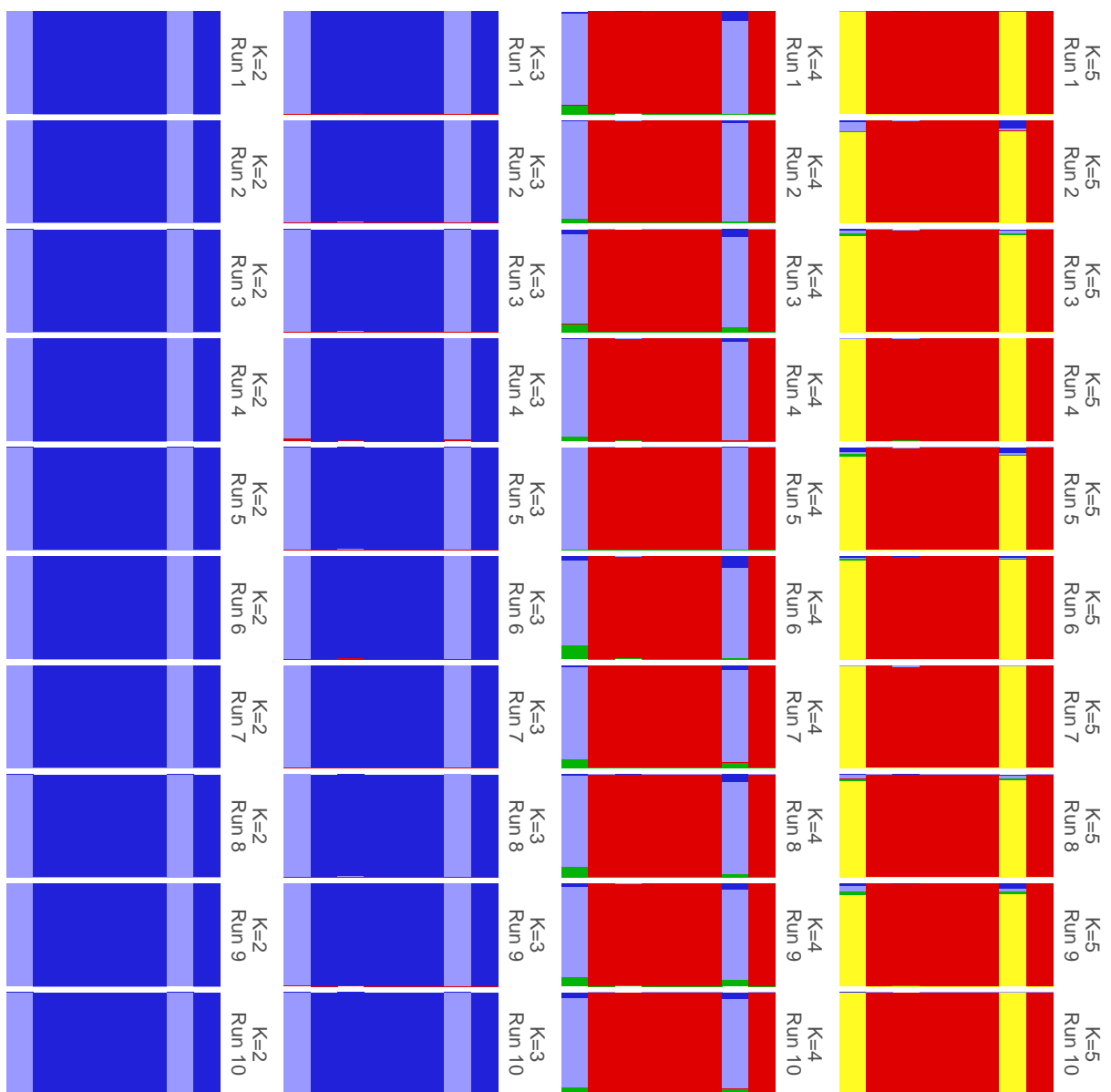


Figure 3.21. Results of each independent *A. americanus* *STRUCTURE* run (rows) for each value of K (columns) showing convergence among runs with the same value for K. Plot was created with *POPHelper* (Francis, 2017).

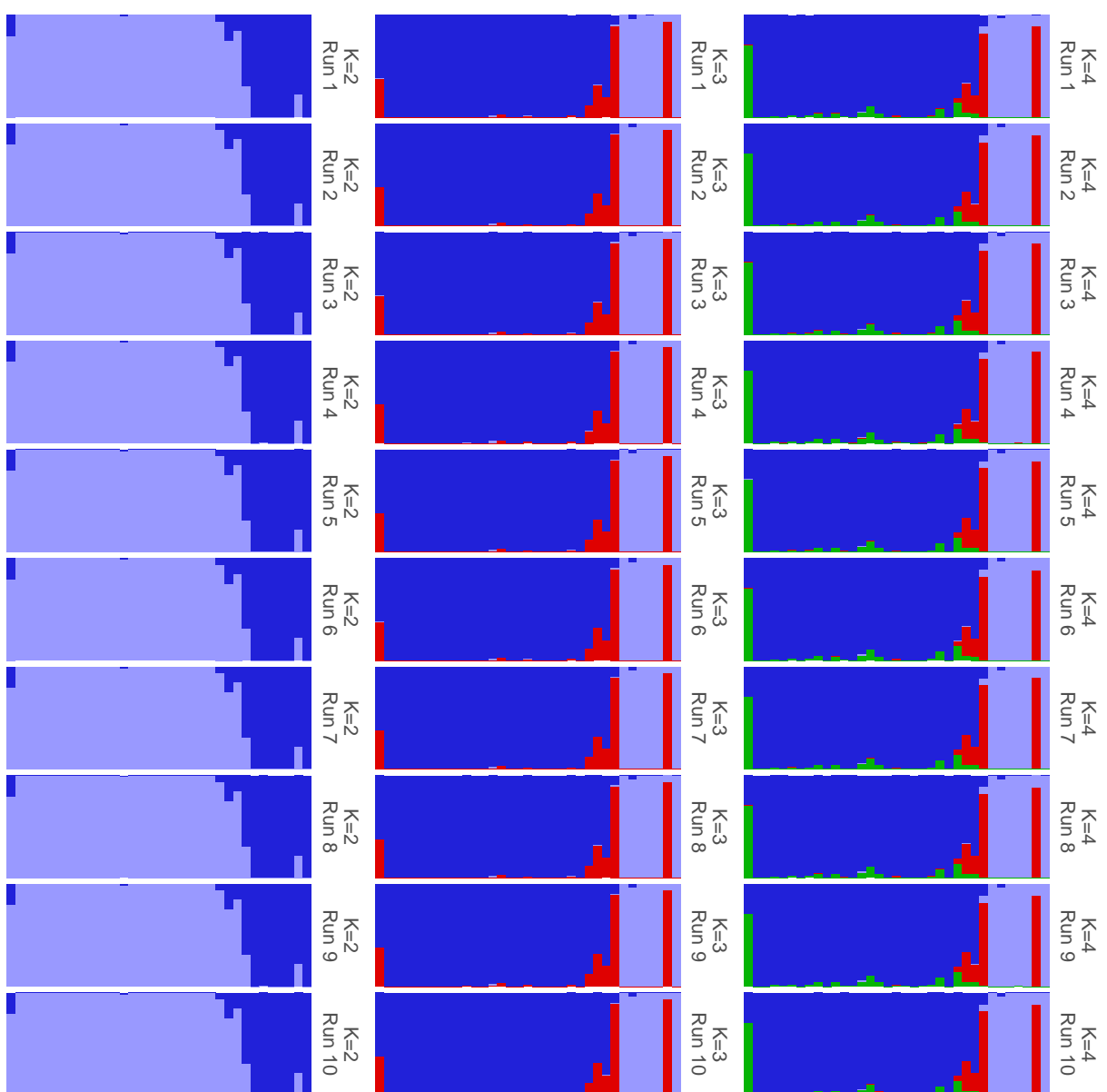


Figure 3.22. Results of each independent combined *A. fowleri* and *A. americanus* *STRUCTURE* run (rows) for each value of K (columns) showing convergence among runs with the same value for K. Plot was created with *POPHELPER* (Francis, 2017).

3.6 Tables

Table 3.1. Samples used in this study

ID	Sample ID	Species	Latitude	Longitude	Passed Filtering	Phycoeval	Structure
003	AHT 2544	<i>quercicus</i>	30.99523	-86.23332	X	X	
004	AHT 2564	<i>terrestris</i>	31.55752	-84.04267	X	X	X
006	AHT 3413	<i>fowleri</i>	33.36940	-88.12941	X		X
009	AHT 3428	<i>terrestris</i>	31.12679	-86.54755	X		X
010	AHT 3459	<i>americanus</i>	34.88028	-87.71849	X		X
011	AHT 3460	<i>americanus</i>	33.78013	-85.58421	X		X
012	AHT 3461	<i>americanus</i>	34.88779	-87.74103	X		X
013	AHT 3462	<i>americanus</i>	33.77001	-85.55434	X		X
014	AHT 3463	<i>americanus</i>	33.71125	-85.59762	X		X
015	AHT 3658	<i>fowleri</i>	32.85842	-86.39697	X		X
016	AHT 3665	<i>fowleri</i>	32.81220	-86.17698	X		X
017	AHT 3813	<i>terrestris</i>	31.13854	-86.53906	X		
018	AHT 3833	<i>terrestris</i>	31.00422	-85.03427	X		X
021	AHT 4373	<i>americanus</i>	38.94913	-95.39818	X		X
022	AHT 5276	<i>terrestris</i>	31.55613	-86.82514			
023	AHT 5277	<i>terrestris</i>	31.15830	-86.55430	X		X

Continued on next page

Table 3.1 – continued from previous page

ID	Sample ID	Species	Latitude	Longitude	Passed Filtering	Phycoeval	Structure
024	AHT 5278	<i>terrestris</i>	31.16105	-86.69868	X		X
025	HERA 10025	<i>fowleri</i>	37.11151	-84.11812	X	X	X
026	HERA 10233	<i>americanus</i>	39.86453	-85.01037	X	X	X
027	HERA 10239	<i>americanus</i>	38.99151	-92.31078	X		X
028	HERA 10248	<i>americanus</i>	41.27319	-73.38974	X		X
029	HERA 10255	<i>americanus</i>	37.11151	-84.11812	X		X
030	HERA 10350	<i>americanus</i>	45.51396	-69.95928	X	X	X
031	HERA 10372	<i>americanus</i>	42.22795	-79.36759	X		X
032	HERA 10396	<i>fowleri</i>	41.80663	-72.73281	X	X	X
033	HERA 10484	<i>marina</i>	25.61296	-80.56606			
034	HERA 10493	<i>fowleri</i>	39.08588	-75.56844	X	X	X
035	HERA 11976	<i>americanus</i>	43.51819	-71.42336	X		X
036	HERA 13722	<i>fowleri</i>	36.55514	-89.18929			
037	HERA 14196	<i>retiformis</i>	33.34906	-112.49010			
038	HERA 14926	<i>microscaphus</i>	33.73033	-113.98078			
039	HERA 15787	<i>americanus</i>	38.88546	-95.29399	X	X	X

Continued on next page

Table 3.1 – continued from previous page

ID	Sample ID	Species	Latitude	Longitude	Passed Filtering	Phycoeval	Structure
040	HERA 20415	<i>woodhousii</i>	34.31743	-92.94602	X	X	X
041	HERA 20514	<i>fowleri</i>	33.95140	-83.36715	X		X
042	INHS 16273	<i>americanus</i>	42.30245	-89.55950	X		X
043	INHS 17016	<i>americanus</i>	37.46121	-88.18728	X		X
044	INHS 19127	<i>fowleri</i>	41.58247	-88.07273			
045	INHS 21799	<i>americanus</i>	46.01258	-94.26710	X		X
046	KAC 016	<i>terrestris</i>	30.54819	-86.93067	X		X
061	KAC 053	<i>fowleri</i>	32.78044	-86.73877			
062	KAC 060	<i>speciosus</i>	27.69185	-99.71955	X		
063	KAC 062	<i>punctatus</i>	29.43603	-103.50564	X		
064	KAC 063	<i>speciosus</i>	29.29522	-103.92916	X		
065	KAC 064	<i>speciosus</i>	29.29522	-103.92916	X		
066	KAC 065	<i>terrestris</i>	30.43282	-81.64088	X		
067	KAC 066	<i>terrestris</i>	30.43282	-81.64088			
068	KAC 067	<i>terrestris</i>	30.43282	-81.64088			
069	KAC 070	<i>americanus</i>	34.79963	-84.57678	X		X

Continued on next page

Table 3.1 – continued from previous page

ID	Sample ID	Species	Latitude	Longitude	Passed Filtering	Phycoeval	Structure
071	KAC 074	<i>terrestris</i>	30.77430	-85.22690	X		X
130	KAC 137	<i>fowleri</i>	33.01461	-86.60953	X		X
150	KAC 157	<i>fowleri</i>	32.43769	-85.63620	X		X
158	KAC 165	<i>fowleri</i>	32.66356	-85.48498	X		X
159	KAC 166	<i>fowleri</i>	32.66356	-85.48498	X		X
163	KAC 174	<i>fowleri</i>	32.62938	-85.63828	X		X
164	KAC 175	<i>fowleri</i>	32.64849	-85.64711	X		X
167	KAC 178	<i>fowleri</i>	32.38644	-85.23561			
168	KAC 179	<i>fowleri</i>	32.38644	-85.23561	X		X
169	KAC 180	<i>fowleri</i>	32.38644	-85.23561	X		X
175	KAC 186	<i>fowleri</i>	32.38579	-85.23565	X		X
190	KAC t2018-02-17-01	<i>americanus</i>	33.55274	-85.82913	X		X
191	KAC t2018-02-17-04	<i>americanus</i>	33.48548	-85.88857	X		X
196	KAC t2018-03-10-2	<i>fowleri</i>	32.93116	-86.08465	X		X
200	KAC t2018-08-18-1	<i>terrestris</i>	30.66902	-81.44013	X		X
201	KAC t2018-08-18-2	<i>terrestris</i>	30.66902	-81.44013			

Continued on next page

Table 3.1 – continued from previous page

ID	Sample ID	Species	Latitude	Longitude	Passed Filtering	Phycoeval	Structure
202	KAC t2018-08-18-3	<i>terrestris</i>	30.43282	-81.64088	X	X	X
203	KAC t2018-08-18-4	<i>terrestris</i>	30.66902	-81.44013	X		X
205	KAC t2019-08-25-2	<i>fowleri</i>	34.21852	-87.36662	X		X
206	KAC 202	<i>fowleri</i>	33.25104	-86.43850	X		X
207	KAC 203	<i>fowleri</i>	32.62294	-85.49660	X		X
208	KAC 204	<i>fowleri</i>	32.62294	-85.49660	X		X
229	KAC 226	<i>fowleri</i>	32.48119	-85.79838	X		X
230	KAC 230	<i>terrestris</i>	30.80933	-86.77686	X		X
231	KAC 232	<i>terrestris</i>	30.80922	-86.78994	X		X
231	KAC 232	<i>terrestris</i>	30.80922	-86.78994	X		X
232	KAC 233	<i>terrestris</i>	30.80922	-86.78994	X		X
233	KAC 234	<i>terrestris</i>	30.80922	-86.78994	X		X
234	KAC 236	<i>terrestris</i>	30.82632	-86.80258	X		X
235	KAC 237	<i>terrestris</i>	30.83733	-86.77630	X		X
236	KAC 238	<i>terrestris</i>	30.82433	-86.76284	X		X
237	KAC 239	<i>terrestris</i>	30.80162	-86.76659	X		X

Continued on next page

Table 3.1 – continued from previous page

ID	Sample ID	Species	Latitude	Longitude	Passed Filtering	Phycoeval	Structure
238	KAC 240	<i>fowleri</i>	32.64328	-85.37114	X		X
239	KAC 241	<i>fowleri</i>	32.64328	-85.37114	X		X
240	KAC 242	<i>americanus</i>	34.50446	-85.63768	X		X
241	KAC 243	<i>nebulifer</i>	30.39140	-90.62049	X	X	
242	KAC 244	<i>fowleri</i>	32.89261	-93.88756	X		X
243	MSB 100793	<i>microscaphus</i>	37.27154	-114.46478	X	X	
244	MSB 100800	<i>woodhousii</i>	36.73612	-114.21972	X	X	X
245	MSB 100913	<i>microscaphus</i>	33.28038	-108.08868		X	
246	MSB 104548	<i>woodhousii</i>	36.49094	-103.20838			
247	MSB 104570	<i>fowleri</i>	34.00087	-95.38229			
248	MSB 104571	<i>americanus</i>	34.00917	-95.38058			
249	MSB 104608	<i>americanus</i>	34.00367	-94.82670			
250	MSB 104644	<i>americanus</i>	36.95124	-94.27782	X		X
251	MSB 104677	<i>cognatus</i>	46.39834	-97.20927	X	X	
252	MSB 104681	<i>hemiophrys</i>	46.47076	-97.04604	X		X
253	MSB 104731	<i>woodhousii</i>	42.61091	-100.65607	X	X	X

Continued on next page

Table 3.1 – continued from previous page

ID	Sample ID	Species	Latitude	Longitude	Passed Filtering	Phycoeval	Structure
254	MSB 75646	<i>woodhousii</i>	33.36365	-104.34282	X	X	X
255	MSB 92689	<i>baxteri</i>	41.21182	-105.82558			
256	MSB 92691	<i>baxteri</i>	41.21182	-105.82558	X	X	
257	MSB 92692	<i>baxteri</i>	41.21182	-105.82558	X	X	
258	MSB 96528	<i>debilis</i>	32.58239	-107.46348			
259	MSB 98058	<i>woodhousii</i>	32.83360	-108.60900			
260	MSB 98065	<i>cognatus</i>	32.63240	-108.73800		X	
261	KAC t1020	<i>terrestris</i>	31.10783	-86.62247	X		X
264	KAC t2004	<i>americanus</i>	33.58295	-85.73524	X		X
265	KAC t2015	<i>americanus</i>	33.58435	-85.74064	X		X
267	KAC t2040	<i>americanus</i>	33.58295	-85.73539	X		X
269	KAC t3040	<i>fowleri</i>	32.38644	-85.23561			
270	UTEP 18705	<i>woodhousii</i>	32.45198	-106.88317	X	X	X
271	UTEP 19941	<i>fowleri</i>	34.79137	-88.95715	X	X	X
272	UTEP 19943	<i>fowleri</i>	33.81998	-88.29533	X		X
273	UTEP 19947	<i>terrestris</i>	31.22432	-88.77548	X	X	X

Continued on next page

Table 3.1 – continued from previous page

ID	Sample ID	Species	Latitude	Longitude	Passed Filtering	Phycoeval	Structure
274	UTEP 20105	<i>woodhousii</i>	33.62853	-103.08198	X		X
275	UTEP 20482	<i>woodhousii</i>	32.90708	-94.74945	X		X
276	UTEP 20921	<i>americanus</i>	35.55405	-91.83443	X		X
277	UTEP 21284	<i>debilis</i>	31.25968	-105.33402		X	
278	UTEP 21286	<i>speciosus</i>	31.70140	-105.47958			
279	UTEP 21724	<i>speciosus</i>	31.26087	-104.60168			
280	UTEP 21881	<i>cognatus</i>	35.53600	-100.44035		X	
281	UTEP 21884	<i>speciosus</i>	32.75472	-101.43208	X		
282	UTEP 21885	<i>speciosus</i>	32.20195	-100.34345	X		X
283	UTEP 21886	<i>woodhousii</i>	35.07800	-100.43392	X		X

Chapter 4

Comparison of Linked versus Unlinked Character Models for Species Tree Inference

4.1 Introduction

Current model-based methods of species tree inference require biologists to make difficult decisions about their genomic data. They must decide whether to assume (1) sites in their alignments are each inherited independently (“unlinked”), or (2) groups of sites are inherited together (“linked”). If assuming the former, they must then decide whether to analyze all of their data or only putatively unlinked variable sites. Our goal in this chapter is to use simulated data to help guide these choices by comparing the robustness of different approaches to errors that are likely common in high-throughput genetic datasets.

Reduced-representation genomic data sets acquired from high-throughput instruments are becoming commonplace in phylogenetics (Leaché & Oaks, 2017), and usually comprise hundreds to thousands of loci from 50 to several thousand nucleotides long. Full likelihood approaches for inferring species trees from such datasets can be classified into two groups based on how they model the evolution of orthologous DNA sites along gene trees within the species tree—those that assume (1) each site evolved along its own gene tree (i.e., each site is “unlinked”) (Bryant et al., 2012; De Maio et al., 2015), or (2) contiguous, linked sites evolved along a shared gene tree (Heled & Drummond, 2010; Liu & Pearl, 2007; Ogilvie et al., 2017; Yang, 2015). We will refer to these as unlinked and linked-character models, respectively. For both models, the gene tree of each locus (whether each locus

is a single site or a segment of linked sites) is assumed to be independent of the gene trees of all other loci, conditional on the species tree. Methods using linked character models become computationally expensive as the number of loci grows large, due to the estimation or numerical integration of all of the gene trees (Ogilvie et al., 2017; Yang, 2015). Unlinked-character models on the other hand are more tractable for a large number of loci, because estimating individual gene trees is avoided by analytically integrating over all possible gene trees (Bryant et al., 2012; De Maio et al., 2015). Whereas unlinked-character models can accommodate a larger number of loci than linked-character models, most genetic data sets comprise linked sites and unlinked-character models are unable to utilize the aggregate information about ancestry contained in such linked sites.

Investigators are thus faced with decisions about how best to use their data to infer a species tree. Should they use a linked-character method that assumes the sites within each locus evolved along a shared gene tree? Ideally, the answer would be “yes,” however this is not always computationally feasible and the model could be violated by intralocus recombination. Alternatively, should investigators remove all but one single-nucleotide polymorphism (SNP) from each locus and use an unlinked-character model? Or, perhaps they should apply the unlinked-character method to all of their sites, even if this violates the assumption that each site evolved along an independent gene tree. Important considerations in such decisions include the sources of error and bias that result from reduced-representation protocols, high-throughput sequencing technologies, and the processing of these data.

Most reduced-representation sequencing workflows employ amplification of DNA using polymerase chain reaction (PCR) which can introduce mutational error at a rate of up to 1.5×10^{-5} substitutions per base (Potapov & Ong, 2017). Furthermore, current high-throughput sequencing technologies have non-negligible rates of error. For example, Illumina sequencing platforms have been shown to have error rates as high as 0.25% per base (Pfeiffer et al., 2018). In hope of removing such errors, it is common for biologists to filter out variants that are not found above some minimum frequency threshold (Linck & Battey, 2019; Rochette et al., 2019). The effect of this filtering will be more pronounced

in data sets with low or highly variable coverage. Also, to avoid aligning paralogous sequences, it is common to remove loci that exceed an upper threshold on the number of variable sites (Harvey et al., 2015). These processing steps can introduce errors and acquisition biases, which have been shown to affect estimates derived from the assembled alignments (Harvey et al., 2015; Huang & Knowles, 2016; Linck & Battey, 2019). Given these issues are likely common in high-throughput genomic data, downstream decisions about what methods to use and what data to include in analyses should consider how sensitive the results might be to errors and biases introduced during data collection and processing.

Our goal is to determine whether linked and unlinked character models differ in their robustness to errors in reduced-representation genomic data, and whether it is better to use all sites or only SNPs for unlinked character methods. Linked-character models can leverage shared information among linked sites about each underlying gene tree. Thus, these models might be able to correctly infer the general shape and depth of a gene tree, even if the haplotypes at some of the tips have errors. Unlinked character models have very little information about each gene tree, and rely on the frequency of allele counts across many characters to inform the model about the relative probabilities of all possible gene trees. Given this reliance on accurate allele count frequencies, we predict that unlinked character models will be more sensitive to errors and acquisition biases in genomic data. To test this prediction that linked character models are more robust to the types of errors contained in reduced-representation data, we simulated data sets with varying degrees of errors related to miscalling rare alleles and heterozygous sites. Our results support this prediction, but also show that with only two species, the region of parameter space where there are differences between linked and unlinked character models is quite limited. Further work is needed to determine whether this difference in robustness between linked and unlinked character models will increase for larger species trees.

4.2 Methods

4.2.1 Simulations of error-free data sets

For our simulations, we assumed a simple two-tipped species tree with one ancestral population with a constant effective size of N_e^R that diverged at time τ into two descendant populations (terminal branches) with constant effective sizes of N_e^{D1} and N_e^{D2} (Fig. 4.1). For two diploid individuals sampled from each of the terminal populations (4 sampled gene copies per population), we simulated 100,000 orthologous biallelic characters under a finite-sites, continuous-time Markov chain (CTMC) model of evolution. We simulated 100 data sets comprised of loci of four different lengths—1000, 500, 250, and 1 characters. We assume each locus is effectively unlinked and has no intra-locus recombination; i.e., each locus evolved along a single gene tree that is independent of the other loci, conditional on the species tree. We chose this simple species tree model for our simulations to help ensure any differences in estimation accuracy or precision were due to differences in the underlying linked and unlinked character models, and *not* due to differences in numerical algorithms for searching species and gene tree space. Furthermore, we simulated biallelic characters, because unlinked-character multi-species coalescent models (Bryant et al., 2012; Oaks, 2019) that are most comparable to linked-character models (Heled & Drummond, 2010; Ogilvie et al., 2017) are limited to characters with (at most) two states.

We simulated the two-tipped species trees under a pure-birth process (Yule, 1925) with a birth rate of 10 using the *Python* package *DendroPy* (Version 4.40, Commit eb69003; Sukumaran & Holder, 2010). This is equivalent to the time of divergence between the two species being Exponentially distributed with a mean of 0.05 substitutions per site. We drew population sizes for each branch of the species tree from a Gamma distribution with a shape of 5.0 and mean of 0.002. We simulated 100, 200, 400, and 100,000 gene trees for data sets with loci of length 1000, 500, 250, and 1, respectively, using the contained coalescent implemented in *DendroPy*. We simulated linked biallelic character alignments

using *Seq-Gen* (Version 1.3.4) (Rambaut & Grass, 1997) with a GTR model with base frequencies of A and C equal to 0 and base frequencies of G and T equal to 0.5. The transition rate for all base changes was 0, except for the rate between G and T which was 1.0.

4.2.2 Introducing Site-pattern Errors

From each simulated dataset containing linked characters described above, we created four datasets by introducing two types of errors at two levels of frequency. The first type of error we introduced was changing singleton character patterns (i.e., characters for which one gene copy was different from the other seven gene copies) to invariant patterns by changing the singleton character state to match the other gene copies. We introduced this change to all singleton site patterns with a probability of 0.2 and 0.4 to create two datasets from each simulated dataset. The second type of error we introduced was missing heterozygous gene copies. To do this, we randomly paired gene copies from within each species to create two diploid genotypes for each locus, and with a probability of 0.2 or 0.4 we randomly replaced one allele of each genotype with the other. For the unlinked character dataset comprised of a single site per locus, we only simulated singleton character pattern error at a probability of 0.4.

4.2.3 Assessing Sensitivity to Errors

For each simulated data set with loci of 250, 500, and 1000 characters, we approximated the posterior distribution of the divergence time (τ) and effective population sizes (N_e^R , N_e^{D1} , and N_e^{D2}) under an unlinked-character model using *ecoevolity* (Version 0.3.2, Commit a7e9bf2; Oaks, 2019) and a linked-character model using the *StarBEAST2* package (Version 0.15.1; Ogilvie et al., 2017) in *BEAST2* (Version 2.5.2; Bouckaert et al., 2014). For both methods, we specified a CTMC model of character evolution and prior distributions that matched the model and distributions from which the data were generated. The prior on the effective size of the root population in the original implementation of *ecoevolity* was parameterized to be relative to the mean effective size of the descendant

populations. We added an option to *ecoevolity* to compile a version where the prior is specified as the absolute effective size of the root population, which matches the model in *StarBEAST2* and the model we used to generate the data. The linkage of sites within loci of our simulated data violates the unlinked-character model of *ecoevolity* (Bryant et al., 2012; Oaks, 2019). Therefore, we also analyzed each data set with *ecoevolity* after selecting, at most, one variable character from each locus; loci without variable sites were excluded.

We analyzed the data sets simulated with 1-character per locus (i.e., unlinked data) with *ecoevolity*. Our goal with these analyses was to verify that the generative model of our simulation pipeline matched the underlying model of *ecoevolity*, and to confirm that any behavior of the method with the other simulated data sets was not being caused by the linkage violation.

For *ecoevolity*, we ran four independent Markov chain Monte Carlo (MCMC) analyses with 75,000 steps and a sample frequency of 50 steps. For *StarBEAST2*, we ran two independent MCMC analyses with 20 million steps and a sample frequency of 5000 steps. To assess convergence and mixing of the *ecoevolity* and *StarBEAST2* MCMC chains, we computed the effective sample size (ESS; Gong & Flegal, 2016) and potential scale reduction factor (PSRF; the square root of Equation 1.1 in Brooks & Gelman, 1998) from the samples of each parameter, and considered an ESS value greater than 200 and PSRF less than 1.2 (Brooks & Gelman, 1998) to indicate adequate convergence and mixing of the chains. Based on preliminary analyses of simulated data sets without errors, we chose to discard the first 501 and 201 samples from the MCMC chains of *ecoevolity* and *StarBEAST2*, leaving 4000 and 7600 posterior samples for each data set, respectively.

4.2.4 Project repository

The full history of this project has been version-controlled and is available at <https://github.com/kerrycobb/align-error-sp-tree-sim>, and includes all of the data and scripts necessary to produce our results.

4.3 Results

4.3.1 Behavior of linked (*StarBEAST2*) versus unlinked (*ecoevolity*) character models

The divergence times estimated by the linked-character method, *StarBEAST2*, were very accurate and precise for all alignment lengths and types and degrees errors, despite poor MCMC mixing (i.e., low ESS values) for shorter loci (Figs. 4.2–4.4). For data sets without error, the unlinked-character method, *ecoevolity*, estimated divergence times with similar accuracy and precision as *StarBEAST2* when all characters are analyzed (Figs. 4.2–4.4). However when alignments contained errors, *ecoevolity* underestimated very recent divergence times with increasing severity as the frequency of errors increased (Figs. 4.2–4.4); estimates of older divergence times were unaffected.

The biased underestimation of divergence times by *ecoevolity* in the face of errors was coupled with overestimation of the ancestral effective population sizes (Figs. 4.5–4.7). When analyzing the alignments without errors, *ecoevolity* essentially returned the prior distribution on the effective size of the ancestral population (Figs. 4.5–4.7). Despite poor MCMC mixing, *StarBEAST2* consistently estimated the effective size of the ancestral population better than *ecoevolity* and was unaffected by errors in the data (Figs. 4.5–4.7), and the precision of *StarBEAST2*'s estimates of N_e^R increased with locus length.

Estimates of the effective size of the descendant populations are largely similar between *StarBEAST2* and *ecoevolity*; both methods underestimate the descendant population sizes when the data sets contain errors, and this downward bias is generally worse for *ecoevolity* (Figs. 4.8–4.10). The degree of underestimation increases with the rate of errors in the data sets for both *StarBEAST2* and *ecoevolity*, and the results were largely consistent across different locus lengths. (Figs. 4.8–4.10).

When we apply *ecoevolity* to data sets simulated with unlinked characters (i.e., data sets simulated with 1-character per locus), we see the same patterns of biased parameter estimates in response to errors (Fig. 4.11) as we did with the linked loci (Figs. 4.2–4.4).

These results rule out the possibility that the greater sensitivity of *ecoevolity* to the errors we simulated is due to violation of the method's assumption that all characters are unlinked.

4.3.2 Analyzing all sites versus SNPs with *ecoevolity*

The unlinked character model implemented in *ecoevolity* assumes that orthologous nucleotide sites evolve independently along separate gene trees. The data however, were simulated under a model assuming that contiguous linked sites evolve along a shared gene tree. It would thus be a violation of the *ecoevolity* model to include all sites in the analysis. However, avoiding this violation by removing all but one variable site per locus drastically reduces the amount of data. When analyzing the simulated data sets without errors, the precision and accuracy of parameter estimates by *ecoevolity* was much greater when all sites of the alignment were used relative to when a single SNP per locus was used despite violating the model (Figs. 4.2–4.10). This was generally true across the different lengths of loci, however, the coverage of credible intervals is lower with longer loci. Analyzing only SNPs does make *ecoevolity* more robust to the errors we introduced. However, this robustness is due to the lack of information in the SNP data leading to wide credible intervals, and in the case of population size parameters, the marginal posteriors essentially match the prior distribution (Figs. 4.8–4.10).

4.3.3 Coverage of credible intervals

The 95% credible intervals for divergence times and effective population sizes estimated from alignments without error in *StarBEAST2* had the expected coverage frequency in that the true value was within approximately 95% of the estimated credible intervals. This was also true for *ecoevolity* when analyzing data sets simulated with un-linked characters (i.e., no linked sites). This coverage behavior is expected, and helps to confirm that our simulation pipeline generated data under the same model used for inference by *StarBEAST2* and *ecoevolity*. As seen previously (Oaks, 2019), analyzing longer linked loci causes the coverage of *ecoevolity* to be lower, due to the violation of the

model's assumption that the sites are unlinked.

4.3.4 MCMC convergence and mixing

Most sets of *StarBEAST2* and *ecoevolity* MCMC chains yielded samples of parameters with a PSRF less than 1.2, indicative of convergence. However, we do see poor mixing ($\text{ESS} < 200$) of the *StarBEAST2* chains as the length of loci decreases (Figs. 4.2–4.10; yellow indicates $\text{ESS} < 200$, red indicates $\text{PSRF} > 1.2$, green indicates both) We only see evidence of poor mixing and convergence for *ecoevolity* when applied to data sets with errors. This is in contrast to *StarBEAST2*, for which the frequency and degree of poor MCMC behavior is largely unaffected by the type or frequency of errors. The proportion of simulation replicates where *StarBEAST2* had an ESS of the ancestral population size less than 200 was high across all analyses (Figs. 4.5–4.7). For the descendant population size, *StarBEAST2* had better ESS values across all analyses, with the exception of rare estimates of essentially zero when analyzing 250 bp loci (Figs. 4.8–4.10).

4.4 Discussion

Phylogeneticists seeking to infer species trees from large, multi-locus data sets are faced with difficult decisions regarding assumptions about linkage across sites and, if assuming all sites are unlinked, what data to include in their analysis. With the caveat that we only explored trees with two species, the results of our simulations provide some guidance for these decisions. As we predicted, the linked-character method we tested, *StarBEAST2*, was more robust to the sequencing errors we simulated than the unlinked character method, *ecoevolity*. However, even with only two species in our simulations, the current computational limitations of linked-character models was apparent from the poor sampling efficiency of the MCMC chains, especially with shorter loci. For data sets with more species and many short loci, linked character models are theoretically appealing, but current implementations may not be computationally feasible. The unlinked character method, *ecoevolity*, was more sensitive to sequence errors, but was still quite robust to

realistic levels of errors and is more computationally feasible thanks to the analytical integration over gene trees.

Overall, for data sets with relatively long loci, as is common with sequence-capture approaches, it might be worth trying a linked-character method. If computationally practical, you stand to benefit from the aggregate information about each gene tree contained in the linked sites of each locus. However, if your loci are shorter, as in restriction-site-associated DNA (RAD) markers, you are likely better off applying an unlinked-character model to all of your data, even though this violates an assumption of the model. Below we discuss why performance differs between methods, locus lengths, and degree of error in the data, and what this means for the analyses of empirical data.

4.4.1 Robustness to character-pattern errors

As predicted, the linked-character model of *StarBEAST2* was more robust to erroneous character patterns in the alignments than the unlinked-character model of *ecoevolity*. This is most evident in the estimates of divergence times, for which the two methods perform very similarly when there are no errors in the data (Row 1 of Figs. 4.2–4.4). When errors are introduced, the divergence time estimates of *StarBEAST2* are unaffected, but *ecoevolity* underestimates recent divergence times as both singleton and heterozygosity errors become more frequent (Rows 2–5 of Figs. 4.2–4.4). However, *ecoevolity* divergence-time estimates are only biased at very recent divergence times, and the effect disappears when the time of divergence is larger than about $8N_e\mu$.

These patterns make sense given that both types of errors we simulated reduce variation *within* each species. Thus, it is not too surprising that the unlinked-character model in *ecoevolity* struggles when there is shared variation between the two populations (i.e., most gene trees have more than two lineages that coalesce in the ancestral population). The erroneous character patterns mislead both models that the effective size of the descendant branches is smaller than they really are (Figs. 4.8–4.10). To explain the shared variation between the species (i.e. deep coalescences) when underestimating the descendant population sizes, the unlinked-character model of *ecoevolity* simultaneously reduces

the divergence time and increases the effective size of the ancestral population. Despite also being misled about the size of the descendant populations (Figs. 4.8–4.10), the linked-character model of *StarBEAST2* seems to benefit from more information about the general shape of each gene tree across the linked sites and can still maintain an accurate estimate of the divergence time (Figs. 4.2–4.4) and ancestral population size (Figs. 4.5–4.7).

This downward biased variation within each species becomes less of a problem for the unlinked-character model as the divergence time gets larger, likely because the average gene tree only has a single lineage from each species that coalesces in the ancestral population. As the coalesced lineage within each species leading back to the ancestral population becomes a large proportion of the overall length of the average gene tree, the proportion of characters that either show fixed differences between the species or are invariant likely provides enough information to the unlinked character model about the time of divergence to overcome the downward biased estimates of the descendant population sizes.

From the *ecoevolity* results, we also see that when faced with heterozygosity errors, accuracy decreases as locus length increases. In contrast, accuracy of *ecoevolity* is not affected by locus length when analyzing data sets with singleton errors. This pattern makes sense in light of how we generated these errors. We introduced singleton errors per-site and heterozygosity errors per-locus. Thus, the same per-locus rate of heterozygosity errors affects many more sites of a dataset with 1000bp loci compared to dataset with 250bp loci.

Unsurprisingly, the MCMC sampling performance of *StarBEAST2* declines with decreasing locus length. There is less information in the shorter loci about ancestry, and thus more posterior uncertainty about the gene trees. This forces *StarBEAST2* to traverse a much broader distribution of gene trees during MCMC sampling, which is difficult due to the constraints imposed by the species tree. This decline in MCMC performance in *StarBEAST2* does not appear to correlate with poor parameter estimates and the distribution of estimates is generally as good or better than those from *ecoevolity*. However,

this might be due to fact that there is no uncertainty in the species tree in any of our analyses, because there are only two species. As the number of species increases, it seems likely that the MCMC performance will further decline and start to affect parameter and topology estimates.

4.4.2 Relevance to empirical data sets

It is reassuring to see the effect of sequence errors on the unlinked-character model is limited to a small region of parameter space, and is only severe when the frequency of errors in the data is large. Our simulated error rate of 40% is likely higher than the rate that these types of errors occur during most sample preparation, high-throughput sequencing, and bioinformatic processing. However, empirical alignments likely contain a mix of different sources of errors and biases from various steps in the data collection process. Also, real data are not generated under a known model with no prior misspecification. Violations of the model might make these methods of species-tree inference more sensitive to lower rates of error.

The degree to which a dataset will be affected by errors from missing heterozygote haplotypes and missing singletons will be highly dependent on the method used to reduce representation of the genome, depth of sequencing coverage (i.e., the number of overlapping sequence reads at a locus), and how the data are processed. To filter out sequencing errors, most pipelines for processing sequence reads set a minimum coverage threshold for variants or a minimum minor allele frequency. This can result in the miscalling or removal of true variation, especially if coverage is low due to random chance or biases in PCR amplification and sequencing. Processing the data in this way can result in biased estimates of parameters that are sensitive to the frequencies of rare alleles (Huang & Knowles, 2016; Linck & Battey, 2019). If the thresholds for such processing steps are stringent, it could introduce levels of error greater than our simulations.

4.4.3 Recommendations for using unlinked-character models

When erroneous character patterns cause *ecoevolity* to underestimate the divergence time it also inflates the effective population size of the ancestral population. We are seeing values of $N_e^R\mu$ consistent with an average sequence divergence between individuals *within* the ancestral population of 3%, which is almost an order of magnitude larger than our prior mean expectation (0.4%). Thus, looking for unrealistically large population sizes estimated for internal branches of the phylogeny might provide an indication that the unlinked-character model is not explaining the data well. However, there is little information in the data about the effective population sizes along ancestral branches, so the parameter that might indicate a problem is going to have very large credible intervals. Nonetheless, many of the posterior estimates of the ancestral population size from our data sets simulated with character-pattern errors are well beyond the prior distribution.

Whether using linked or unlinked-character models with empirical high-throughput data sets, it is good practice to perform analyses on different versions of the aligned data that are assembled under different coverage thresholds for variants or alleles. Variation of estimates derived from different assemblies of the data might indicate that the model is sensitive to the errors or acquisition biases in the alignments. This is especially true for data where sequence coverage is low for samples and/or loci. Given our findings, it might be helpful to compare the estimates of the effective population sizes along internal branches of the tree. Seeing unrealistically large estimates for some assemblies of the data might indicate that the model is being biased by errors or acquisition biases present in the character patterns.

Consistent with what has been shown in previous work (Oaks, 2019; Oaks et al., 2019), *ecoevolity* performed better when all sites were utilized despite violating the assumption that all sites are unlinked. This suggests that investigators might obtain better estimates by analyzing all their data under unlinked-character models, rather than discarding much of it to avoid violating an assumption of the model. Given that the model of unlinked characters implemented in *ecoevolity* does not use information about linkage among sites

(Bryant et al., 2012; Oaks, 2019), it is not surprising that this model violation does not introduce a bias. Linkage among sites does not change the gene trees and site patterns that are expected under the model, but it does reduce the variance of those patterns due to them evolving along fewer gene trees. As a result, the accuracy of the parameter estimates is not affected by the linkage among sites within loci, but the credible intervals become too narrow as the length of loci increase (Oaks, 2019; Oaks et al., 2019). However, it remains to be seen whether the robustness of the model’s accuracy to linked sites holds true for larger species trees.

4.4.4 Other complexities of empirical data in need of exploration

Our goal was to compare the theoretical performance of linked and unlinked character models, not their current software implementations. Accordingly, to minimize differences in performance that are due to differences in algorithms for exploring the space of gene and species trees, we restricted our simulations to two species model and a small number of individuals. Nonetheless, exploring how character-pattern errors and biases affect the inference of larger species trees would be informative. The species tree topology is usually a parameter of great interest to biologists, so it would be interesting to know whether the linked model continues to be more robust to errors than the unlinked model as the number of species increases. We saw the MCMC performance of *StarBEAST2* decline concomitantly with locus length in our simulations due to greater uncertainty in gene trees. Given that data sets frequently contain loci shorter than 250 bp, it is important to know whether good sampling of the posterior of linked-character models becomes prohibitive for larger trees. Also, *ecoevolity* greatly overestimated the effective size of the ancestral population in the face of high rates of errors in the data. Exploring larger trees will also determine whether this behavior is limited to the root population or is a potential problem for all internal branches of the species tree.

Exploring other types of errors and biases would also be informative. To generate alignments of orthologous loci from high-throughput data, sequences are matched to a similar portion of a reference sequence or clustered together based on similarity. To avoid

aligning paralogous sequences it is necessary to establish a minimum level of similarity for establishing orthology between sequences. This can lead to an acquisition bias due to the exclusion of more variable loci or alleles from the alignment (Huang & Knowles, 2016). Furthermore, when a reference sequence is used, this data filtering will not be random with respect to the species, but rather there will be a bias towards filtering loci and alleles with greater sequence divergence from the reference. Simulations exploring the affect of these types of data acquisition biases would complement the errors we explored here.

In our analyses, there was no model misspecification other than the introduced errors (except for the linked sites violating the unlinked-character model). With empirical data, there are likely many model violations, and our prior distributions will never match the distributions that generated the data. Introducing other model violations and misspecified prior distributions would thus help to better understand how species-tree models behave on real data sets. Of particular concern is whether misspecified priors will amplify the effect of character-pattern errors or biases.

We found that character-pattern errors that remove variation from within species can cause unlinked-character models to underestimate divergence times and overestimate ancestral population sizes in order to explain shared variation among species. This raises the question of whether we can explicitly model and correct for these types of data collection errors in order to avoid biased parameter estimates. An approach that could integrate over uncertainty in the frequency of these types of missing-allele errors would be particularly appealing.

References

- Bouckaert, R., Heled, J., Kühnert, D., Vaughan, T., Wu, C.-H., Xie, D., Suchard, M. A., Rambaut, A., & Drummond, A. J. (2014). BEAST 2: A Software Platform for Bayesian Evolutionary Analysis (A. Prlic, Ed.). *PLoS Computational Biology*, 10(4), e1003537. <https://doi.org/10.1371/journal.pcbi.1003537>

- Brooks, S. P., & Gelman, A. (1998). General methods for monitoring convergence of iterative simulations. *Journal of computational and graphical statistics*, 7(4), 434–455.
- Bryant, D., Bouckaert, R., Felsenstein, J., Rosenberg, N. A., & RoyChoudhury, A. (2012). Inferring Species Trees Directly from Biallelic Genetic Markers: Bypassing Gene Trees in a Full Coalescent Analysis. *Molecular Biology and Evolution*, 29(8), 1917–1932. <https://doi.org/10.1093/molbev/mss086>
- De Maio, N., Schrempf, D., & Kosiol, C. (2015). PoMo: An Allele Frequency-Based Approach for Species Tree Estimation. *Systematic Biology*, 64(6), 1018–1031. <https://doi.org/10.1093/sysbio/syv048>
- Gong, L., & Flegal, J. M. (2016). A Practical Sequential Stopping Rule for High-Dimensional Markov Chain Monte Carlo. *Journal of Computational and Graphical Statistics*, 25(3), 684–700. <https://doi.org/10.1080/10618600.2015.1044092>
- Harvey, M. G., Judy, C. D., Seeholzer, G. F., Maley, J. M., Graves, G. R., & Brumfield, R. T. (2015). Similarity thresholds used in DNA sequence assembly from short reads can reduce the comparability of population histories across species. *PeerJ*, 3, e895. <https://doi.org/10.7717/peerj.895>
- Heled, J., & Drummond, A. J. (2010). Bayesian Inference of Species Trees from Multilocus Data. *Molecular Biology and Evolution*, 27(3), 570–580. <https://doi.org/10.1093/molbev/msp274>
- Huang, H., & Knowles, L. L. (2016). Unforeseen Consequences of Excluding Missing Data from Next-Generation Sequences: Simulation Study of RAD Sequences. *Systematic Biology*, 65(3), 357–365. <https://doi.org/10.1093/sysbio/syu046>
- Hunter, J. D. (2007). Matplotlib: A 2D Graphics Environment. *Computing in Science & Engineering*, 9(3), 90–95. <https://doi.org/10.1109/MCSE.2007.55>
- Leaché, A. D., & Oaks, J. R. (2017). The Utility of Single Nucleotide Polymorphism (SNP) Data in Phylogenetics. *Annual Review of Ecology, Evolution, and Systematics*, 48(1), 69–84. <https://doi.org/10.1146/annurev-ecolsys-110316-022645>

- Linck, E., & Battey, C. J. (2019). Minor allele frequency thresholds strongly affect population structure inference with genomic data sets. *Molecular Ecology Resources*, 19(3), 639–647. <https://doi.org/10.1111/1755-0998.12995>
- Liu, L., & Pearl, D. K. (2007). Species Trees from Gene Trees: Reconstructing Bayesian Posterior Distributions of a Species Phylogeny Using Estimated Gene Tree Distributions (T. Buckley, Ed.). *Systematic Biology*, 56(3), 504–514. <https://doi.org/10.1080/10635150701429982>
- Oaks, J. R. (2019). Full Bayesian Comparative Phylogeography from Genomic Data (L. Kubatko, Ed.). *Systematic Biology*, 68(3), 371–395. <https://doi.org/10.1093/sysbio/syy063>
- Oaks, J. R., Siler, C. D., & Brown, R. M. (2019). The comparative biogeography of Philippine geckos challenges predictions from a paradigm of climate-driven vicariant diversification across an island archipelago. *Evolution*, 73(6), 1151–1167. <https://doi.org/10.1111/evo.13754>
- Ogilvie, H. A., Bouckaert, R. R., & Drummond, A. J. (2017). StarBEAST2 Brings Faster Species Tree Inference and Accurate Estimates of Substitution Rates. *Molecular Biology and Evolution*, 34(8), 2101–2114. <https://doi.org/10.1093/molbev/msx126>
- Pfeiffer, F., Gröber, C., Blank, M., Händler, K., Beyer, M., Schultze, J. L., & Mayer, G. (2018). Systematic evaluation of error rates and causes in short samples in next-generation sequencing. *Scientific Reports*, 8(1), 10950. <https://doi.org/10.1038/s41598-018-29325-6>
- Potapov, V., & Ong, J. L. (2017). Examining Sources of Error in PCR by Single-Molecule Sequencing (R. Kalender, Ed.). *PLOS ONE*, 12(1), e0169774. <https://doi.org/10.1371/journal.pone.0169774>
- Rambaut, A., & Grass, N. C. (1997). Seq-Gen: An application for the Monte Carlo simulation of DNA sequence evolution along phylogenetic trees. *Bioinformatics*, 13(3), 235–238. <https://doi.org/10.1093/bioinformatics/13.3.235>

- Rochette, N. C., Rivera-Colón, A. G., & Catchen, J. M. (2019). Stacks 2: Analytical methods for paired-end sequencing improve RADseq-based population genomics. *Molecular Ecology*, 28(21), 4737–4754. <https://doi.org/10.1111/mec.15253>
- Sukumaran, J., & Holder, M. T. (2010). DendroPy: A Python library for phylogenetic computing. *Bioinformatics*, 26(12), 1569–1571. <https://doi.org/10.1093/bioinformatics/btq228>
- Yang, Z. (2015). The BPP program for species tree estimation and species delimitation. *Current Zoology*, 61(5), 854–865. <https://doi.org/10.1093/czoolo/61.5.854>
- Yule, G. U. (1925). A mathematical theory of evolution, based on the conclusions of Dr. JC Willis, FR S. *Philosophical transactions of the Royal Society of London. Series B, containing papers of a biological character*, 213(402-410), 21–87.

4.5 Figures

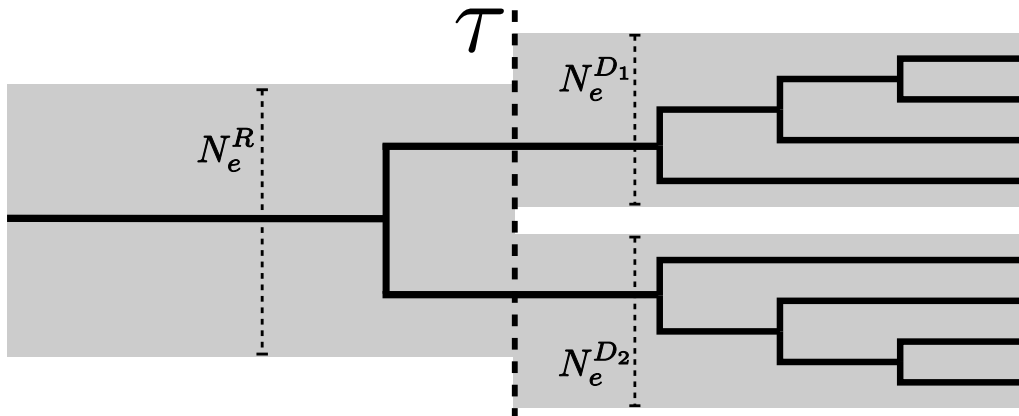


Figure 4.1. An illustration of the species-tree model we used to simulate data. N_e^R , N_e^{D1} , and N_e^{D2} represent the constant effective population sizes of the root, and each of the two terminal populations. τ represents the instantaneous separation of the ancestral population into two descendant populations. One hypothetical gene tree is shown to illustrate the gene trees simulated under a contained coalescent process for 4 haploid gene copies sampled from each of the terminal branches of the species tree.

Divergence Time — 1000bp loci

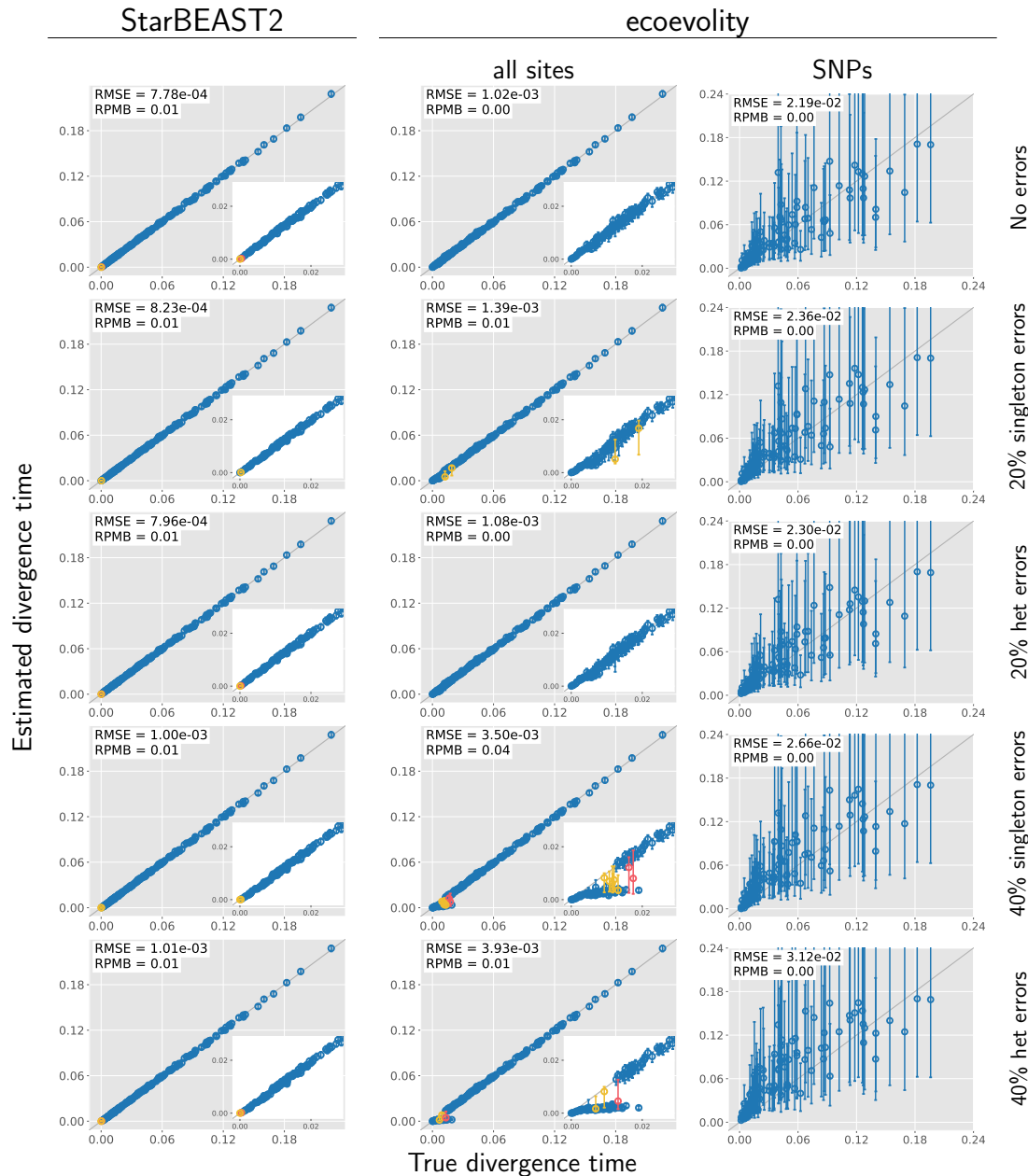


Figure 4.2. Accuracy and precision of divergence-time estimates (in units of expected substitutions per site) with 1000 base pair loci. The left column shows estimates from *StarBEAST2*, and the center and right column shows estimates from *ecoevolity* using all sites and (at most) one SNP per locus. The top row shows estimates from 200 data sets simulated without character-pattern errors. Rows labelled 20% and 40% singleton errors show estimates from the same alignments after singleton site patterns were changed to invariant sites with probabilities 0.2 and 0.4, respectively. Rows labelled 20% and 40% het errors show estimates from the same (error-free) alignments after we randomly paired gene copies within each species into two diploid genotypes, and for each genotype we randomly replaced one allele with the other with probability 0.2 and 0.4, respectively. Each plotted circle and associated error bars represent the posterior mean and 95% credible interval. Circles and error bars are colored yellow if the effective sample size (ESS) of the estimate was less than 200, red if the potential scale reduction factor (PSRF) was greater than 1.2, and green if both conditions were true. The root mean square error (RMSE) and rate of poor MCMC behavior (RPMB) is given for each plot, the latter of which is the proportion of estimates with ESS < 200 and/or PSRF > 1.2. We generated the plots using matplotlib Version 3.1.1 (Hunter, 2007).

Divergence Time — 500bp loci

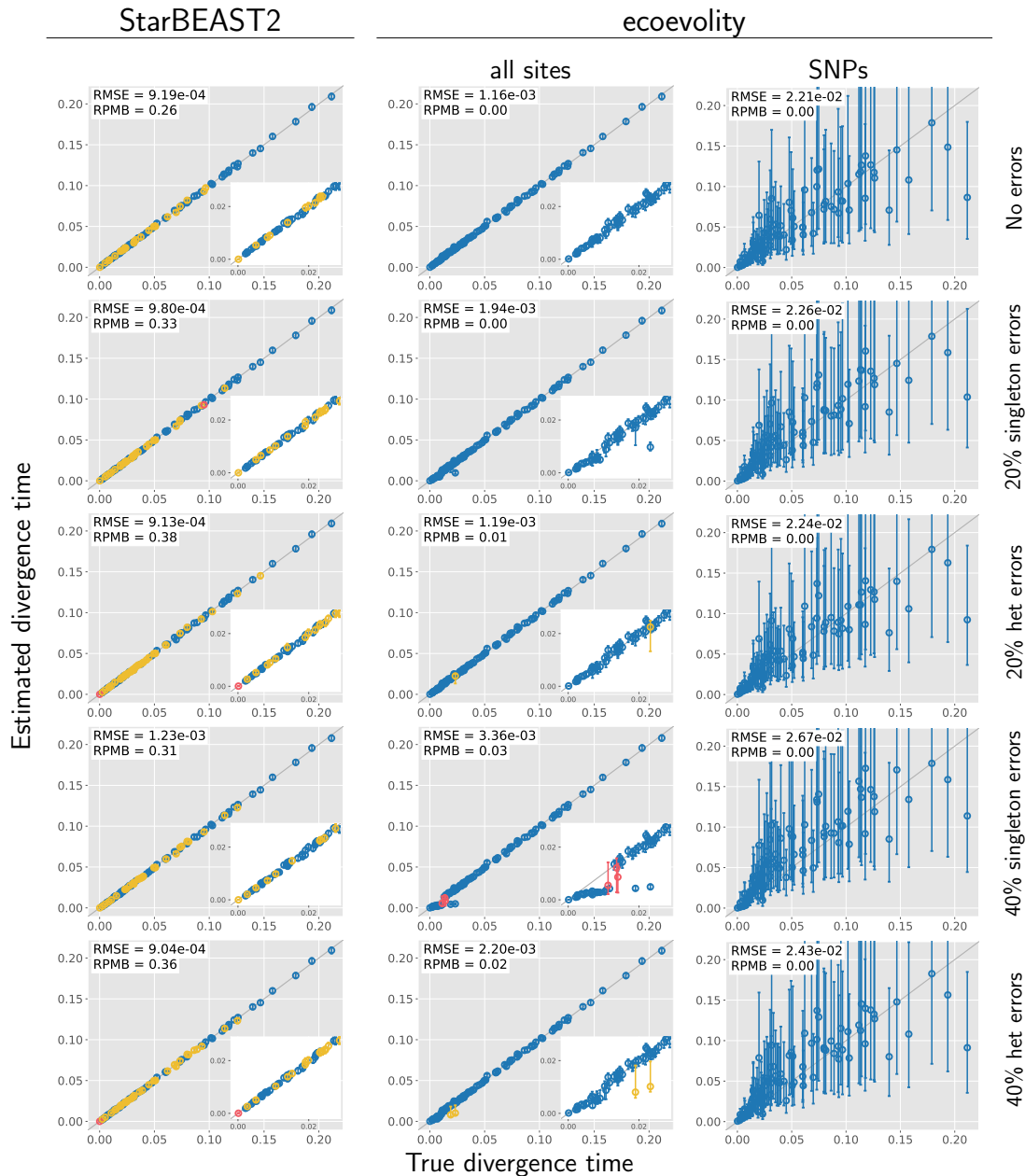


Figure 4.3. Accuracy and precision of divergence-time estimates (in units of expected substitutions per site) with 500 base pair loci. The left column shows estimates from *StarBEAST2*, and the center and right column shows estimates from *ecoevolity* using all sites and (at most) one SNP per locus. The top row shows estimates from 200 data sets simulated without character-pattern errors. Rows labelled 20% and 40% singleton errors show estimates from the same alignments after singleton site patterns were changed to invariant sites with probabilities 0.2 and 0.4, respectively. Rows labelled 20% and 40% het errors show estimates from the same (error-free) alignments after we randomly paired gene copies within each species into two diploid genotypes, and for each genotype we randomly replaced one allele with the other with probability 0.2 and 0.4, respectively. Each plotted circle and associated error bars represent the posterior mean and 95% credible interval. Circles and error bars are colored yellow if the effective sample size (ESS) of the estimate was less than 200, red if the potential scale reduction factor (PSRF) was greater than 1.2, and green if both conditions were true. The root mean square error (RMSE) and rate of poor MCMC behavior (RPMB) is given for each plot, the latter of which is the proportion of estimates with ESS < 200 and/or PSRF > 1.2. We generated the plots using matplotlib Version 3.1.1 (Hunter, 2007).

Divergence Time — 250bp loci

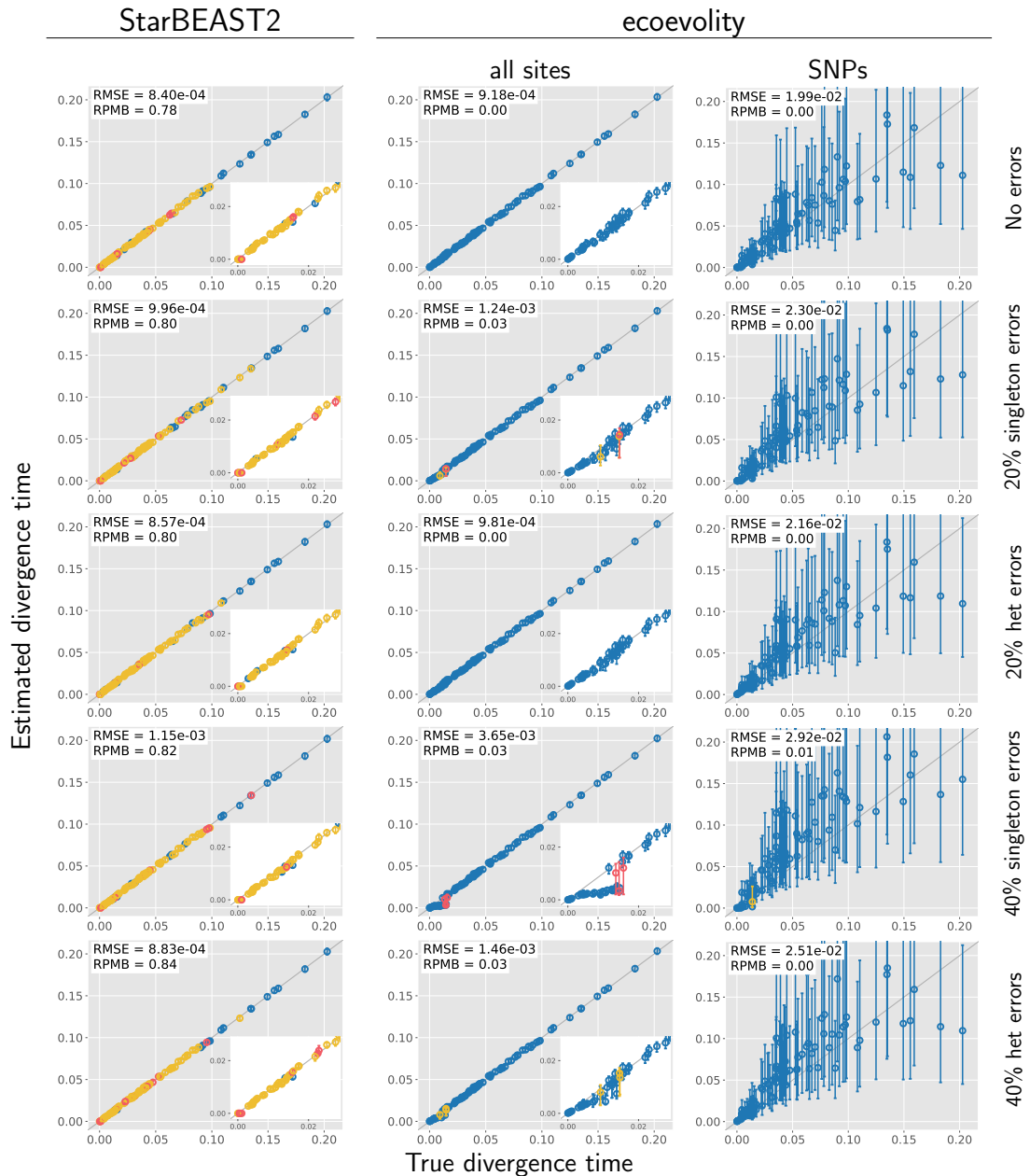


Figure 4.4. Accuracy and precision of divergence-time estimates (in units of expected substitutions per site) with 250 base pair loci. The left column shows estimates from *StarBEAST2*, and the center and right column shows estimates from *ecoevolity* using all sites and (at most) one SNP per locus. The top row shows estimates from 200 data sets simulated without character-pattern errors. Rows labelled 20% and 40% singleton errors show estimates from the same alignments after singleton site patterns were changed to invariant sites with probabilities 0.2 and 0.4, respectively. Rows labelled 20% and 40% het errors show estimates from the same (error-free) alignments after we randomly paired gene copies within each species into two diploid genotypes, and for each genotype we randomly replaced one allele with the other with probability 0.2 and 0.4, respectively. Each plotted circle and associated error bars represent the posterior mean and 95% credible interval. Circles and error bars are colored yellow if the effective sample size (ESS) of the estimate was less than 200, red if the potential scale reduction factor (PSRF) was greater than 1.2, and green if both conditions were true. The root mean square error (RMSE) and rate of poor MCMC behavior (RPMB) is given for each plot, the latter of which is the proportion of estimates with ESS < 200 and/or PSRF > 1.2. We generated the plots using matplotlib Version 3.1.1 (Hunter, 2007).

Ancestral $N_e\mu$ — 1000bp loci

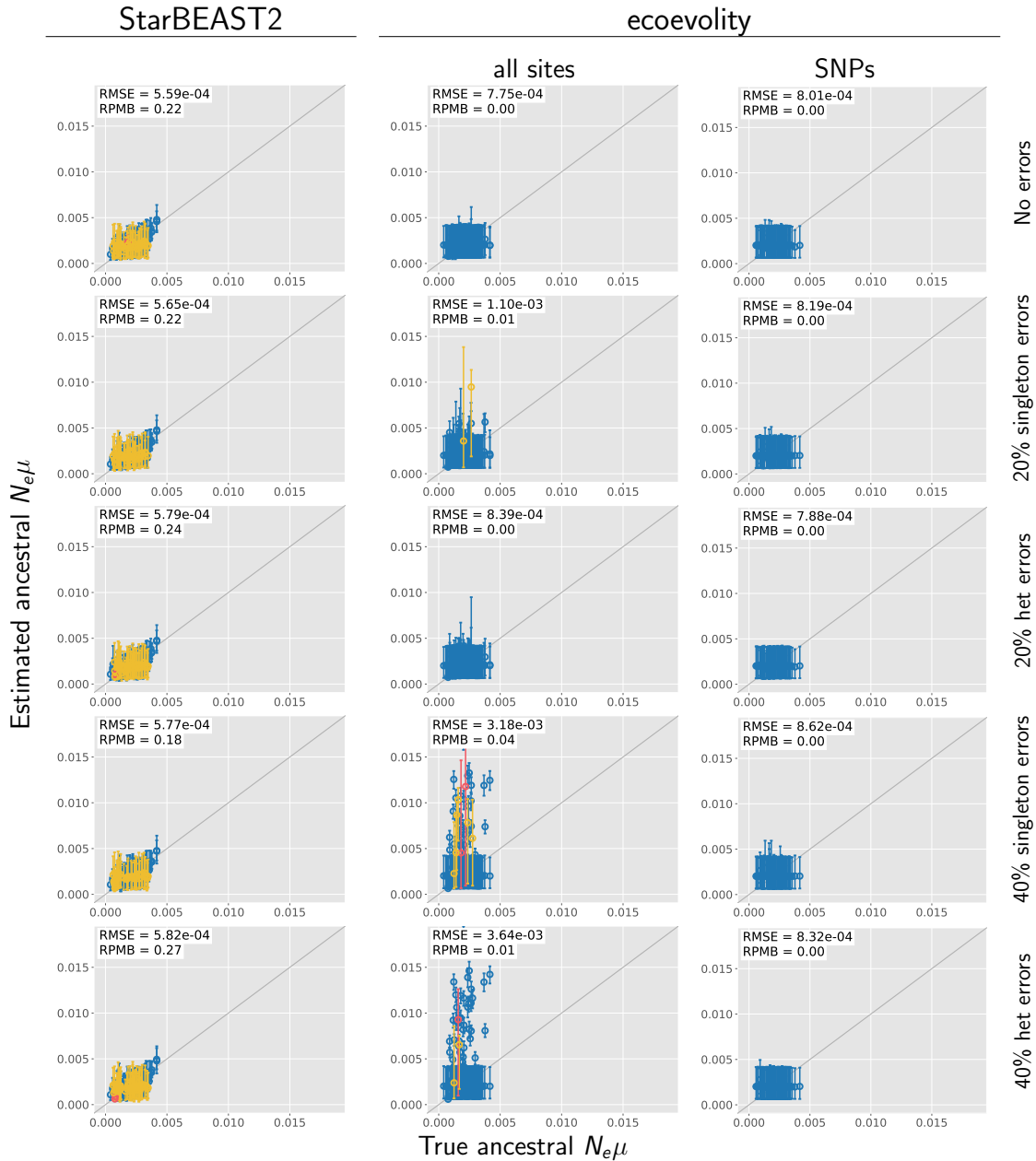


Figure 4.5. Accuracy and precision of estimates of root effective population size scaled by the mutation rate ($N_e^R \mu$) with 1000 base pair loci. The left column shows estimates from *StarBEAST2*, and the center and right column shows estimates from *ecoevolity* using all sites and (at most) one SNP per locus. The top row shows estimates from 200 data sets simulated without character-pattern errors. Rows labelled 20% and 40% singleton errors show estimates from the same alignments after singleton site patterns were changed to invariant sites with probabilities 0.2 and 0.4, respectively. Rows labelled 20% and 40% het errors show estimates from the same (error-free) alignments after we randomly paired gene copies within each species into two diploid genotypes, and for each genotype we randomly replaced one allele with the other with probability 0.2 and 0.4, respectively. Each plotted circle and associated error bars represent the posterior mean and 95% credible interval. Circles and error bars are colored yellow if the effective sample size (ESS) of the estimate was less than 200, red if the potential scale reduction factor (PSRF) was greater than 1.2, and green if both conditions were true. The root mean square error (RMSE) and rate of poor MCMC behavior (RPMB) is given for each plot, the latter of which is the proportion of estimates with ESS < 200 and/or PSRF > 1.2. We generated the plots using matplotlib Version 3.1.1 (Hunter, 2007).

Ancestral $N_e\mu$ — 500bp loci

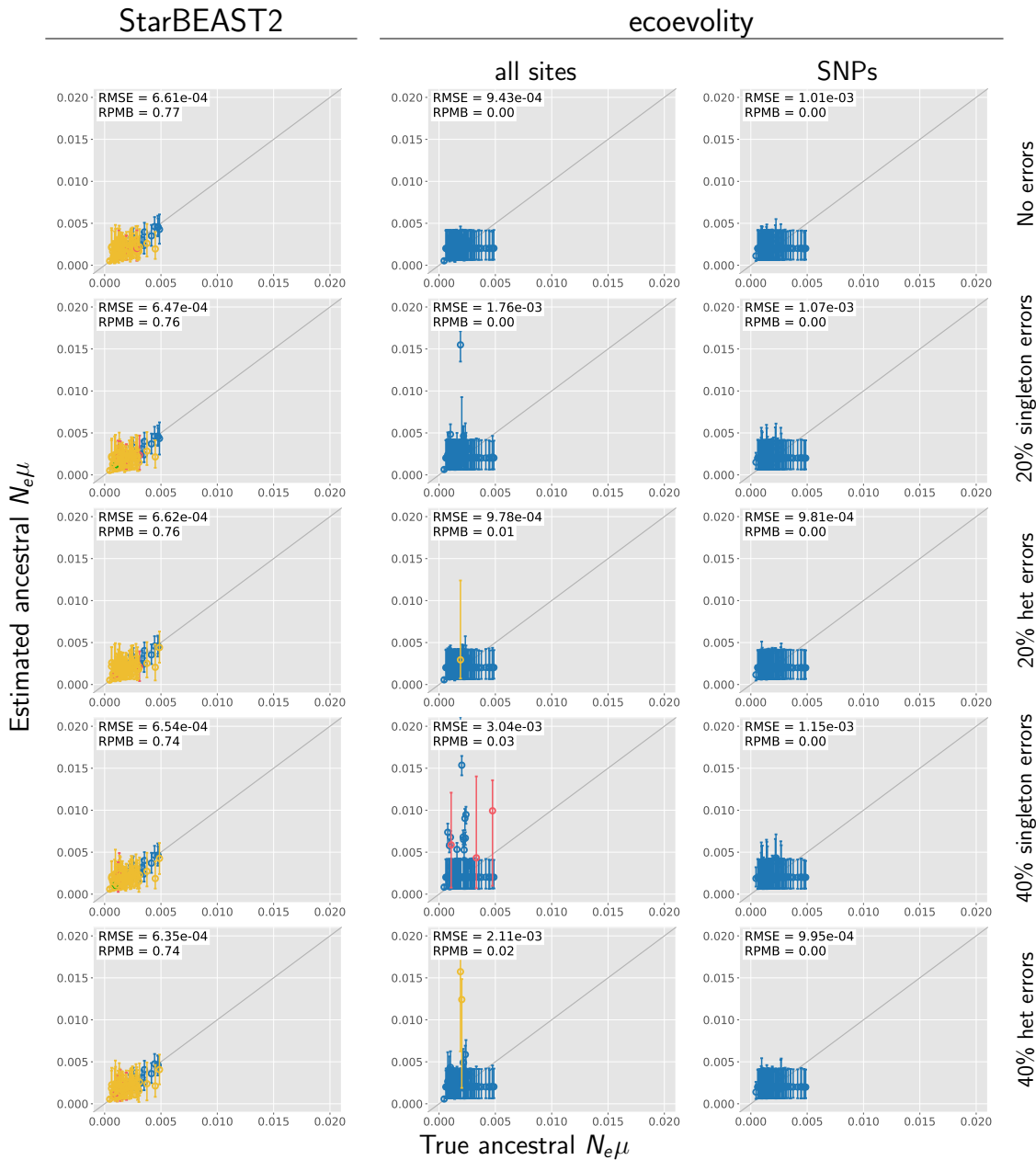


Figure 4.6. Accuracy and precision of estimates of root effective population size scaled by the mutation rate ($N_e^R\mu$) with 500 base pair loci. The left column shows estimates from *StarBEAST2*, and the center and right column shows estimates from *ecoevolity* using all sites and (at most) one SNP per locus. The top row shows estimates from 200 data sets simulated without character-pattern errors. Rows labelled 20% and 40% singleton errors show estimates from the same alignments after singleton site patterns were changed to invariant sites with probabilities 0.2 and 0.4, respectively. Rows labelled 20% and 40% het errors show estimates from the same (error-free) alignments after we randomly paired gene copies within each species into two diploid genotypes, and for each genotype we randomly replaced one allele with the other with probability 0.2 and 0.4, respectively. Each plotted circle and associated error bars represent the posterior mean and 95% credible interval. Circles and error bars are colored yellow if the effective sample size (ESS) of the estimate was less than 200, red if the potential scale reduction factor (PSRF) was greater than 1.2, and green if both conditions were true. The root mean square error (RMSE) and rate of poor MCMC behavior (RPMB) is given for each plot, the latter of which is the proportion of estimates with ESS < 200 and/or PSRF > 1.2. We generated the plots using matplotlib Version 3.1.1 (Hunter, 2007).

Ancestral $N_e\mu$ — 250bp loci

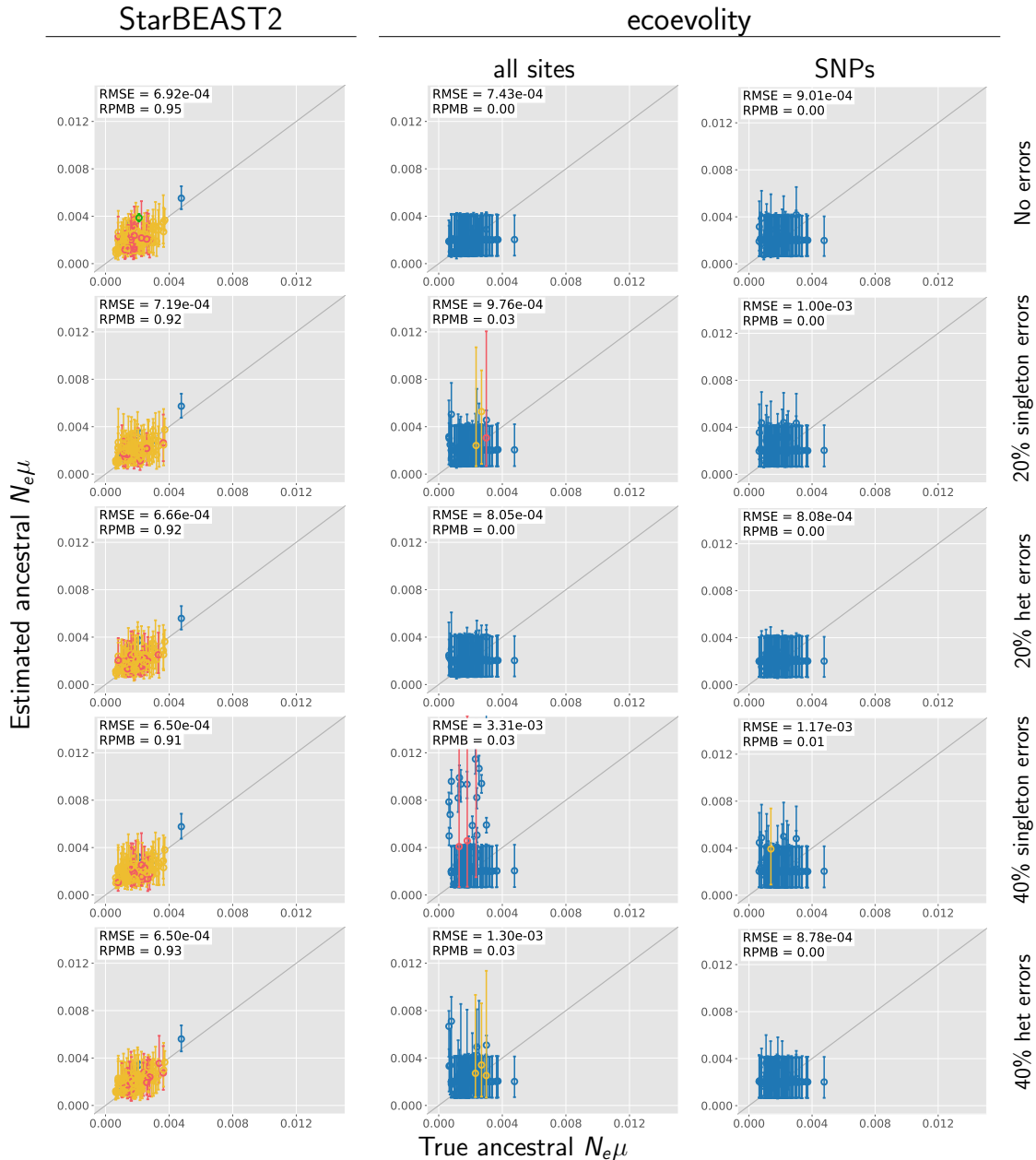


Figure 4.7. Accuracy and precision of estimates of root effective population size scaled by the mutation rate ($N_e^R\mu$) with 250 base pair loci. The left column shows estimates from *StarBEAST2*, and the center and right column shows estimates from *ecoevolity* using all sites and (at most) one SNP per locus. The top row shows estimates from 200 data sets simulated without character-pattern errors. Rows labelled 20% and 40% singleton errors show estimates from the same alignments after singleton site patterns were changed to invariant sites with probabilities 0.2 and 0.4, respectively. Rows labelled 20% and 40% het errors show estimates from the same (error-free) alignments after we randomly paired gene copies within each species into two diploid genotypes, and for each genotype we randomly replaced one allele with the other with probability 0.2 and 0.4, respectively. Each plotted circle and associated error bars represent the posterior mean and 95% credible interval. Circles and error bars are colored yellow if the effective sample size (ESS) of the estimate was less than 200, red if the potential scale reduction factor (PSRF) was greater than 1.2, and green if both conditions were true. The root mean square error (RMSE) and rate of poor MCMC behavior (RPMB) is given for each plot, the latter of which is the proportion of estimates with ESS < 200 and/or PSRF > 1.2. We generated the plots using matplotlib Version 3.1.1 (Hunter, 2007).

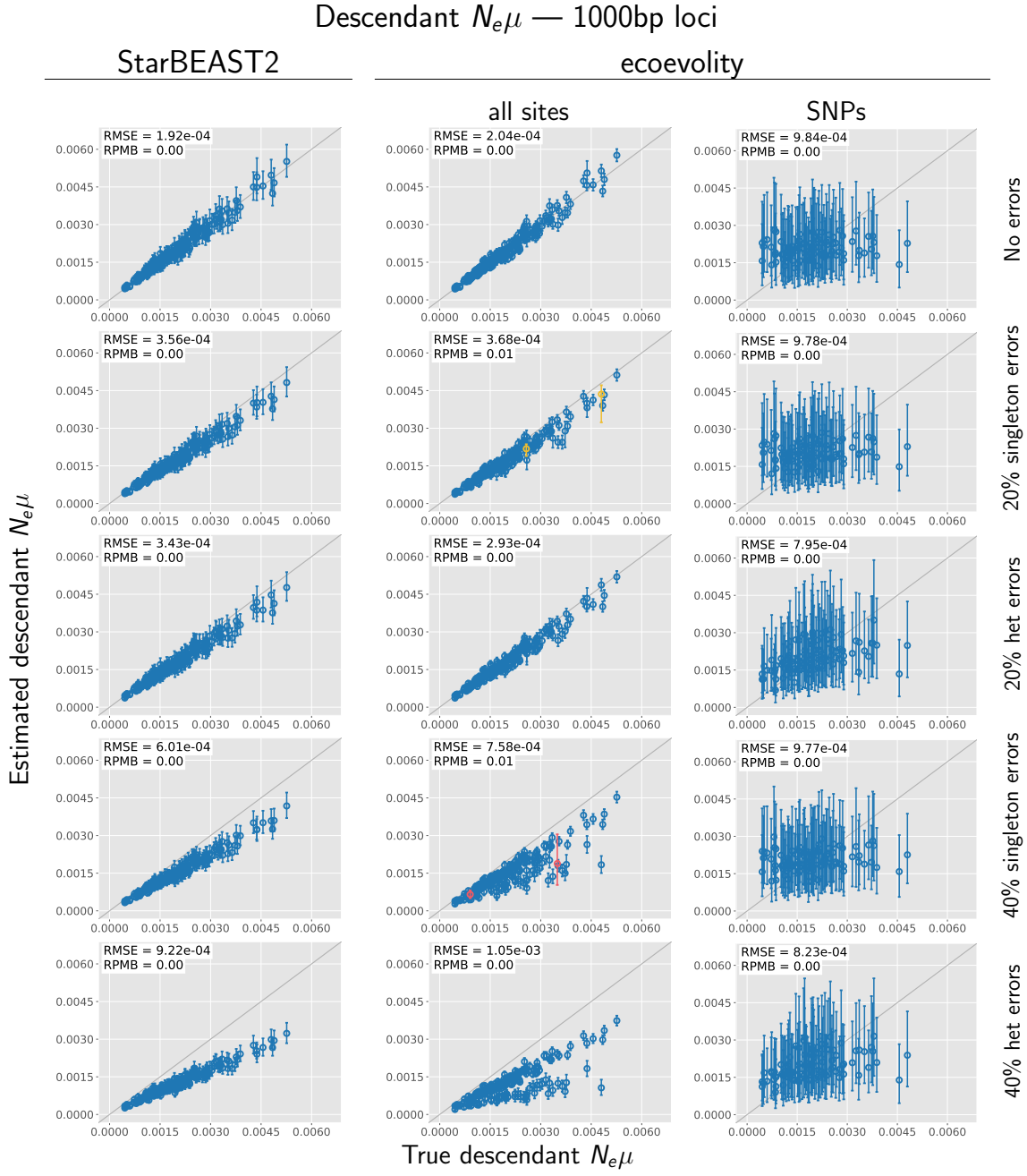


Figure 4.8. Accuracy and precision of estimates of effective population sizes of the descendant branches of the tree scaled by the mutation rate ($N_e^D\mu$) with 1000 base pair loci. The left column shows estimates from *StarBEAST2*, and the center and right column shows estimates from *ecoevolity* using all sites and (at most) one SNP per locus. The top row shows estimates from 200 data sets simulated without character-pattern errors. Rows labelled 20% and 40% singleton errors show estimates from the same alignments after singleton site patterns were changed to invariant sites with probabilities 0.2 and 0.4, respectively. Rows labelled 20% and 40% het errors show estimates from the same (error-free) alignments after we randomly paired gene copies within each species into two diploid genotypes, and for each genotype we randomly replaced one allele with the other with probability 0.2 and 0.4, respectively. Each plotted circle and associated error bars represent the posterior mean and 95% credible interval. Circles and error bars are colored yellow if the effective sample size (ESS) of the estimate was less than 200, red if the potential scale reduction factor (PSRF) was greater than 1.2, and green if both conditions were true. The root mean square error (RMSE) and rate of poor MCMC behavior (RPMB) is given for each plot, the latter of which is the proportion of estimates with ESS < 200 and/or PSRF > 1.2. We generated the plots using matplotlib Version 3.1.1 (Hunter, 2007).

Descendant $N_e\mu$ — 500bp loci

StarBEAST2

ecoevolity

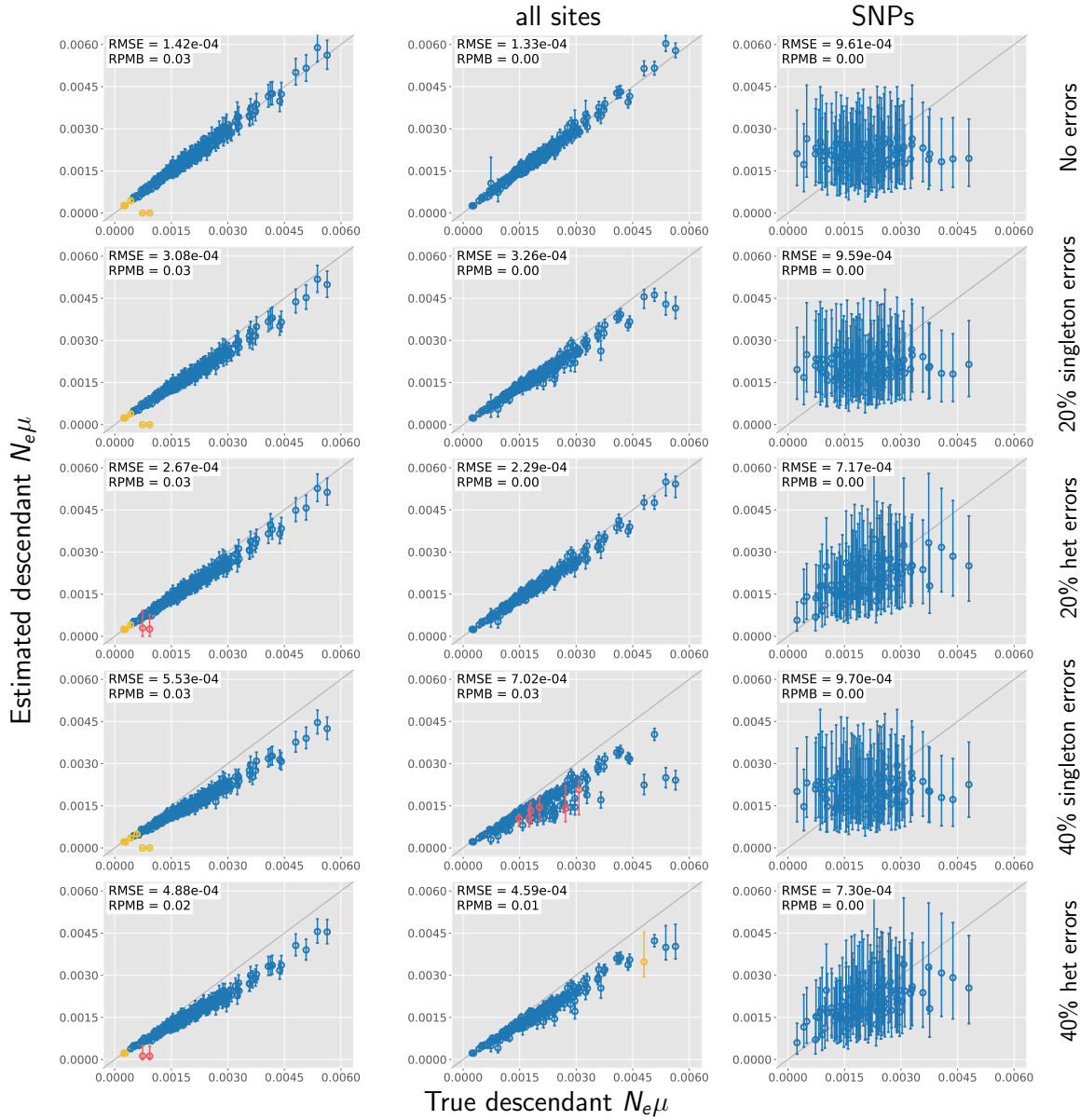


Figure 4.9. Accuracy and precision of estimates of effective population sizes of the descendant branches of the tree scaled by the mutation rate ($N_e^D \mu$) with 500 base pair loci. The left column shows estimates from *StarBEAST2*, and the center and right column shows estimates from *ecoevolity* using all sites and (at most) one SNP per locus. The top row shows estimates from 200 data sets simulated without character-pattern errors. Rows labelled 20% and 40% singleton errors show estimates from the same alignments after singleton site patterns were changed to invariant sites with probabilities 0.2 and 0.4, respectively. Rows labelled 20% and 40% het errors show estimates from the same (error-free) alignments after we randomly paired gene copies within each species into two diploid genotypes, and for each genotype we randomly replaced one allele with the other with probability 0.2 and 0.4, respectively. Each plotted circle and associated error bars represent the posterior mean and 95% credible interval. Circles and error bars are colored yellow if the effective sample size (ESS) of the estimate was less than 200, red if the potential scale reduction factor (PSRF) was greater than 1.2, and green if both conditions were true. The root mean square error (RMSE) and rate of poor MCMC behavior (RPMB) is given for each plot, the latter of which is the proportion of estimates with ESS < 200 and/or PSRF > 1.2. We generated the plots using matplotlib Version 3.1.1 (Hunter, 2007).

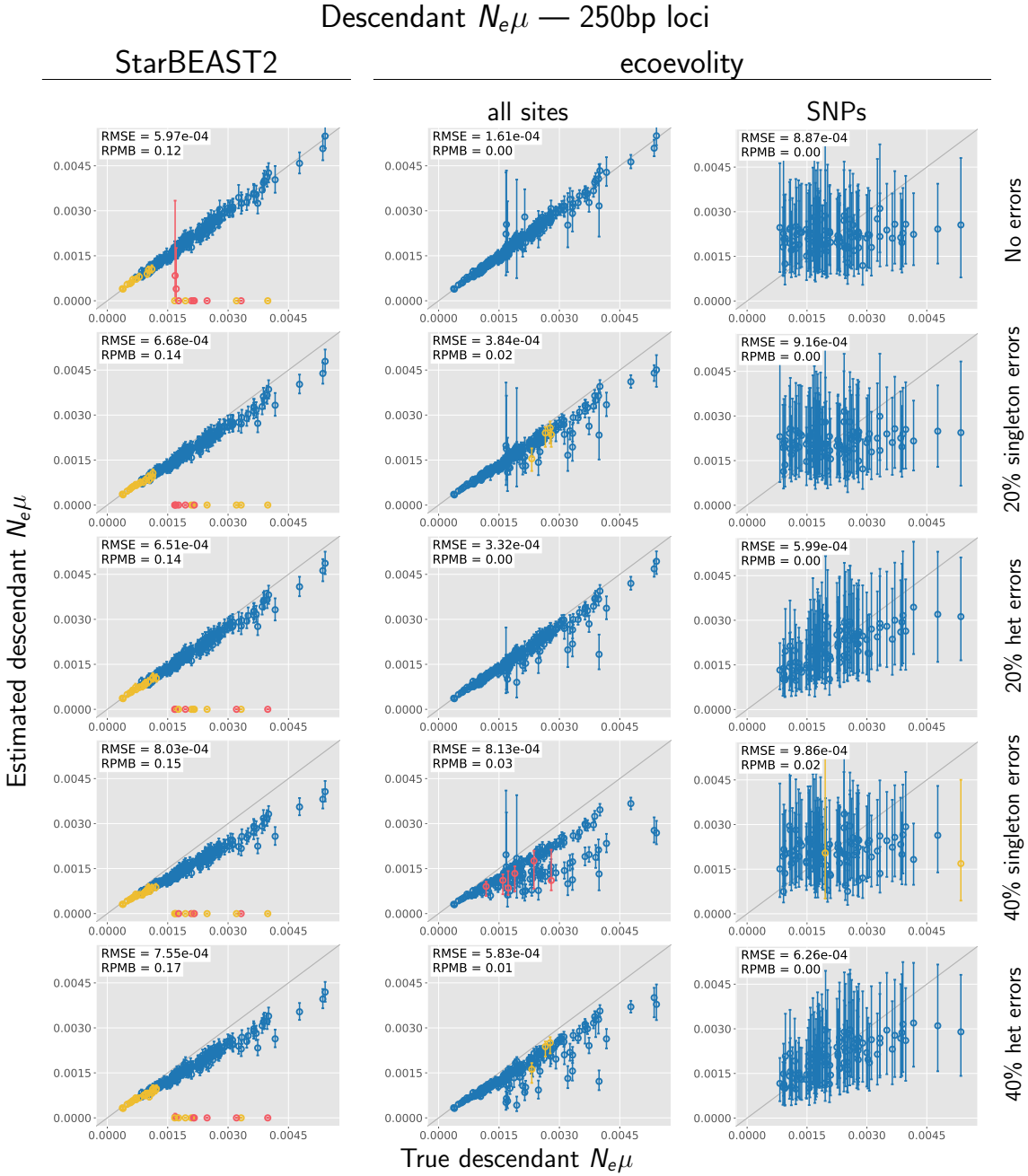


Figure 4.10. Accuracy and precision of estimates of effective population sizes of the descendant branches of the tree scaled by the mutation rate ($N_e^D\mu$) with 250 base pair loci. The left column shows estimates from *StarBEAST2*, and the center and right column shows estimates from *ecoevolity* using all sites and (at most) one SNP per locus. The top row shows estimates from 200 data sets simulated without character-pattern errors. Rows labelled 20% and 40% singleton errors show estimates from the same alignments after singleton site patterns were changed to invariant sites with probabilities 0.2 and 0.4, respectively. Rows labelled 20% and 40% het errors show estimates from the same (error-free) alignments after we randomly paired gene copies within each species into two diploid genotypes, and for each genotype we randomly replaced one allele with the other with probability 0.2 and 0.4, respectively. Each plotted circle and associated error bars represent the posterior mean and 95% credible interval. Circles and error bars are colored yellow if the effective sample size (ESS) of the estimate was less than 200, red if the potential scale reduction factor (PSRF) was greater than 1.2, and green if both conditions were true. The root mean square error (RMSE) and rate of poor MCMC behavior (RPMB) is given for each plot, the latter of which is the proportion of estimates with ESS < 200 and/or PSRF > 1.2. We generated the plots using matplotlib Version 3.1.1 (Hunter, 2007).

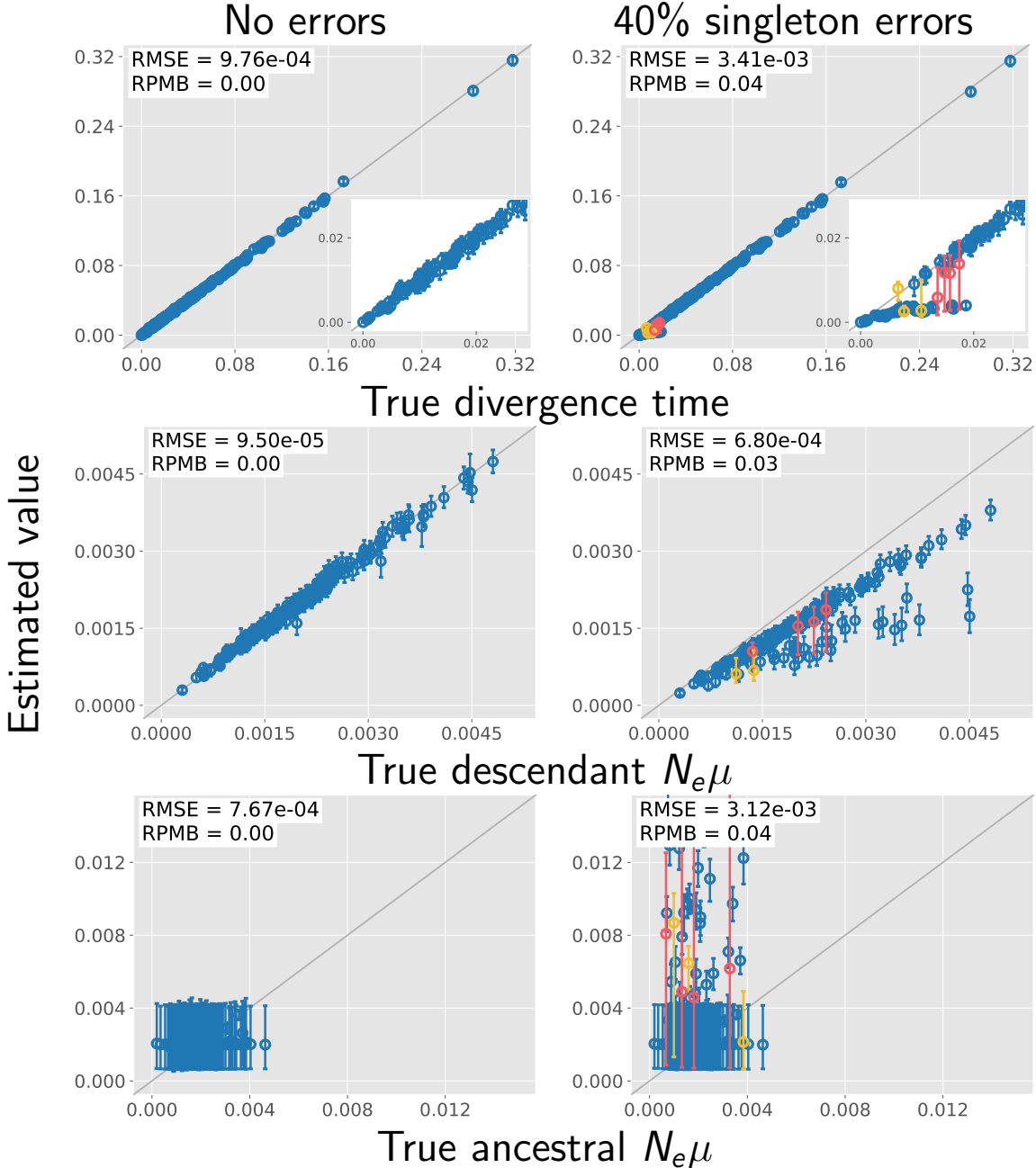


Figure 4.11. The performance of *ecoevolity* with data sets simulated with unlinked characters. Each plotted circle and associated error bars represent the posterior mean and 95% credible interval. Circles and error bars are colored yellow if the effective sample size (ESS) of the estimate was less than 200, red if the potential scale reduction factor (PSRF) was greater than 1.2, and green if both conditions were true. The root mean square error (RMSE) and rate of poor MCMC behavior (RPMB) is given for each plot, the latter of which is the proportion of estimates with $\text{ESS} < 200$ and/or $\text{PSRF} > 1.2$. Inset plots magnify estimates of most recent divergence times. We generated the plots using matplotlib Version 3.1.1 (Hunter, 2007).